

R-matrix calculations of polarisation effects in low-energy positron-molecule collisions

Rui Zhang

A thesis submitted to the University College London
for the degree of Doctor of Philosophy

Department of Physics and Astronomy
University College London

September 2010

I, Rui Zhang, confirm that the work presented in this thesis is my own. Where information has been derived from other sources, I confirm that this has been indicated in the thesis.

Abstract

The study of the interaction of positrons with atoms and molecules has become increasingly popular, because more and more experimental activities have become feasible. Although exchange effects are absent, the polarisation effects, caused by the attractive nature between the positron and the target electrons, make the positron-molecule collisions more difficult to handle than the corresponding electron collisions.

This thesis gives the calculations of positron collisions with polar molecule H_2O and non-polar molecules, H_2 and C_2H_2 at energies below the positronium formation threshold. All calculations were carried out using the modified version of the UK molecular R -matrix code. Due to the large permanent dipolar nature of water molecule, the three models tested give very similar results. However, for positron collision with non-polar molecules, the polarisation effects can be very important in the calculation. The molecular R -matrix with pseudostates (MRMPS) method has been employed to analyse the positron collision with non-polar molecules, and found to lead to an excellent representation of target polarisation.

C_2H_2 is the simplest molecule that has very enhanced annihilation parameter Z_{eff} , which can be determined by the total scattering wavefunction. So a new sub-code was developed for calculating Z_{eff} based on the UK R -matrix polyatomic code and employed to treat positron collisions with H atom, H_2 and C_2H_2 molecules. It has been found that Z_{eff} values are also sensitive to the degree of polarisation included in calculations and are greatly improved by use of the MRMPS method.

Contents

1	Introduction	11
1.1	Overview	11
1.2	Positron interactions	15
1.3	The positron-molecule scattering problem	18
1.4	Positron annihilation in molecules	21
1.5	Objectives	24
1.6	Layout of the thesis	24
2	General Theory	26
2.1	Born-Oppenheimer approximation	26
2.2	Hartree-Fock self consistent field method	28
2.3	Configuration interaction	30
2.4	Fixed-nuclei formulation of the scattering problem	32
3	R-matrix theory	35
3.1	Overview	35
3.2	The inner region	36
3.2.1	The inner region wave function	37
3.2.2	Derivation of the R -matrix	39
3.3	The outer region	41
3.3.1	Outer region wave function	44
3.4	Molecular R -matrix with pseudostates method	45
3.5	The Partitioned R -matrix method	48
3.6	Computational implementation	49

CONTENTS

4	Positron Annihilation	56
4.1	Introduction	56
4.2	Dirac delta functions	58
4.3	Normalisation of elastic scattering wave function	59
4.4	Annihilation tests	61
4.5	Conclusion	64
5	Positron collisions with water	65
5.1	Introduction	65
5.2	Target calculation	67
5.3	Scattering calculation	68
5.4	Results and discussion	69
5.5	DCS correction	76
5.6	Conclusion	77
6	Positron collisions with H₂ molecule	79
6.1	Introduction	79
6.2	Calculations	80
6.3	Results and discussion	84
6.4	Conclusion	89
7	Positron collisions with C₂H₂	91
7.1	Introduction	91
7.2	Target calculation	92
7.3	Scattering calculation	96
7.4	Results	98
7.5	Conclusions	103
8	Annihilation rates of low-energy positron scattering with molecules	105
8.1	Introduction	105
8.2	Calculations	107
8.3	Z_{eff} results for H ₂	107
8.4	Z_{eff} results for C ₂ H ₂	111
8.5	Conclusion	111

CONTENTS

9	Conclusion	112
	Bibliography	115

List of Figures

1.1	Track of a positron experimentally	12
1.2	Positronium beam apparatus in University College London	14
1.3	Flow chart of experimental positron and positronium collisions	14
1.4	Flow diagram of a positron emission tomography scan	15
1.5	Excitation cross sections for positron collision with H atom	17
1.6	The s -wave phase shifts for positron/electron collisions with Ar	20
1.7	Total cross sections for positron collision with He	22
1.8	Feynman diagrams of the mechanisms of positron annihilation	23
2.1	Coordinate of a molecular system	28
2.2	Potential energy of H ₂ molecule	31
2.3	Coordinates of a molecular system in the laboratory frame.	33
2.4	Electronic coordinates of a molecular system in the BODY frame	34
3.1	Division of configuration space in the fixed nuclei R -matrix theory.	37
3.2	Flow diagram for the inner region target calculation using the UK R - matrix package	51
3.3	Flow diagram for the scattering calculation in the inner region.	52
3.4	Flow diagram for the scattering calculation in the outer region	54
4.1	Flow diagram for the inner region Z_{eff} calculation.	60
4.2	Z_{eff} for positron-H annihilation with A _g symmetry with no potential and square-well potential	63

LIST OF FIGURES

4.3	Z_{eff} for H atom calculated for several methods as a function of the collision energies	63
4.4	Z_{eff} for H atom in terms of J	64
5.1	The equilibrium nuclear condifuration of water	66
5.2	Comparison of the dipole Born corrections between the frame transformation correction by program POLYDCS and direct Born correction . .	71
5.3	Elastic integral cross sections for positron-water collisions for several theoretical models	71
5.4	Differential cross section for positron-water collisions at 0.25 eV and 2 eV	72
5.5	Differential cross section for positron-water collisions at 5 eV and 10 eV	73
5.6	Comparison of experiment with theory for the elastic integral cross sections for positron-water collisions	74
5.7	Calculated elastic (rotationally summed) integral cross sections for positron-water collisions as a function of the collision energy	74
5.8	Elastic (rotationally summed) momentum transfer cross sections for positron and electron water scattering as a function of the collision energy	75
5.9	A comparison of theoretical ICS with uncorrected and corrected experiment for positron-water collisions.	77
6.1	Target state distribution of Σ_g^+ symmetry for H_2 with $\beta = 1.4$ and deletion threshold $\delta_{thrs h-tar} = 2 \times 10^{-4}$	83
6.2	Cross sections of Σ_g^+ symmetry with various R -matrix radius, PCOs models and orthogonalizing deletion thresholds.	84
6.3	Comparison of eigenphase sums for Σ_g^+ symmetry for static model, SP model, close-coupling without MRMPS model and close-coupling with MRMPS model.	85
6.4	Comparison of eigenphase sums for Σ_g^+ symmetry with various PCOs models in the function of energies.	85
6.5	Comparison of eigenphase sums for Π_u, Σ_u^+ and Π_g symmmtries, respectively.	86
6.6	Total elastic cross sections for various models without and with MRMPS method.	87
6.7	Calculated total elastic cross sections with MRMPS method compared with various available theoretical studies as a function of energy.	88

LIST OF FIGURES

6.8	A comparison of experiment with our MRMPS calculation for total elastic cross sections for positron-H ₂ collisions.	88
7.1	Target state distributions of Σ_g^+ symmetry for various α_0 with $\beta = 1.4$ and deletion threshold $\delta_{thrshtar} = 2 \times 10^{-4}$ based on <i>spd</i> -PCOs model.	96
7.2	Target state distributions of Σ_g^+ symmetry for C ₂ H ₂	97
7.3	Comparison of eigenphase sums for different R-matrix calculations with semi-empirical results for Σ_g^+ symmetry.	99
7.4	The scattering length for positron-C ₂ H ₂ collision using MRMPS method in terms of J	100
7.5	Calculated positron-C ₂ H ₂ total elastic scattering cross sections for Σ_g^+ symmetry corresponding to different MRMPS calculations.	101
7.6	Elastic integral cross sections for positron-C ₂ H ₂ collision using various R -matrix models.	102
7.7	Comparisons of calculated integral cross sections with other theoretical and experimental studies for positron-C ₂ H ₂ scattering at energies below 5 eV.	103
7.8	Comparisons of calculated integral cross sections with various models for positron-C ₂ H ₂ scattering at energies below 5 V.	104
8.1	Z_{eff} for H ₂ molecule in terms of energies	108
8.2	Z_{eff} of H ₂ molecule for different number of target states included in the calculation.	109
8.3	Z_{eff} for H ₂ molecule in terms of J	110
8.4	Scattering length for H ₂ molecule in terms of J	110
8.5	Z_{eff} for positron-C ₂ H ₂ annihilation at static level	111

List of Tables

4.1	Experimental values of Z_{eff} for various atoms and molecules at room temperature	57
5.1	Vertical excitation energy for H ₂ O target states.	68
5.2	Coefficients for fit function given by eq. (5.1) used to represent the angular behaviour of the positron (and electron) DCS in the forward region	76
6.1	Polarizabilities of H ₂ for the basis of spd-PCOs with $\beta = 1.4$ for different α_0	82
6.2	Polarizabilities of H ₂ for the basis of PCOs with $\beta = 1.4$ and $\alpha_0 = 0.10$.	82
6.3	Polarizabilities of H ₂ for the basis of PCOs with $\beta = 1.4$ and $\alpha_0 = 0.17$.	82
7.1	Target configurations of different models for C ₂ H ₂	93
7.2	Polarisabilities of C ₂ H ₂ in a_0^3 for the basis of PCOs with $\beta = 1.4$ and $\alpha_0 = 0.17$ for different models. The experimental data are from Nakagawa (1995).	94
7.3	Polarisabilities of C ₂ H ₂ for the basis of PCOs with $\beta = 1.4$ and $\alpha_0 = 0.17$ for different MRMPS calculations based on model 4.	96
7.4	Dimension of the Hamiltonian matrix for scattering calculations for different MRMPS calculations.	98
7.5	scattering length a_{scat} for positron-C ₂ H ₂ collision.	100

Acknowledgements

First, I would like to express my sincerest thanks to my supervisor Prof. Jonathan Tennyson for his guidance, tremendous patience and encouragement during the years of training through my PhD. He can give excellent advice to any question I have met in my study. Great thanks to him for giving me the opportunity to develop my ability to analyze issues and programming skills.

I also thank my second supervisor Dr. Jan Franz for his practical advice, encouraging comments and support. Also thanks to him for his work on writing new codes GAUSDELTA without which Chapter 8 of this thesis would not have been possible. Thank also goes to Prof. K.L. Baluja for his valuable advice to my PhD research.

Thanks also to Alex Faure for his generous provision of his electron-water scattering calculations to my latest publication and work presented here. I would also like to thank Alex Harvey for the very useful discussions on calculation of A_{Ek} coefficients. Thanks also go to Pavlos Galiatsatos for his support of OMP version of SCATCI which greatly saving running time of my jobs; Prof. Nella Laricchia and her group for providing their experimental data for my theoretical studies; David Rage for the IT support; Hemal Varambhia, Gabriela Halmová, Chiarra Piccarreta and Amar Dora for their useful discussions and support.

I would like to express my thanks to my other co-workers and all members in the TAMPA group for their support and friendship.

Finally, Many thanks to my husband and my parents for being supportive and loving. Special thanks to my mum for getting up at 5am every day and meeting me up on the internet because that time is 10pm in UK when would not interfere me with anything.

Chapter 1

Introduction

1.1 Overview

The positron, e^+ , is the antimatter version of the electron. The positron has a positive electronic charge of $+1$, which is $+1.6 \times 10^{-19}$ C, the converse of the electron. Besides the charge and directly related properties (e.g. wave function), the positron has the same properties as electron, such as mass (9.10×10^{-31} kg) and spin ($1/2$). In 1928, Dirac first predicted the existence of the positron from theory when he studied on the expression of relativistic quantum mechanics (Dirac, 1928). Actually, Dirac was not aware of the prediction of a new particle, but thought it to be electrons with positive charge and negative energy. Being enlightened by Chung-yao Chao's experiment in 1930 on absorption and the scattering of gamma rays which gave absolutely greater results (Anderson and Anderson, 1983) than theoretical prediction (Gray, 1929), his classmate Carl D Anderson, in 1933, used the same radioactive source as Chao's experiment but in the cloud chamber to detect cosmic radiation (Anderson, 1933). In this experiment, the tracks of positrons were, for the first time, observed (see Figure 1.1). Meanwhile, the reason for the odd results from Chao's experiment was revealed by Anderson: the additional gamma rays not predicted in the calculations were due to the electron-positron interaction during the absorption process and the gamma rays produced. These gamma rays, each with energy about 0.5 MeV, came from the electron-positron annihilation (Anderson and Anderson, loc. cit., pp136). This observation not only validated relativistic quantum field theory but also introduced a new research

1.1 Overview

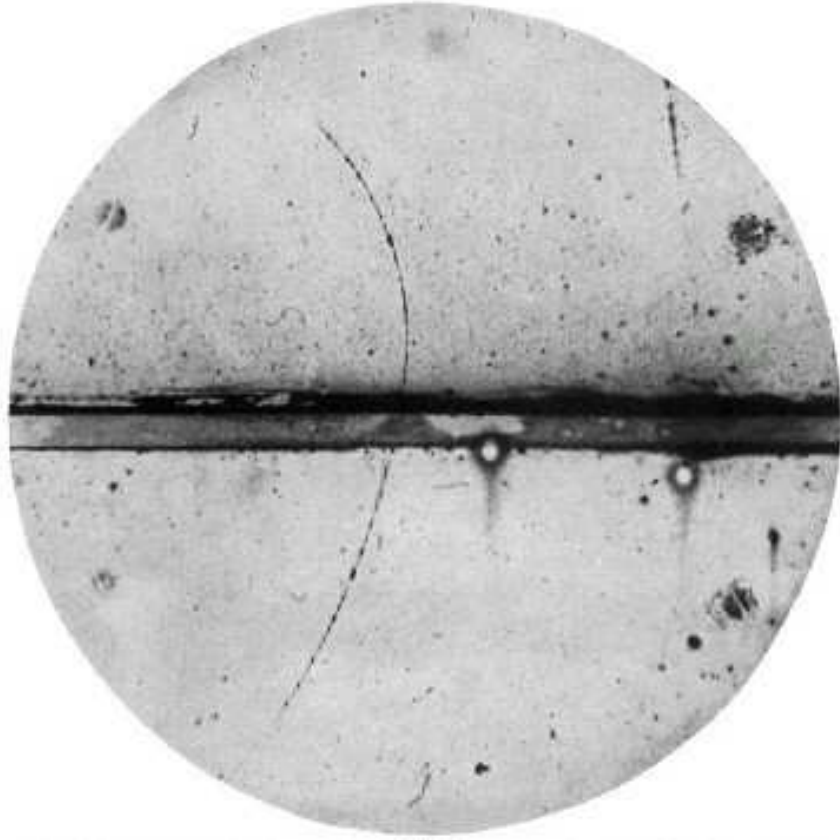


Figure 1.1: Track of positron when passing through the lead plate. The track coming from below the plate is of a positron which is bent less in the magnetic field (URL: <http://en.wikipedia.org/wiki/Positron>).

field: antimatter.

The positron is a stable particle in a vacuum. However, it may annihilate with a molecular electron resulting in two or more gamma ray photons at low energies:



At high energies, electron-positron annihilation may yield other particles, such as D mesons. The annihilation process needs to comply with the charge conservation, energy conservation, linear and angular momentum conservation, no matter how many gamma rays and which kind of particle are emitted. The ratio for producing three versus two gamma rays is only 1/372 as found by Alkhorayef et al. (2009) experimentally. The value of this ratio is even less for four versus two gamma rays. Any matter can annihilate with its antimatter.

There is also a strongly correlated positron-electron configuration called positron-

1.1 Overview

ium, in which the electron and positron combines to a quasi-stable bound state. It was first discovered by Deutsch (1951*a,b*). Positronium has the form of virtual states at collision energies below the positronium formation threshold and provides a real open channel for positron collisions at energies above the threshold. The two particles move around the centre of mass. The electron and the positron finally annihilate with each other yielding two gamma ray photons, the lifetime of positronium is 125 ps for the singlet state (*para*-positronium), and 142 ns for the triplet state (*ortho*-positronium) in vacuum, respectively. The lowest energy of positronium is -6.8 eV, so the positronium formation threshold is given by

$$E_{th} = E_{ion} - 6.8eV \quad (1.2)$$

where E_{ion} is the ionization energy of the atoms or molecules involved.

Positronium is the bound state of positron-electron pair. There is no static potential in the positronium system due to the superposition of the centres of mass and charge. A positronium can bind to electron to form a negative ion Ps^- ($e^-e^+e^-$), which was discovered by Mills (1981), when both the electrons are in singlet spin states. Positronium also can bind to a positron to be a new charged species with singlet spin state and sufficiently small mass (Armour, 1983); a hydrogen atom to produce the positronium-hydride molecule PsH . It is possible to form the positronium molecule Ps_2 with the two positrons and the two electrons being in singlet spin states.

Figure 1.2 shows the world's only positronium beam producing equipment which is located at University College London. Figure 1.3 is the schematic illustration of this apparatus to measure total cross sections for positron and positronium collision with molecules (Beale et al., 2006). Using this apparatus, many reliable experimental measurements of Ps collisions have been made, e.g. Armitage et al. (2006).

The theoretical study of positronium molecule collisions is very complicated and little has been done in this area. In this thesis, the study of positron annihilation with normal matter is considered.

Positrons not only exist in cosmic rays, but also can be found in nuclear reaction involving radioactive nuclei. They can be produced by process of positron emission radioactive decay. A significant application of positrons is via positron emission tomography (PET). These scans can give, for the first time, detailed imaging examination of human brain function, cancer diagnosis and other physiological disease (see

1.1 Overview



Figure 1.2: Positronium beam apparatus in University College London (picture taken directly from laboratory of Positron-, Positronium-, and Electron-Collisions group at UCL).

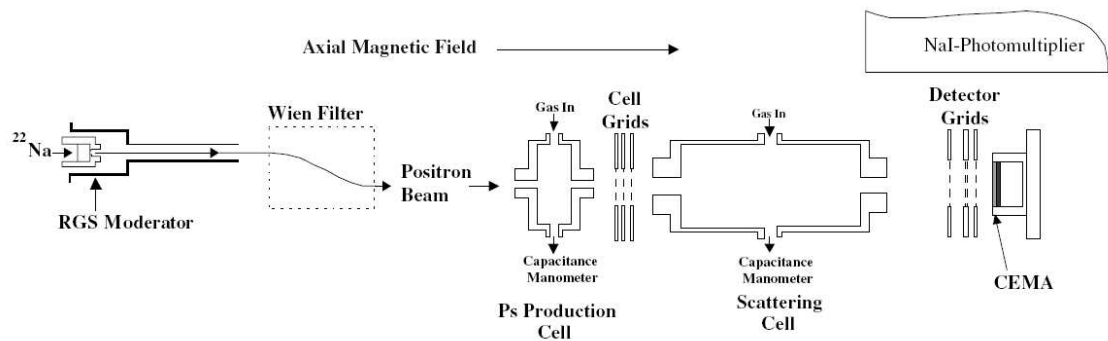


Figure 1.3: Flow chart of the measurement for positron and positronium collisions with atoms and molecules (Beale et al., 2006).

1.2 Positron interactions

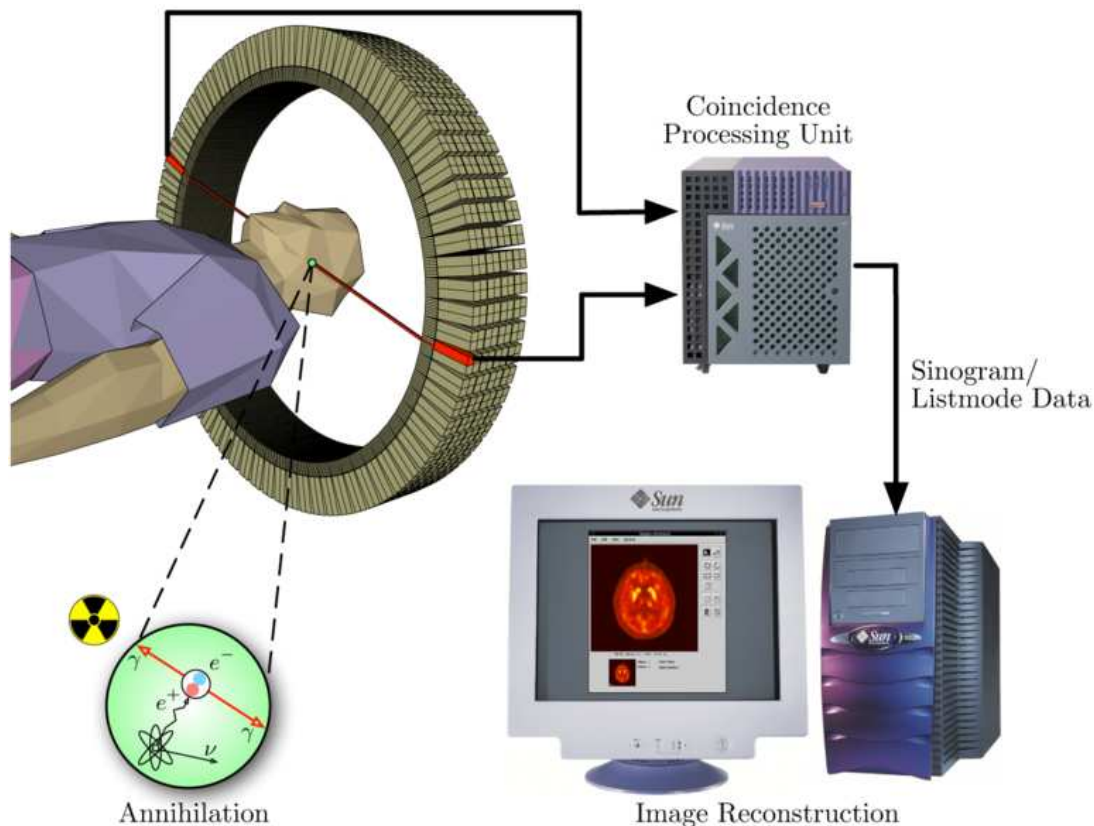


Figure 1.4: Flow schematic diagram of a PET scan (image URL: <http://en.wikipedia.org/wiki/File:PET-schema.png>)

figure 1.4). PET scans use a small dose of a radioactive isotope which decays by emitting a positron. The positron then encounters an electron in the human body producing two gamma ray photons. The gamma rays generated from this procedure are detected by the PET scanner. Then a three-dimensional image of the detected region can be produced. Although taking a PET scan involves ionizing radiation, it is believed to be a safe technique and that the small amount of radiation is not harmful to the human body.

1.2 Positron interactions

The key processes for low-energy positron collisions with molecules can be categorized as follows:

- Elastic scattering:

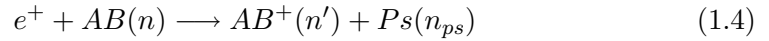


1.2 Positron interactions

At all energies, elastic scattering occurs for positron collision with atoms and molecules. The electronic and vibrational states are not changed after elastic scattering, but the direction of scattered positron may have changed. Integral cross section and differential cross sections, which are feasibly to measure experimentally, are always regarded as important physical quantity for elastic positron scattering. It should be noted that the measured 'elastic' cross sections usually include rotational excitation, maybe and vibrational excitation, as these can not be resolved experimentally and are often neglected in theoretical approximation.

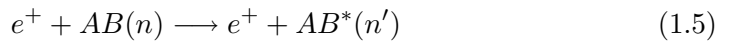
As the incident energy increases, inelastic scattering becomes possible, e.g. positronium formation, target excitation and ionization.

- Positronium formation:



As the positron energy is increased above the positronium formation threshold given by equation 1.2, positronium production begins. In this process, the incident positron captures one electron from the target molecule. If positronium is formed, the system becomes more complicated to treat theoretically as exchange effect between the electrons in the positronium atom and the electron in the residual ion, and positronium-ion polarisation need to be considered accurately.

- Electronic excitation:



where AB^* is the electronically excited target. The energy that the positron loose after scattering corresponds to one of the target excitation energies. The target is in a electronically excited state(n') after scattering. As positrons do not couple target states with different spin symmetries, only singlet target states can be excited for a target with a singlet ground state. In electron collisions, singlet and triplet excited electronic states can be reached. However, for positron collisions, the excitation occurs only when the total spin of the target is unchanged.

Figure 1.5 shows the 1S-2S and 1S-2P excitation cross sections for positron collisions with hydrogen atom. 30 target states and pseudostates, and three positronium states were included in the calculation. It can be seen from figure 1.5(a)

1.2 Positron interactions

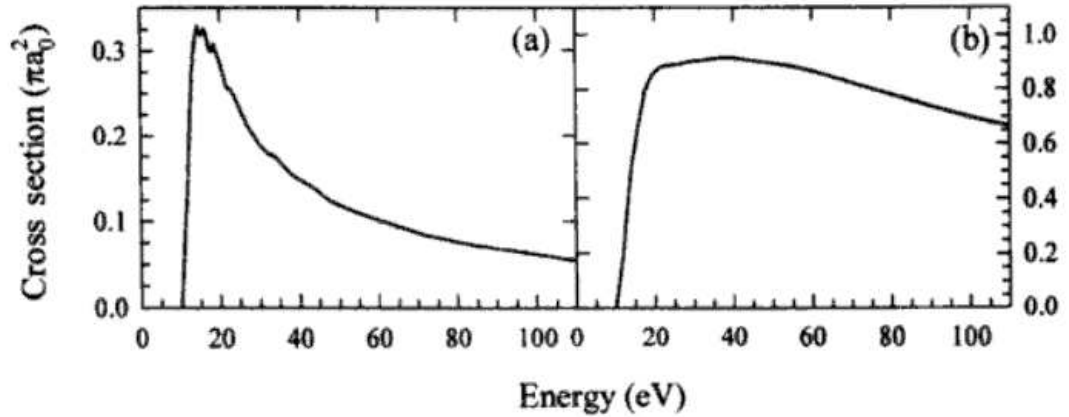
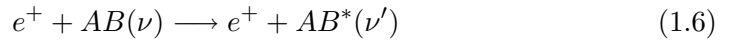


Figure 1.5: Excitation cross sections for positron-H collision using coupled-state approximation: (a)1S-2S; (b)1S-2P (Kernoghan, 1996)

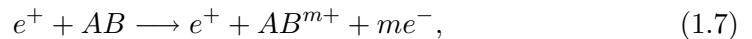
that the 1S-2S cross section rises suddenly near the excitation threshold, 10.2 eV, and reaches the maximum value at about 15 eV. It falls quickly above 15 eV. Figure 1.5(b) shows that after reaching a peak of the value of $0.9 \pi a_0^2$ at 20 eV, the 1S-2P cross section falls slowly at higher energies.

- Vibrational excitation:



The target is excited from an initial state (ν) to a vibrationally excited state (ν').

- Ionization:

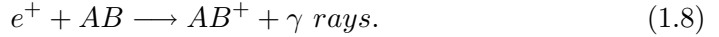


When the total energy of the system is higher than the ionization threshold, single ionization may occur. For electron impact ionization, it is impossible to distinguish the two emerging electrons as we can not tell which was the incident electron and which was the electron originally bound in the target. Positron impact ionization does not have this problem. However, we have the possibility of positronium formation which also ionized the target, which makes the problem more complicated. It should be noted that the positronium formation cross sections is generally smaller than the ionization cross section at scattering energies above the ionization threshold. Because the positronium formation is mainly into

1.3 The positron-molecule scattering problem

its ground state at lower energies, while at higher energies formation is mainly into excited states (Charlton and Humberston, 2001).

- Annihilation:



Positron annihilation with one electron of the target, may occur at all incident energies. The annihilation parameter, Z_{eff} , is an important one and its calculation provides a severe challenge for theory.

1.3 The positron-molecule scattering problem

Positron-molecule interactions are very different from electron-molecule ones due to the opposite sign of the charge of the projectiles. First of all, the electron-electron exchange effects with the target electrons which exist in electron collisions, are absent for positron-molecule interactions as the incident positron is distinguishable from the molecular electrons. For positron scattering, the projectile is attractive to the electrons in the target and repulsive to the nuclei. These effects make the static interaction between the positron and the target repulsive, while it is attractive for electron-molecule scattering. However, the polarisation potential is attractive, as for the electron case, due to the quadratic nature in the charge of the projectile as shown in the definition (Alder and Winther, 1975):

$$V_p(r) = -\frac{4\pi}{9} \frac{Z^2 e^2}{r^4} \alpha, \quad (1.9)$$

where α is the dipole polarisability. Hence, usually, the total cross section for positron-molecule interaction is smaller than the corresponding electron case at low energies. This also makes positrons less likely to be bound than electrons. Positronium formation and electron-positron annihilation only occurs when positrons are involved, they do not occur during electron collisions.

Although one does not need to consider exchange effects, which leads to a simplification of any calculation, positron collisions with molecules are more difficult to treat than corresponding electron collisions due to the attractive nature between the scattered positron and target electrons. This attraction results in great difficulty in accurately modelling polarisation effects in the positron collisions. Various models are used in this thesis to represent polarisation effects.

1.3 The positron-molecule scattering problem

The positron-molecule collision problem can be treated at different levels, which are described as follows:

- Static

The scattering positron is considered to be a separate entity to the target whose wavefunction is frozen in the collision. No polarisation effects are included. For positron calculation with polar molecule, in which the polarisation effects are not the dominant long-range interaction, the static model is believed to give tolerable results. However, for non-polar targets, the static model does not produce satisfactory results, particularly at low energies, due to the lack of the dominant polarisation effects.

- Static plus polarisation (SP)

At this level, two-particle-one-hole configurations are included to represent the polarisation. This means all single excitations are carried out for the target electron. Square-integrable (L^2) configurations are used to represent polarisation and correlation effects.

- Close-coupling (CC)

In this approximation, polarisation effects are treated by coupling the target states and incident positrons in the close-coupling expansion. The total scattering wavefunction is expanded in terms of an, in principle, complete set of eigenstates of the isolated target ψ_i (Lane, 1980):

$$\Phi_E = \sum_i F_i(\mathbf{r}_p)\psi_i \quad (1.10)$$

where F_i are the functions of the scattered positron with position vector \mathbf{r}_p . Functions F_i satisfies the coupled equations

$$[\nabla_p^2 + k_n^2]F_i(\mathbf{r}_p) = \sum_j V_{ij}F_j(\mathbf{r}_p) \quad (1.11)$$

where ∇_p^2 is the Laplacian operator and k_n is channel linear momentum. V_{ij} is the multipole scattering potentials.

Close-coupling method also includes quadratically integrable (L^2) configurations in the scattering wavefunction.

1.3 The positron-molecule scattering problem

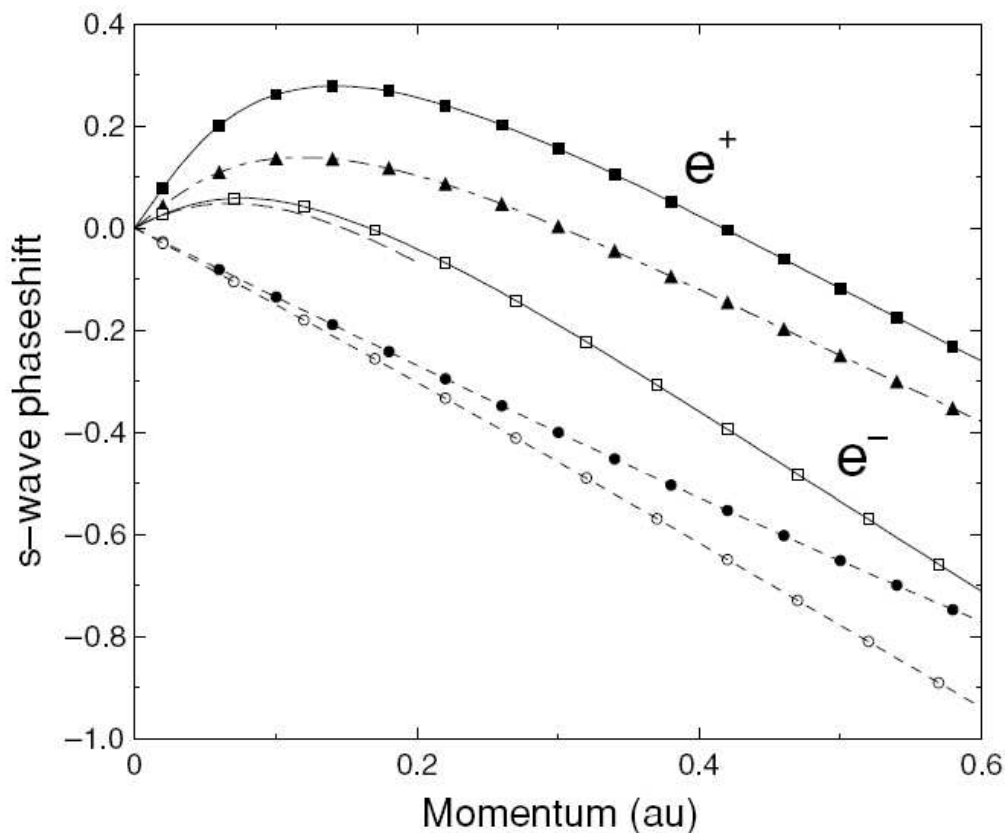


Figure 1.6: The s -wave phase shifts for positron/electron scattering with Ar. open symbols represent electrons and full symbols represent positrons. For positron case: dashed curve with circles, only static potential is considered; dot-dash curve with triangles, only polarisation potential included in the calculation; solid curve with squares, both polarisation potential and Ps-formation potential are included.

The effect of virtual positronium formation plays an important role for some positron collisions with atom or molecule. For example, the virtual positronium formation can contribute about 30% to the total correlation potential for positron collisions with hydrogen atoms and about 20% for collisions with helium atoms (Gribakin and King, 1994). The reason that virtual Ps formation attracts researchers' attention is the fact that there is a significant difference between the polarisation calculation and the precise variational results which are obtained by finding the minimum energy of the trial wavefunction based on the variational principle. The discrepancy is believed to arise from the contribution of virtual Ps formation. This means that an incident positron may form a virtual positronium atom with a target electron.

1.4 Positron annihilation in molecules

It can be seen from Figure 1.6 that phase-shifts which include the contribution of virtual Ps formation are much higher than results including static or polarisation potentials only (Gribakin and King, 1994). The importance of virtual Ps formation also can be demonstrated by comparison of the results of scattering cross section calculations (see Figure 1.7). As shown, the contribution from the virtual Ps formation leads to an excellent agreement with the accurate variational calculations (Humberston, 1978) and various measurements.

1.4 Positron annihilation in molecules

Positron annihilation with atoms and molecules is one of the most important features by which positron collisions differ from the corresponding electron collisions. Obtaining the annihilation parameter Z_{eff} is an important objective for positron researchers. The dimensionless parameter Z_{eff} is usually characterized by the effective number of active electrons of the target available to annihilate with the incoming positron with momentum k . Z_{eff} is also affected by the temperature (T) of incident positron. Usually, Z_{eff} is given as a single number at room temperature T=296K. Positron annihilation with atoms and molecules may yield one, two or three γ -rays, also may result in electron emission (Charlton and Humberston, 2001). Among these processes, the probability of annihilation into two γ rays is the major channel. Non-radiative or one gamma ray annihilation, processes (a) and (b) in figure 1.8, only occur if a nucleus or an atom are involved in order to satisfy energy and momentum conservation.

The original definition of the annihilation parameter for a positron in an atomic or molecular gas is given by

$$Z_{eff} = \frac{\lambda}{\pi r_0^2 c n} \quad (1.12)$$

where λ is the observed rate of the free-positron annihilation processes; $r_0 = e^2/4\pi\epsilon_0 mc^2$ is the classical radius of an electron; c is the velocity of light; n is the electron density of target being in the vicinity of positron. The spin-averaged annihilation cross section at an incident energies below the positronium formation threshold is usually given by

$$\sigma_{ann} = \frac{\lambda}{n\nu} = \pi r_0^2 \frac{c}{\nu} Z_{eff} \quad (1.13)$$

where ν is the velocity of the incident positron.

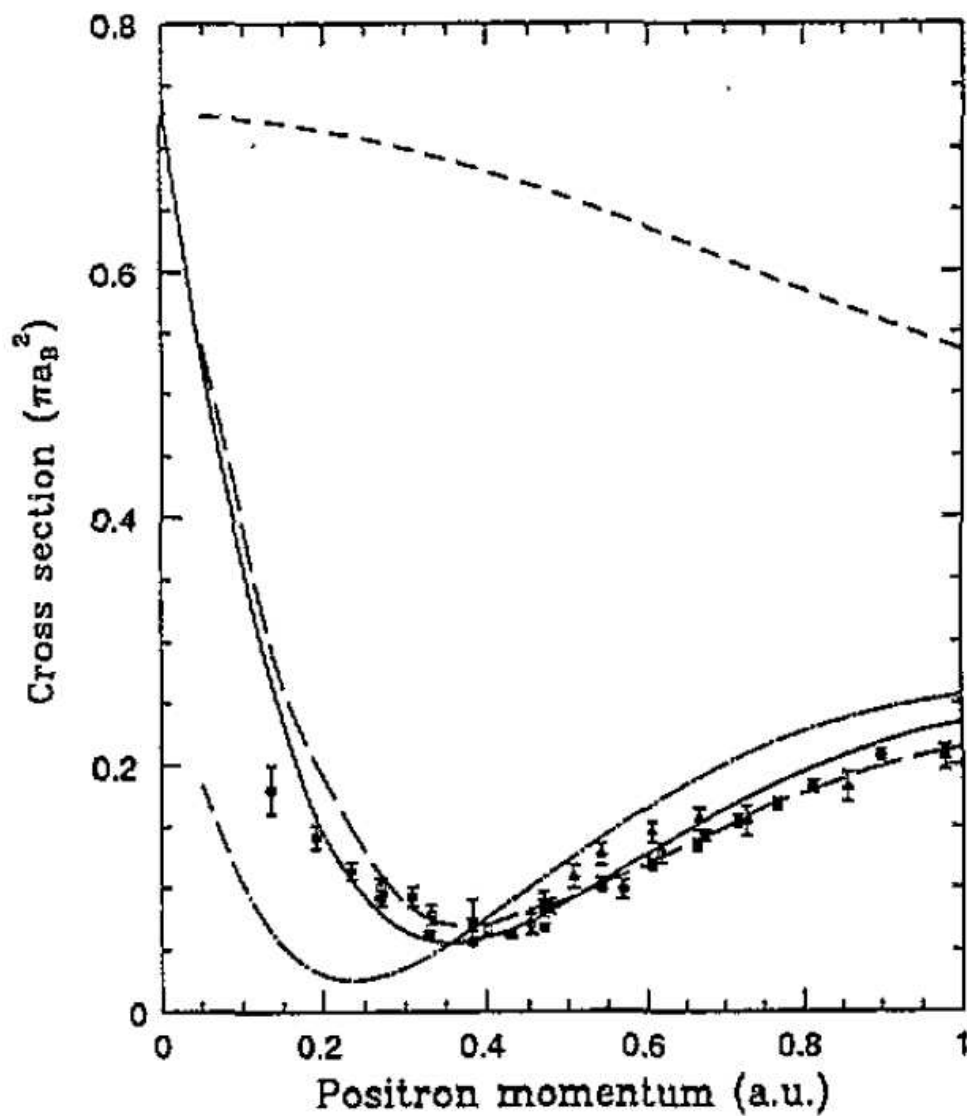


Figure 1.7: Cross sections for positron collision with helium: dash curve, static potential only; dot-dash, the polarisation potential only; solid curve, with Ps-formation potential added to polarisation one; long dash curve is the theoretical variational calculations (Humberston, 1978). Compared to measurements (Stein et al., 1978; Cantre et al., 1972; Sinapius et al., 1980)

1.4 Positron annihilation in molecules

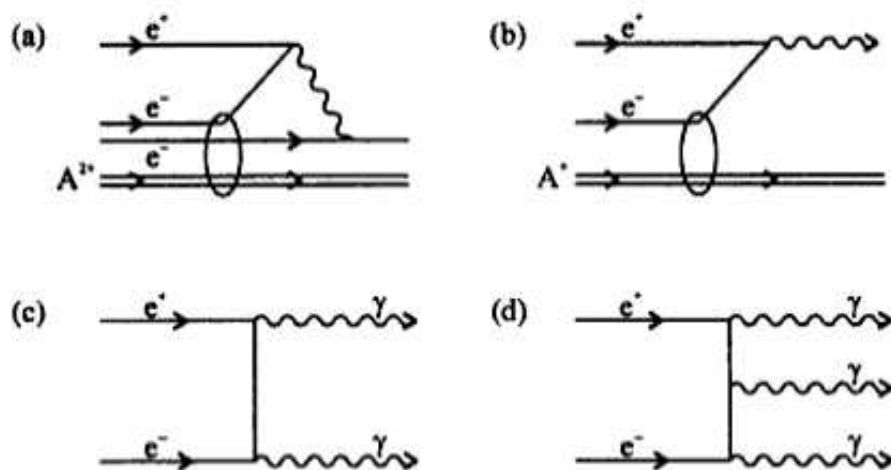


Figure 1.8: Mechanisms which may result from positron annihilation with an electron: (a) nonradiative, (b) one gamma ray, (c) two gamma rays, (d) three gamma rays. From Charlton and Humberston (2001).

Z_{eff} can be obtained from the total scattering wavefunction $\Psi(r_1 \cdots r_Z; r_p)$, normalized to unit positron density,

$$Z_{eff} = \sum_{i=1}^Z \int |\Psi(r_1 \cdots r_Z; r_p)|^2 \delta(r_p - r_i) dr_1 \cdots dr_Z dr_p \quad (1.14)$$

where r_1, \dots, r_Z are the coordinates of the Z electrons of the target and r_p is the coordinate of positron. It can be seen from equation (1.14) that Z_{eff} is sensitive to the accuracy of the total wave function Ψ . This means that to obtain an accurate Z_{eff} value, the wave function Ψ must provide an accurate representation of the positron-electron coordinate particularly as the electron-positron distance $r_{ip} \rightarrow 0$. If the first Born approximation is employed for the annihilating system, with the positron represented by a plane wave and the target undisturbed in the static atomic field, then Z_{eff} would be equal to the number of target electrons Z .

It is well known that the value of Z_{eff} is always larger than the total electron number Z . For example, the experimental result of Z_{eff} for Hydrogen molecule is 14.7 (Laricchia et al., 1987). Particularly, for some organic molecules the measured Z_{eff} values are much larger than Z . For acetylene molecule, $Z_{eff}=3160$ and $Z=14$. This phenomenon is assumed to be due to the formation of pseudo-bound-state for the positron with molecule (Paul and Saint-Pierre, 1963), which means the electrons

1.5 Objectives

in the molecule have more time to react with the positron. At very low energy, the distortion of molecule is much stronger than at higher energy resulting in the fact that Z_{eff} decreases with increasing positron energy below the threshold of positronium formation.

In this thesis, all Z_{eff} results are calculated for positron energies below the positronium formation threshold.

1.5 Objectives

The objectives of this thesis are as follows:

- To build target models for polar molecule H_2O , non-polar molecules H_2 and C_2H_2 by which the vertical excitation energies, dipole moments and polarisabilities can be obtained satisfactorily.
- To construct scattering calculations using the R -matrix method and show how important polarisation effects can be included in calculations.
- Using the Molecular R -matrix with pseudostates method to treat positron-molecule collisions at energies below the positronium formation threshold to show the improvement this method can contribute. To obtain eigenphase sums, elastic (rotationally summed) differential, integral and momentum transfer cross sections.
- To modify the R -matrix code and specify the outer region wave function to calculate annihilation parameter Z_{eff} for molecules with H_2 and C_2H_2 as test cases.

1.6 Layout of the thesis

Chapter 2 introduces some approximation methods which are applied to solving the positron-molecule collision problem. The Born-Oppenheimer approximation, Hartree-Fock self consistent field method, configuration interaction method and fixed-nuclei formulation of the scattering problem are discussed.

Chapter 3 describes derivation of the molecular R -matrix method and its extensions, the molecular R -matrix with pseudostates method and the partitioned R -matrix method. Eigenphase, integral cross section and other quantities and observables ob-

1.6 Layout of the thesis

tained using the R -matrix method are presented. The structure of the codes used to implement the R -matrix theory is also introduced.

Chapter 4 discusses the annihilation parameter in positron collisions based on the R -matrix method. It gives a method for the accurate formulation of outer region wave functions. Annihilation parameters from initial tests for positron-H and positron- H_2^+ at energies below the positronium formation threshold are used as test cases.

Chapters 5-8 describe the calculations and results for positron-molecule collisions using the R -matrix method.

Chapter 5 presents the positron collisions with H_2O molecule at energies below the positronium formation threshold. Static, static plus polarisation and close coupling with natural orbital models are used to describe the increasing level of polarisation effects included in the calculation. Differential cross sections are calculated for collision energies of 0.25 eV, 2 eV, 5 eV and 10 eV. Integral cross sections and momentum transfer cross sections are also calculated and compared to measurements and the corresponding electron case.

Chapter 6 discusses positron scattering by H_2 molecule. Several models are employed to treat this problem. Particularly, the molecular R -matrix with pseudostates (MRMPS) method is introduced into our calculation to allow for the polarisation effects which need to be represented appropriately. Integral cross sections are obtained at energies below the positronium formation threshold and compared to previous theoretical results and observations.

Chapter 7 discusses positron scattering by the C_2H_2 molecule using the MRMPS method. Various MRMPS models are tested to generate good target representations. Polarisabilities for each model are discussed. Integral cross sections are calculated below 5 eV and compared to experimental data.

Annihilation is one of the most significant features of positron collisions. Chapter 8 applies the modified R -matrix method to calculations of the annihilation parameter Z_{eff} for positron collision with H_2 and C_2H_2 .

Chapter 9 give the conclusions for the positron calculation performed. Future work that could arise from the research presented is discussed.

General Theory

2.1 Born-Oppenheimer approximation

For molecular systems with N_e electrons and N_n nuclei (see figure 2.1), the full non-relativistic Hamiltonian in atomic units can be written as

$$H = -\frac{1}{2} \sum_{i=1}^{N_e} \nabla_i^2 - \sum_{A=1}^{N_n} \frac{1}{2M_A} \nabla_A^2 - \sum_{A=1}^{N_n} \sum_{i=1}^{N_e} \frac{Z_A}{|\mathbf{r}_i - \mathbf{R}_A|} + \sum_{j=1}^{N_e} \sum_{i>j}^{N_e} \frac{1}{|\mathbf{r}_i - \mathbf{r}_j|} + \sum_{A=1}^{N_n} \sum_{B>A}^{N_n} \frac{Z_A Z_B}{|\mathbf{R}_A - \mathbf{R}_B|}. \quad (2.1)$$

The first and second terms are the kinetic energies of the electrons and the nuclei, respectively. The third term describes the attractive electron-nucleus Coulomb potential. The subsequent two terms represent the repulsive electron-electron and nuclear-nuclear potentials, respectively. If one can treat the electronic motion and the nuclear motion separately, the total molecular wavefunction can be formed by a product of electronic and nuclear wavefunctions to give what is generally called the Born-Oppenheimer approximation.

The Born-Oppenheimer approximation is based on the property that the electrons in a molecule are much lighter than the nuclei and therefore move much more rapidly. This approximation assumes that electrons surrounding the nuclei can respond instantaneously to even a small motion of the nuclei in order to make adjustment to the given potential of the nuclei. Hence, the nuclei can be assumed to be fixed. That means the kinetic energy term for the nuclei in equation (2.1) is neglected and the inter-nuclear

2.1 Born-Oppenheimer approximation

Coulomb interaction can be treated as a constant. The Hamiltonian now becomes

$$H_{elec} = -\frac{1}{2} \sum_{i=1}^{N_e} \nabla_i^2 - \sum_{A=1}^{N_n} \sum_{i=1}^{N_e} \frac{Z_A}{|\mathbf{r}_i - \mathbf{R}_A|} + \sum_{j=1}^{N_e} \sum_{i>j} \frac{1}{|\mathbf{r}_i - \mathbf{r}_j|}. \quad (2.2)$$

and the time-independent Schrödinger equation may be written as

$$H_{elec} \psi_{elec}(r_i; R_A) = \varepsilon_{elec} \psi_{elec}(r_i; R_A). \quad (2.3)$$

Its solutions depend demonstrably on the electronic position r_i and parametrically on the nuclear position R_A . That means for any configuration of the nuclei (e.g. vibration), the electronic wavefunction ψ_{elec} is modified to a different function of the electronic coordinates. However, the nuclear repulsion term is not included in equation (2.2). Adding the repulsive Coulomb interaction between nuclei to the electronic energy eigenvalue gives

$$E_{elec} = \varepsilon_{elec} + \sum_{A=1}^{N_n} \sum_{B>A} \frac{Z_A Z_B}{|\mathbf{R}_A - \mathbf{R}_B|}. \quad (2.4)$$

The same assumptions can be used to solve the nuclear motion as used for the electronic part of the problem. Since the electronic motion is much faster than the nuclear motion, the electronic motions of equation (2.1) can be accounted for the average distribution of electronic density. Consequently, the Hamiltonian for the nuclear motion in the averaged field of the electrons is

$$\begin{aligned} H_{nucl} &= -\sum_{A=1}^{N_n} \frac{1}{2M_A} \nabla_A^2 + \left\langle \psi_{elec} \left| -\sum_{i=1}^{N_e} \frac{1}{2} \nabla_i^2 - \sum_{A=1}^{N_n} \sum_{i=1}^{N_e} \frac{Z_A}{|\mathbf{r}_i - \mathbf{R}_A|} + \sum_{j=1}^{N_e} \sum_{i>j} \frac{1}{|\mathbf{r}_i - \mathbf{r}_j|} \right| \psi_{elec} \right\rangle \\ &\quad + \sum_{A=1}^{N_n} \sum_{B>A} \frac{Z_A Z_B}{\mathbf{R}_{AB}} \\ &= -\sum_{A=1}^{N_n} \frac{1}{2M_A} \nabla_A^2 + \varepsilon_{elec}(\mathbf{R}_A) + \sum_{A=1}^{N_n} \sum_{B>A} \frac{Z_A Z_B}{\mathbf{R}_{AB}} \\ &= -\sum_{A=1}^{N_n} \frac{1}{2M_A} \nabla_A^2 + E_{elec}(\mathbf{R}_A) \end{aligned} \quad (2.5)$$

The eigenvalue of the total energy $E(R_A)$, depending on the position of the nuclei R_A , gives an interatomic potential for the nuclear motion. Hence in the Born-Oppenheimer approximation the nuclei move in the potential energy produced by the stationary electronic state.

2.2 Hartree-Fock self consistent field method

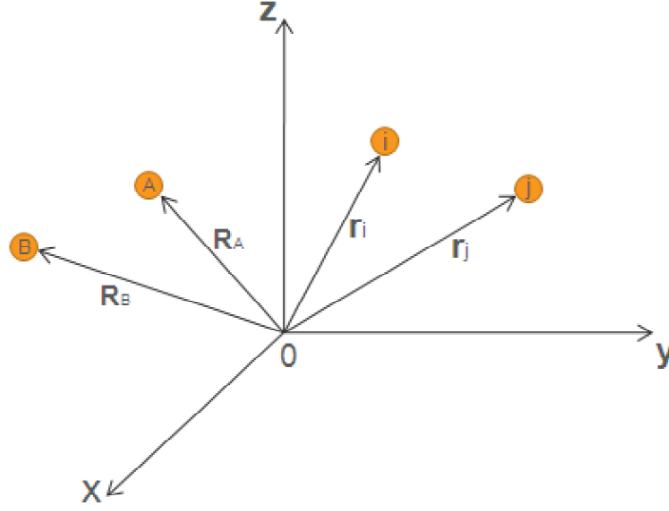


Figure 2.1: Coordinate of a molecular system. e_i and e_j are electrons; A and B are nuclei (Szabó and Ostlund, 1996).

2.2 Hartree-Fock self consistent field method

The simplest wave function for a N-electron atomic or molecular system can be described by a Slater determinant (Szabó and Ostlund, 1996)

$$|\Psi\rangle = |\chi_1\chi_2 \dots \chi_a\chi_b \dots \chi_N\rangle \quad (2.6)$$

where χ_i are spin-orbitals. The Hartree-Fock approach includes the averaged electron-electron repulsions into the wavefunction (2.6), by assuming that each electron is placed in the potential of the nuclei and the averaged field of residual (N-1) electrons. According to the variational principle, the best wave function gives the lowest value of electronic energy E_0 , which is closest to the exact electronic energy of the system. For normalized wave functions:

$$E_0(\Psi_0) = \langle \Psi_0 | \hat{H}_{elec} | \Psi_0 \rangle = \sum_a \langle a | \hat{h} | a \rangle + \frac{1}{2} \sum_{ab} \langle aa | bb \rangle - \langle ab | ba \rangle \quad (2.7)$$

where

$$\langle ij | kl \rangle = \int d\tau_1 d\tau_2 \chi_i^*(x_1) \chi_j(x_1) r_{12}^{-1} \chi_k^*(x_2) \chi_l(x_2), \quad (2.8)$$

2.2 Hartree-Fock self consistent field method

the spin-orbitals are orthogonal,

$$\langle \chi_i | \chi_j \rangle = \delta_{ij}. \quad (2.9)$$

\hat{h} is the one-electron Hamiltonian

$$\hat{h}(1) = -\frac{1}{2}\nabla_1^2 - \sum_{A=1}^{N_n} \frac{Z_A}{r_{1A}} \quad (2.10)$$

The spin-orbitals are modified by minimising E_0 . Thus, the HF eigenvalue equation can be written as

$$\hat{f}(1)\chi_a(1) = \varepsilon_a\chi_a(1) \quad (2.11)$$

where ε_a is the orbital energy of χ_a . Operator \hat{f} is defined as the Fock operator, and contains the core-Hamiltonian operator \hat{h} and the one-electron potential operator G .

$$\hat{f}(1) = \hat{h}(1) + G(1) \quad (2.12)$$

G is called the Hartree-Fock potential and can be written as

$$G(1) = \sum_{b \neq a} [\mathcal{J}_b(1) - \mathcal{K}_b(1)] \quad (2.13)$$

where \mathcal{J}_b is defined as the Coulomb operator and represents the Coulombic repulsion between electrons 1 and 2,

$$\mathcal{J}_b(1)\chi_a(1) = \left[\int d\tau_2 \chi_b(2)^* \frac{1}{r_{12}} \chi_b(2) \right] \chi_a(1) \quad (2.14)$$

and \mathcal{K}_b is the exchange operator which represents the effect of the Pauli principle

$$\mathcal{K}_b(1)\chi_a(1) = \left[\int d\tau_2 \chi_b(2)^* \frac{1}{r_{12}} \chi_a(2) \right] \chi_b(1). \quad (2.15)$$

In short, the Hartree-Fock approximation simplifies a complicated many-electron problem to an effective one-electron problem by treating electron-electron repulsion in an averaged way. Usually the nonlinear HF equations are solved iteratively by the self-consistent field (SCF) approach. In this method, the one-particle HF potentials are constructed using a set of spin-orbitals, then a set of HF equations are solved to get a new set of improved spin-orbitals which are substituted back to construct new Fock operator and so on until the solutions are self-consistent.

2.3 Configuration interaction

2.3 Configuration interaction

In some cases, the Hartree-Fock self consistent field method does not give a good representation of states due to use of only a single Slater determinant to describe the many-electron system. The configuration interaction (CI) method gives a better description of the system; this method includes dynamical correlation effects between electrons.

The interaction between electrons needs to be considered carefully. Motion for one electron may lead to very different repulsion to others. This phenomenon is called electron correlation. The CI method aims to include the electron correlation in the calculation. The correlation energy may be added to the Hartree-Fock energy E_{HF} to give total non-relativistic electronic energy of the system,

$$E_0 = E_{corr} + E_{HF} \quad (2.16)$$

The full wavefunction can be represented by a linear combination of N-electron Slater determinants of configuration state functions (CSFs)

$$\Phi_{CI} = \sum_i C_i \Phi_i \quad (2.17)$$

$$= c_0 \Phi_0 + \sum_{ar} c_a^r \Phi_a^r + \frac{1}{2!} \sum_{abrs} c_{ab}^{rs} \Phi_{ab}^{rs} + \dots \quad (2.18)$$

where Φ_0 is the HF wavefunction; Φ_a^r are the singly excited determinants with one electron excited from an occupied spin-orbital χ_a in Φ_0 to a virtual spin orbital χ_r ; Φ_{ab}^{rs} are the doubly excited configurations with two electrons excited from spin-orbitals χ_a and χ_b in Φ_0 to orbitals χ_r and χ_s . If N-tuply excited configurations are included, the CI expansion for an N-electron wave function is complete and called 'Full' CI. Thus, the exact solution for a given orbital set would be obtained by diagonalising the N-electron Hamiltonian operator. However, in practice only a finite set of N-electron wavefunctions can be included considering the size of Hamiltonian matrix obtained. Figure 2.3 shows the potential energy curves of the small molecule H_2 as a function of the bond length for different methods.

The CI expansion based on HF spin-orbitals converges slowly. In order to obtain a spinless one-electron basis for which the CI expansion convergents faster than HF orbitals, natural orbitals (NOs) (Löwdin, 1955) can be used. To define the NOs, the

2.3 Configuration interaction

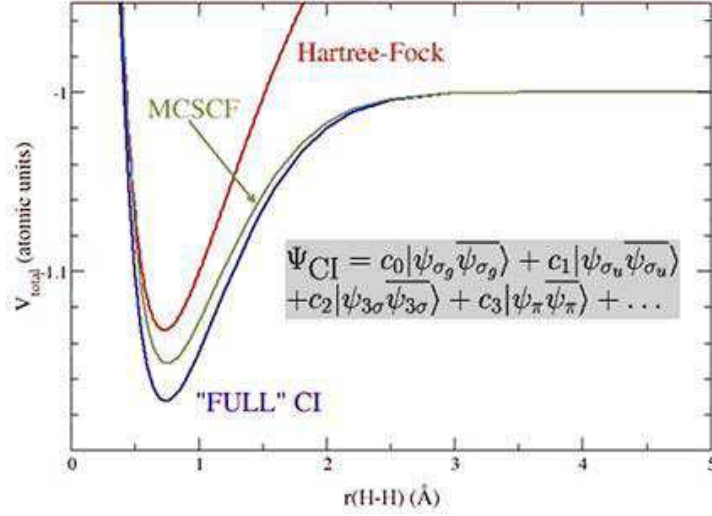


Figure 2.2: Potential energy for the H_2 molecule (Harvey, "Molecular Electronic Structure", University of Bristol, 2001)

one electron density matrix can be written as:

$$\gamma(\mathbf{x}_1, \mathbf{x}'_1) = N \int d\mathbf{x}_2 \cdots d\mathbf{x}_N \Phi(\mathbf{x}_1, \mathbf{x}_2, \cdots, \mathbf{x}_N) \Phi^*(\mathbf{x}'_1, \mathbf{x}_2, \cdots, \mathbf{x}_N) \quad (2.19)$$

It also can be expanded in the orthonormal basis of HF spin orbitals as

$$\gamma(\mathbf{x}_1, \mathbf{x}'_1) = \sum_{ij} \psi_i(\mathbf{x}_1) \gamma_{ij} \psi_j^*(\mathbf{x}'_1) \quad (2.20)$$

If Φ is the HF ground state wave function Φ_0 , it becomes

$$\gamma^{HF}(\mathbf{x}_1, \mathbf{x}'_1) = \sum_a \psi_a(\mathbf{x}_1) \psi_a^*(\mathbf{x}'_1) \quad (2.21)$$

In most of the cases, Φ is not Φ_0 . Then the one electron reduced density matrix is not diagonal in the basis of HF spin orbitals. The matrix γ is Hermitian, so it can be transformed to a diagonal matrix and rewritten as

$$\gamma(\mathbf{x}_1, \mathbf{x}'_1) = \sum_i \lambda_i \eta_i(\mathbf{x}_1) \eta_i^*(\mathbf{x}'_1) \quad (2.22)$$

where the orthonormal spin orbitals η_i are called natural orbitals; λ_i are the eigenvalues of the density matrix, representing the average number of electrons in each NO and called the occupation numbers. In the R -matrix method, NOs with relatively small occupation number can be neglected due to the less importance to the CI expansion.

2.4 Fixed-nuclei formulation of the scattering problem

Only the NOs with the largest occupation number, which give the lowest eigenenergy, are included in the CI expansion.

In practice, a full CI can only be performed for small molecules with few electrons. A complete active space configuration interaction (CAS CI) can be employed. In the CASCI method, all excitations are performed within a defined set of spin orbitals. It is usually necessary to freeze some electrons in a core. Hence, the lowest energy orbitals are kept doubly occupied in all configurations. Due to the fact that positrons do not couple to the target states with different spin, only singlet excited states are needed in the close-coupling expansion for stable, singlet target molecules.

2.4 Fixed-nuclei formulation of the scattering problem

Assume the nuclei are fixed. Then, only the electronic Hamiltonian for the particle-molecule collision system needs to be solved. Two reference frames (Lane, 1980) can be used to simplify the equations describing the collision process: the BODY frame (figures 2.4) and the laboratory (LAB) frame (figures 2.3). Both frames are systems centred at the centre of mass. The BODY frame is a coordinate system whose z axis is taken along the maximum symmetry axis of the molecule. While in the LAB frame the z axis lies along the initial momentum vector of the incident particle. \mathbf{r} and \mathbf{R} are the position vectors of the electrons and nuclei of the molecule, respectively and \mathbf{r}_p represents the coordinate of the scattering particle in the BODY frame and the primed coordinates refer to the LAB frame.

The Hamiltonian for the particle-molecule collision system can be written as

$$H_{N+1} = -\frac{1}{2}\nabla_\gamma^2 + H_N^{elec} + V_{p-m} \quad (2.23)$$

where ∇_p^2 is the Laplacian of the scattering particle in the BODY frame. H_N^{elec} is the N -electron target Hamiltonian given by equation (2.2) and V_{p-m} is the positive charged particle-target molecule interaction potential energy,

$$V_{p-m}(\mathbf{r}'_p, \mathbf{r}', \mathbf{R}) = \sum_{A=1}^{N_n} \frac{Z_A}{|\mathbf{r}'_p - \mathbf{R}_A|} - \sum_{j=1}^{N_e} \frac{1}{|\mathbf{r}'_p - \mathbf{r}'_j|}. \quad (2.24)$$

For a target molecule the electronic states are represented by functions $\psi_A^{elec}(\mathbf{r}, \mathbf{R})$, where A represents the electronic quantum numbers. These wave functions must satisfy the electronic Schrödinger equation (2.3). In the fixed-nuclei formulation, the

2.4 Fixed-nuclei formulation of the scattering problem

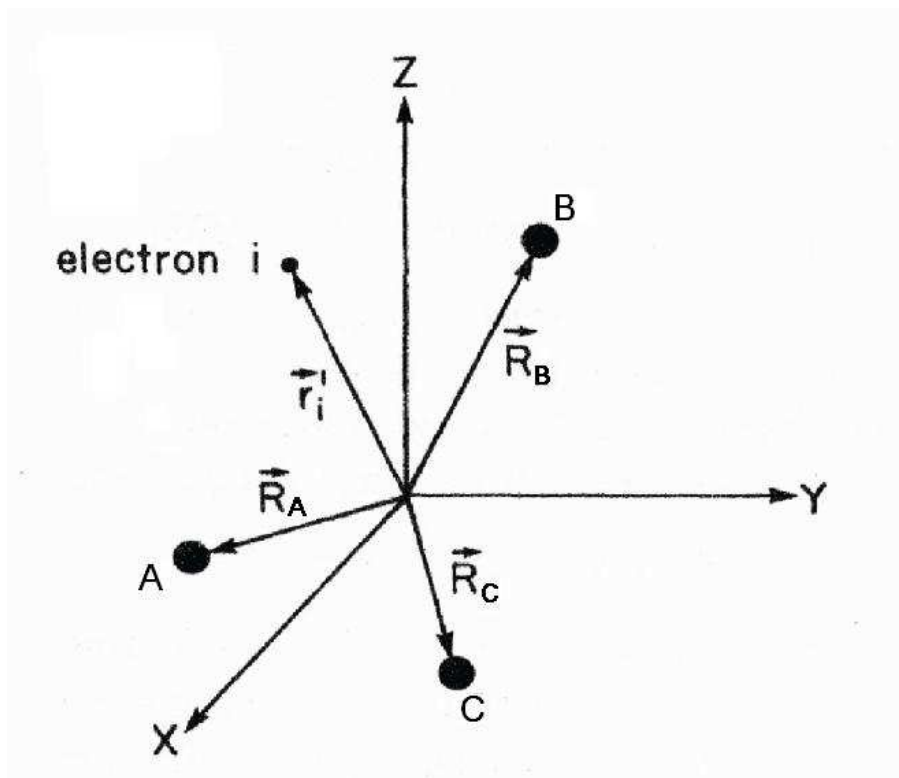


Figure 2.3: Coordinates of a molecular system in the LAB frame: e_i is the electron; A, B and C are nuclei (Lane, 1980).

Schrödinger equation for the $N_e + 1$ system is written as

$$(H_{N+1} - \varepsilon)\Psi_\varepsilon^{FN}(\mathbf{r}_p, \mathbf{r}; \mathbf{R}) = 0 \quad (2.25)$$

The fixed-nuclei approximation is valid in the region where the collision time is very short. However, this approximation is not applicable when the motion of positrons is dominated by strong long-range interactions.

2.4 Fixed-nuclei formulation of the scattering problem

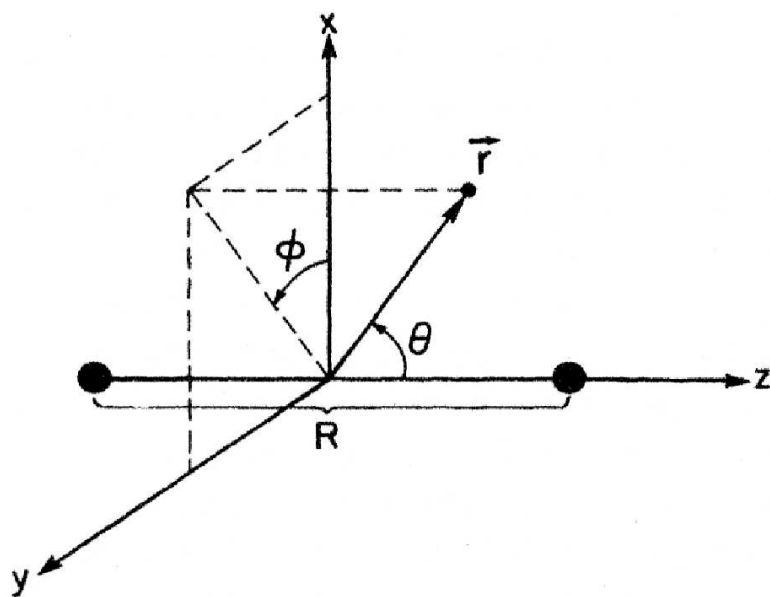


Figure 2.4: Electronic coordinates of a molecular system in the BODY frame (Lane, 1980).

R-matrix theory

3.1 Overview

R-matrix theory was originally established for applications to nuclear physics by Wigner (1946*a,b*) and Wigner and Eisenbud (1947). Lane and Thomas (1958) gave an early review of the *R*-matrix method for nuclear collisions. The first application of *R*-matrix techniques to atomic scattering by electrons was performed by Burke and co-workers (Burke et al., 1971; Burke and Robb, 1975; Burke, 1976). Schneider (1975), Schneider and Hay (1976) and Burke et al. (1977) applied molecular *R*-matrix theory to electron-molecule scattering; followed by developments by several groups, including Burke et al. (1983), Tennyson et al. (1984) and Nestmann et al. (1994), for the study of electron collisions with diatomic molecules and polyatomic molecules.

The first time that the molecular *R*-matrix theory was adapted to positron-molecule collisions was the study of low energy positron-H₂ and positron-N₂ scattering by Tennyson (1986). For positron studies, the kinetic and Coulomb one electron integrals are treated separately. The exchange effects that exist in electron codes could be set to zero for positron collisions. After the initial studies, the theory was applied to various diatomic targets (Tennyson and Morgan, 1987; Tennyson and Danby, 1988; Danby and Tennyson, 1988, 1990b, 1991) using the diatomic *R*-matrix code for which Slater Type Orbitals (STOs) are used to represent the target wave function. However, insufficient positron-electron correlation was included in these calculations causing the reported results to poorly reproduce the low-energy collision behaviour. Twenty years later,

3.2 The inner region

the molecular R -matrix method was reactivated and developed for low energy positron collisions, that is energies below the positronium formation threshold by Franz et al. (2008) using the polyatomic R -matrix code. Both the target wave function and the continuum functions in the inner region are represented by Gaussian Type Orbitals (GTOs) in the polyatomic R -matrix code.

The scattering process can be described by the time-independent Schrödinger equation

$$H_{N+1}\Psi = E\Psi \quad (3.1)$$

in which H_{N+1} is the Hamiltonian operator, given by

$$H_{N+1} = -\frac{1}{2} \sum_{i=1}^{N+1} \nabla_i^2 - \sum_{i=1}^N \sum_{j=1}^{N_m} \frac{Z_j}{|\mathbf{r}_i - \mathbf{R}_j|} + \sum_{i>j=1}^N \frac{1}{|\mathbf{r}_i - \mathbf{r}_j|} + \sum_{i>j=1}^{N_m} \frac{Z_i Z_j}{|\mathbf{R}_i - \mathbf{R}_j|} \quad (3.2)$$

$$- \sum_{i=1}^N \frac{1}{|\mathbf{r}_p - \mathbf{r}_i|} + \sum_{j=1}^{N_m} \frac{Z_j}{|\mathbf{r}_p - \mathbf{R}_j|} \quad (3.3)$$

where N_m is the number of nuclei; Z_j are the nuclear charges. Atomic units, for which $\hbar = 1$, $m_e = 1$ and $e = 1$, are used for all the equations in this chapter.

Within the R -matrix method, to get solutions of the scattering processes, the configuration space is divided into two regions (see figure 3.1): an inner region and an outer region. The inner region ($r \leq a$), is defined by a sphere of radius a centred on the molecular centre of mass which is normally defined by a equals 10 to 15 a_0 . This sphere must include the entire target wave functions. In this region, although exchange effects are absent in positron collisions, the positron-electron correlation is very important because of the attractive nature of the positron-electron interaction and must be treated in detail.

The outer region potential are given by the target multipole moments as $r \geq a$. These are similar to the corresponding electron case but with the opposite charge of the projectile. The two regions are connected by matching the inner and outer region wave functions at $r = a$.

3.2 The inner region

The wave function of the target molecule is described by a set of basis functions representing the molecular orbitals formed as linear combinations of atomic orbitals centred on the nuclei. Early positron-molecule collisions using R -matrix method employed

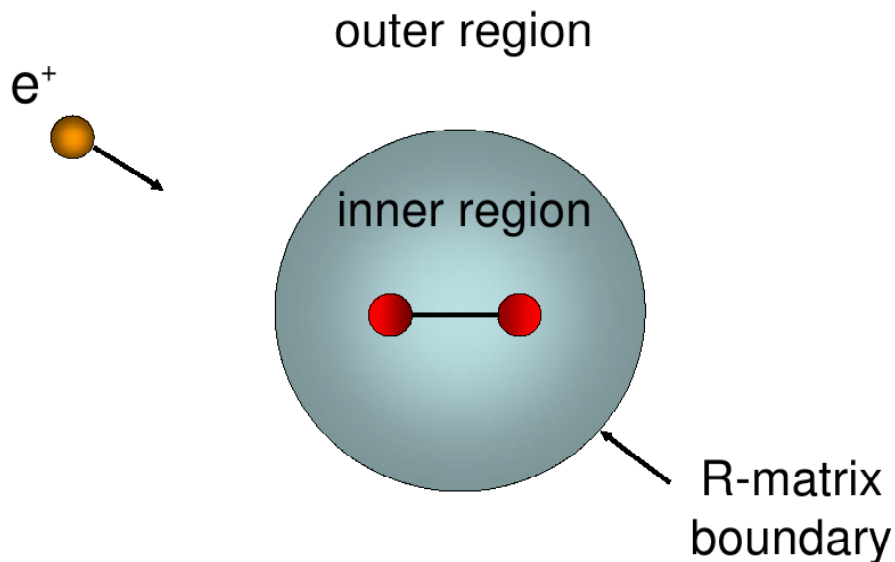


Figure 3.1: Division of configuration space in the fixed nuclei *R*-matrix theory.

Slater-type orbitals (see Slater (1960)) to represent diatomic targets (Tennyson, 1986; Tennyson and Danby, 1988; Danby and Tennyson, 1990a,b, 1991). However, Gaussian-type orbitals (GTOs) are usually used to represent polyatomic molecules and only these are considered here.

3.2.1 The inner region wave function

In the inner region, the total wave function describing the collision process with energy E (corresponding to the solution of equation (3.1)) takes the following form:

$$\Psi(E) = \sum_k \psi_k A_{Ek} \quad (3.4)$$

3.2 The inner region

where ψ_k are energy-independent basis states constructed by the close-coupling expansion:

$$\psi_k = \sum_{ij} a_{ijk} \tilde{\Phi}_i(x_1, \dots, x_N, \sigma_p) u_{ij}(x_p) + \sum_i b_{ik} \chi_i(x_1, \dots, x_p), \quad (3.5)$$

where x_p is the coordinate representing the positron; $\tilde{\Phi}_i$ are channel functions formed by coupling the target states ψ_i^N with the spin-angle functions of the scattered particle $Y_l^m(\vartheta_p, \varphi_p) s(\sigma_p)$; $u_{ij}(x_p)$ are continuum orbitals and χ_i are quadratically integrable (L^2) correlation functions constructed from occupied and virtual molecular orbitals of the target. For electron collision, there should be an antisymmetrization operator in the first term of equation (3.5). While for the positron case, the projectile is distinguishable from the target electrons, so the need for antisymmetrization is removed. The ' L^2 ' functions are important both for relaxing the orthogonality between the target and continuum orbitals, and for representing short-range polarisation effects not included in the truncated close-coupling expansion. For example, if the positron and the electrons share a common orbital set then the positron is allowed to occupy orbitals already fully occupied by electrons.

The continuum basis functions, which have the form $f_{il_i}(r) = \frac{1}{r} u_{il}(r) Y_{l_i}^{m_i}(\theta, \phi)$, in diatomic R -matrix method are obtained numerically from the solution of the second-order differential equation:

$$\left[\frac{d^2}{dr^2} - \frac{l(l+1)}{r^2} + 2V_0(r) + k_i^2 \right] u_{il}(r) = 0 \quad (3.6)$$

with the R -matrix boundary conditions

$$u_{il}(0) = 0, \quad \frac{a}{u_{il}(a)} \frac{du_{il}}{dr} \Big|_{r=a} = b, \quad (3.7)$$

where $V_0(r)$ is the single centre potential and k_j^2 are the eigenenergies. b in the boundary condition is an arbitrary constant, usually chosen to be zero. The continuum basis functions also form an orthonormal set

$$\int_0^a u_i u_j dr = \delta_{ij} \quad (3.8)$$

To get continuum orbitals, Schmidt orthogonalisation is used to orthogonalise the continuum molecular orbitals to the target orbitals. Subsequently, the continuum molecular orbitals are orthogonalised with themselves using symmetric or Löwdin orthogonalisation (Löwdin, 1950).

3.2 The inner region

The diatomic code actually required a 'Buttle' correction (Buttle, 1967) to be added to the diagonal elements of the R -matrix to solve the convergence problem of the R -matrix expansion (shown below). But in the polyatomic R -matrix code, a 'Buttle' correction is not required because the above artificial boundary condition is also not used in the polyatomic code. Gaussian functions are used to represent continuum basis functions in the polyatomic code. The continuum functions are obtained by fitting GTO basis sets to Bessel functions in the inner region (Nestmann and Peyerimhoff, 1990). A program GTOBAS was produced to represent both Bessel and Coulomb functions by fitting GTO continuum basis sets (Faure et al., 2002). All integrals involving continuum basis functions are evaluated in the configuration space. Spatial integration outside the R -matrix sphere is subtracted from an infinite range integrals (Tennyson and Morgan, 1999).

3.2.2 Derivation of the R -matrix

The variational coefficients a_{ijk} and b_{ik} of equation (3.5) are obtained by diagonalizing the Hamiltonian H_{N+1} . However, the Hamiltonian H_{N+1} is not Hermitian in the inner region due to a surface term at $r = a$ which results from the kinetic energy operators. So a Bloch operator (Bloch, 1957) is introduced to ensure that operator $H_{N+1} + L_{N+1}$ is Hermitian within the volume $r \leq a$

$$L_{N+1} = \sum_{i=1}^{N+1} \frac{1}{2} \delta(r_i - a) \left(\frac{d}{dr_i} - \frac{b}{r_i} \right) \quad (3.9)$$

where b is an arbitrary constant, normally choose to be zero. Hence, a_{ijk} and b_{ik} are obtained by diagonalizing $H_{N+1} + L_{N+1}$

$$\langle \psi_k | H_{N+1} + L_{N+1} | \psi_{k'} \rangle \quad (3.10)$$

The Schrödinger equation 3.1 can be rewritten by adding the Bloch operator

$$(H_{N+1} + L_{N+1} - E) |\Psi\rangle = L_{N+1} |\Psi\rangle \quad (3.11)$$

which gives the formal solution

$$|\Psi\rangle = (H_{N+1} + L_{N+1} - E)^{-1} L_{N+1} |\Psi\rangle \quad (3.12)$$

Referring to equation (3.10), the inner region wave functions ψ_k are the eigenfunctions of the Hamiltonian matrix $(H_{N+1} + L_{N+1})$ with eigenvalues E_k .

$$\langle \psi_k | H_{N+1} + L_{N+1} | \psi_{k'} \rangle = \delta_{kk'} E_k \quad (3.13)$$

3.2 The inner region

So the inverse operator in equation (3.12) can be expanded in terms of ψ_k , giving

$$|\Psi\rangle = \sum_k |\psi_k\rangle \frac{1}{(E_k - E)} \langle \psi_k | L_{N+1} | \Psi \rangle \quad (3.14)$$

which, by comparison with equation (3.4), gives

$$A_{Ek} = \frac{\langle \psi_k | L_{N+1} | \Psi \rangle}{E_k - E}. \quad (3.15)$$

Expanding the Bloch operator in terms of the channel functions described above,

$$|\psi_i^N Y_{l_i}^{m_i}\rangle \frac{1}{2} \sum_{i=1}^{N+1} \sum_{j=1} |\psi_j^N Y_{l_j}^{m_j}\rangle \delta(r_i - a) \left(\frac{d}{dr_i} - \frac{b}{r_i} \right) \langle \psi_j^N Y_{l_j}^{m_j} |. \quad (3.16)$$

A_{Ek} therefore becomes

$$A_{Ek} = \frac{1}{2} \sum_{i=1}^{N+1} \sum_{j=1} \frac{\langle \psi_k | \psi_j^N Y_{l_j}^{m_j} \rangle \delta(r_i - a) \left(\frac{d}{dr_i} - \frac{b}{r_i} \right) \langle \psi_j^N Y_{l_j}^{m_j} | \Psi \rangle}{E_k - E}. \quad (3.17)$$

We can define the reduced radial wave function evaluated on the boundary of the inner region as

$$F_j(a) = \langle \psi_j^N Y_{l_j}^{m_j} | \Psi \rangle \quad (3.18)$$

as well as the surface amplitudes

$$\omega_{jk}(a) = \langle \psi_j^N Y_{l_j}^{m_j} | \psi_k \rangle. \quad (3.19)$$

The Dirac brackets in equations (3.18) and (3.19) denote that the integrations are carried out over the entire electronic space and coordinates except the radial coordinate of the scattered positron or electron. The coefficient A_{Ek} takes the form

$$A_{Ek} = \frac{1}{2a} \sum_{j=1} \frac{\omega_{jk}^\dagger(a) \left(aF_j'(a) - bF_j(a) \right)}{E_k - E} \quad (3.20)$$

In order to define the total scattering wave function it is essential to construct F_j and their derivatives F_j' at the R -matrix boundary. Substituting (3.20) into (3.4), and then projecting it onto the channel basis function $|\psi_i^N Y_{l_i}^{m_i}\rangle$

$$\langle \psi_i^N Y_{l_i}^{m_i} | \Psi \rangle = \frac{1}{2a} \sum_{k,j} \frac{\omega_{jk}^\dagger(a) \left(aF_j'(a) - bF_j(a) \right)}{E_k - E} \langle \psi_i^N Y_{l_i}^{m_i} | \psi_k \rangle. \quad (3.21)$$

One obtains

$$F_i = \frac{1}{2a} \sum_{ijk} \frac{\omega_{jk}^\dagger(a) \omega_{ik}(a)}{E_k - E} \left(aF_j'(a) - bF_j(a) \right) \quad (3.22)$$

3.3 The outer region

whose elements can be defined as the R -matrix

$$R_{ij} = \frac{1}{2a} \sum_k \frac{\omega_{jk}^\dagger(a) \omega_{ik}(a)}{E_k - E} \quad (3.23)$$

The surface amplitudes $\omega_{jk}(a)$ and the R -matrix poles E_k are obtained from the eigenvalues and eigenvectors of the Hamiltonian matrix given by equation (3.13). Hence, the reduced radial function and therefore coefficient A_{EK} can be rewritten in terms of the R -matrix

$$F_i(a) = \sum_j R_{ij} \left(aF_j'(a) - bF_j(a) \right) \quad (3.24)$$

and

$$A_{Ek} = \frac{1}{2a(E_k - E)} \sum_{ij} w_{ik}^T R_{ij}^{-1} F_j \quad (3.25)$$

The total scattering wave function Ψ in the inner region can be established by determining the R -matrix, reduced radial function F and coefficient A_{EK} for any incident energy E .

3.3 The outer region

To solve the positron/electron-molecule scattering problem, in the outer region ($r \geq a$), where the correlation effects vanish, the close-coupling expansion of the wave function is used in terms of the channel basis function $\psi_i^N Y_{l_i}^{m_i}$ (Gillan et al., 1995)

$$\Psi = \sum_i \psi_i^N Y_{l_i}^{m_i} \mathbf{r}_p^{-1} F_i(\mathbf{r}_p) \quad (3.26)$$

In this equation, the scattered positron is represented by the reduced radial wave functions $F(r)$ as the multi-centre quadratically integrable functions χ_i^N vanish in the outer region. The wave functions ψ_i are target states. For positron-molecule scattering, each target state can lead to several channels, which means even a one target state scattering calculation yields a multi-channel problem.

Substituting the outer region wave function into the Schrödinger equation (3.1) and projecting onto the channel functions $\psi_i Y_{l_i}^{m_i}$ leads to n-coupled second-order differential equations for the reduced radial functions (Burke et al., 1971)

$$\left(\frac{d^2}{dr^2} - \frac{l_i(l_i + 1)}{r^2} + k_i^2 \right) F_i(r) = 2 \sum_j V_{ij}(r) F_j(r) \quad (3.27)$$

3.3 The outer region

where V_{ij} is the long-range potential matrix given by the multipole expansion

$$V_{ij}(r) = \sum_{\lambda=0}^{\lambda_{max}} \frac{\alpha_{ij}^{\lambda}}{r^{\lambda+1}}, r \geq a \quad (3.28)$$

in which the potential coefficients are determined by Burke et al. (1977)

$$\alpha_{ij}^{\lambda} = \left(\frac{2l_i + 1}{2l_j + 1} \right)^{\frac{1}{2}} C(l_i \lambda l_j; m_i m_{\lambda} m_j) C(l_i \lambda l_j; 000) Q_{ij}^{(\lambda)} \quad (3.29)$$

where $C(l_1 l_2 l_3; m_1 m_2 m_3)$ is a Clebsch-Gordan coefficient. $Q_{ij}^{(\lambda)}$ is the target moment in which $\lambda = 1$ for representing dipoles, $\lambda = 2$ for quadrupoles, and $\lambda = 0$ for the Coulomb potential given by an ionic target.

In equation (3.27), the channel energies are

$$k_i^2 = 2(E - E_i), \quad (3.30)$$

where E_i is the eigenenergy of the target state χ_i and E is the scattering energy. If $k_i^2 \geq 0$, it gives an open channel since it can be reached asymptotically. Whereas if $k_i^2 < 0$, it gives a closed channel.

Solving equation (3.27) yields n_a (the number of open channels) linearly independent, asymptotic solutions at each incident energy,

$$F_{ij} \underset{r \rightarrow \infty}{\sim} \frac{1}{\sqrt{k_j}} (\sin \theta_j \delta_{ij} + \cos \theta_j K_{ij}) \quad (3.31)$$

and n_c , which is the number of close channels, solutions satisfying the asymptotic boundary conditions

$$F_{ij} \underset{r \rightarrow \infty}{\sim} e^{-|k_j|r}. \quad (3.32)$$

In equation (3.31),

$$\begin{aligned} \theta_j &= k_j r - \frac{1}{2} l_j \pi - \eta_j \ln(2k_j r) + \sigma_{l_j} \\ \eta_j &= -(Z - N)/k_j \\ \sigma_{l_j} &= \arg \Gamma(l_j + 1 + i\eta_j) \end{aligned}$$

The coefficient K_{ij} is a $n_a \times n_a$ dimensional real symmetric matrix. To obtain this K -matrix, $n + n_a$ linearly independent solutions $v_{ij}(r)$ of equation (3.31) are introduced:

$$\begin{aligned} v_{ij} \underset{r \rightarrow \infty}{\sim} \sin \theta_i \delta_{ij} + O(r^{-1}) & \quad i = 1 \cdots n, \quad j = 1 \cdots n_a \\ v_{ij} \underset{r \rightarrow \infty}{\sim} \cos \theta_i \delta_{ij-n_a} + O(r^{-1}) & \quad i = 1 \cdots n, \quad j = n_a + 1 \cdots 2n_a \\ v_{ij} \underset{r \rightarrow \infty}{\sim} \exp(-|k_i|r) \delta_{ij-n_a} + O(r^{-1}) & \quad i = 1 \cdots n, \quad j = 2n_a + 1 \cdots n + n_a \end{aligned} \quad (3.33)$$

3.3 The outer region

where n is the total number of the coupled equations ($n = n_a + n_c$). The solution can be written:

$$F_{ij}(r) = \sum_{l=1}^{n+n_a} x_{lj} v_{il}(r) \quad i = 1 \cdots n, \quad j = 1 \cdots n_a \quad (3.34)$$

where the coefficients x_{lj} are given by

$$x_{lj} = k_j^{\frac{1}{2}} \delta_{lj} \quad l = 1 \cdots n_a \quad (3.35)$$

$$\sum_{l=1}^{n+n_a} x_{lj} \left(v_{il}(a) - \sum_{m=1}^n R_{im} \left(a \frac{dv_{ml}}{dr} - b v_{ml} \right) \Big|_{r=a} \right) = 0 \quad i = 1 \cdots n \quad (3.36)$$

which together give the K -matrix

$$K_{ij} = k_i^{\frac{1}{2}} x_{i+n_a, j} \quad i, j = 1 \cdots n_a \quad (3.37)$$

The eigenphase sums can be obtained from the diagonalised K -matrix K_{ii}^D , as

$$\delta(E) = \sum_i \arctan(K_{ii}^D) \quad (3.38)$$

where the sum runs over the n_a channels. The K -matrix can be transformed into the scattering matrix \mathbf{S} , which is given by

$$\mathbf{S} = \frac{(\mathbf{1} + i\mathbf{K})}{(\mathbf{1} - i\mathbf{K})} \quad (3.39)$$

The T -matrix is given by

$$\mathbf{T} = \mathbf{S} - \mathbf{1} = \frac{2i\mathbf{K}}{(\mathbf{1} - i\mathbf{K})} \quad (3.40)$$

and can be used to calculate the integral cross section (ICS) and differential cross sections (DCS). The integral cross section for excitation from the state i to state i' can be written as (Burke, 1982)

$$\sigma(i \rightarrow i') = \frac{\pi}{k_i^2} \sum_S \frac{(2S+1)}{2(2S_i+1)} \sum_{\Gamma l l'} |T_{ii'l'}^{\Gamma S}|^2 \quad (3.41)$$

where S_i is the spin angular momentum of the i^{th} target state, S is the total spin angular momentum, Γ runs over symmetry, l and l' are orbital angular momentum quantum numbers related to i and i' states. The number of partial waves required to converge the cross section can be very large if the interaction potential includes long-range dipole terms. However, the partial-wave expansion does not converge in the fixed-nuclei approximation. The dipole Born approximation is used to solve this problem since it can be used to calculate the contribution of all partial waves to the

3.3 The outer region

cross section for a charged particle in a dipole potential, both summed and individually. Contribution of high partial waves to the total cross section can be obtained by adding the TCS calculated using the Born approximation and then subtracting the contribution of low partial waves. Consequently, the DCS can be obtained by

$$\frac{d\sigma^{total}}{d\Omega} = \frac{d\sigma^{Born}}{d\Omega} + \sum_{L=0}^{L_{max}} (A_L - A_L^{Born}) P_L(\cos \theta) \quad (3.42)$$

where the first term is the plane wave Born cross section and the second term is the cross section derived from a finite expansion of the first Born cross section containing the same number of partial waves as $\sigma(i \rightarrow i')$. The coefficients A_L are obtained as partial wave expansions up to L_{max} (Itikawa, 2000).

The above procedure is a simple way to implement the Born correction, which has a consequence that $\Delta\sigma$ might be negative if one or more of the differences in the sum are obtained, allowing unphysically negative DCS, to be obtained. Another approach was introduced (Fliflet and McKoy, 1980; Itikawa, 2000; Rescigno et al., 1992) to calculate the DCS via the scattering amplitude. This method always give positive results for all angles. Both methods are discussed in Chapter 5 where a comparison of DCS calculations for positron-H₂O collision is performed.

3.3.1 Outer region wave function

One merit of the R -matrix method is that one does not need to calculate the outer region wave function. However, there are occasions, for example when calculating the annihilation parameter Z_{eff} (see Chapter 4), that the exact form of the wave function is required.

As mentioned above, eq (3.33) can be written in matrix form, and then the regular solution

$$\underline{F} = \begin{pmatrix} \underline{F}^{oo} & \underline{F}^{oc} \\ \underline{F}^{co} & \underline{F}^{cc} \end{pmatrix} \underset{r \rightarrow \infty}{\sim} \begin{pmatrix} \sin \underline{\theta} & \underline{0} \\ \underline{0} & \underline{0} \end{pmatrix}$$

and the irregular solution

$$\underline{G} = \begin{pmatrix} \underline{G}^{oo} & \underline{G}^{oc} \\ \underline{G}^{co} & \underline{G}^{cc} \end{pmatrix} \underset{r \rightarrow \infty}{\sim} \begin{pmatrix} \cos \underline{\theta} & \underline{0} \\ \underline{0} & e^{-\underline{\psi}} \end{pmatrix}$$

can be obtained, where \underline{F} and \underline{G} are both n by n dimensional matrices; \underline{F}^{oo} and \underline{G}^{oo} are n_a by n_a matrices; \underline{F}^{cc} and \underline{G}^{cc} are n_c by n_c matrices ($n_c = n - n_a$); \underline{F}^{oc} and \underline{G}^{oc} are

3.4 Molecular R -matrix with pseudostates method

n_a by n_c matrices; F^{co} and G^{co} are n_c by n_a matrices. The underline denotes matrix here. Compared to equation (3.34), in the matrix notation we then have

$$\begin{pmatrix} \mathcal{F}^o \\ \mathcal{F}^c \end{pmatrix} = \begin{pmatrix} \underline{F}^{oo} & \underline{F}^{oc} \\ \underline{F}^{co} & \underline{F}^{cc} \end{pmatrix} \begin{pmatrix} \underline{x}^o \\ \underline{x}^c \end{pmatrix} + \begin{pmatrix} \underline{G}^{oo} & \underline{G}^{oc} \\ \underline{G}^{co} & \underline{G}^{cc} \end{pmatrix} \begin{pmatrix} \underline{y}^o \\ \underline{y}^c \end{pmatrix}$$

Compared to equation (3.31) and (3.32), we can write

$$\begin{aligned} \underline{x}^o &\equiv \underline{k}^{-\frac{1}{2}} \\ \underline{y}^o &\equiv \underline{k}^{-\frac{1}{2}} \underline{K} \\ \underline{y}^c &\equiv \underline{0} \end{aligned}$$

The outer region trial function can be written as

$$\mathcal{F} \underset{r \rightarrow \infty}{\sim} \underline{k}^{-\frac{1}{2}} [\underline{F} + \underline{G}\underline{K}] \quad (3.43)$$

To find the normalisation of the wave function, one can transform the asymptotic form involving S-matrix

$$F_{ij} \underset{r \rightarrow \infty}{\sim} \frac{1}{\sqrt{k_i}} (e^{-i\theta_i} - e^{i\theta_i} S_{ij}), \quad (3.44)$$

which is easy to find the standard normalisation, to K-matrix asymptotic form:

$$F_{ij} \underset{r \rightarrow \infty}{\sim} \frac{2i}{\sqrt{k_i}(1 - K_{ij})} (\sin \theta_i + K_{ij} \cos \theta_i) \quad (3.45)$$

Taking a system with no long-range potential, like H atom, as an example, the asymptotic scattering solutions can be written as

$$F_{ij} \underset{r \rightarrow \infty}{\sim} \frac{2i}{\sqrt{k_i}(1 - K_{ij})} (j_i \delta_{ij} + \eta_i K_{ij}) \quad (3.46)$$

where j_i is a Spherical Bessel function representing the regular solution and spherical Neumann function η_i represents the irregular solution

$$j_l(x) = (-x)^l \left(\frac{1}{x} \frac{d}{dx} \right)^l \frac{\sin x}{x} \quad (3.47)$$

$$\eta_l(x) = -(-x)^l \left(\frac{1}{x} \frac{d}{dx} \right)^l \frac{\cos x}{x} \quad (3.48)$$

3.4 Molecular R -matrix with pseudostates method

The standard close-coupling expansion used in the standard R -matrix method is incomplete since not all excited target states are included in the expansion and no continuum

3.4 Molecular R -matrix with pseudostates method

states of the target are considered. This lack of completeness leads to a significant loss of the polarisation effects for low energy collisions. Especially for non-polar species, these polarisation effects contribute an important part to the collision processes. The *ab initio* convergent close-coupling method (Bray et al., 2002) provides this completeness by employing Sturmian functions as basis functions for electron-atom collisions, but this method has so far only been applied to atoms with one active electron. Therefore, the R -matrix with pseudostates (RMPS) method was introduced to augment the close-coupling expansion by Bartschat et al. (1996), and can be used to treat targets with many active electrons. The process of completing the close-coupling expansion by use of pseudostates has proved to be a successful method in charged particle-atom collisions. Gorfinkiel and Tennyson (2004, 2005) extended the application of pseudostates to electron collisions from ionic and neutral molecular targets within the UK R -matrix polyatomic code (Morgan et al., 1998). This procedure is known as the molecular RMPS (MRMPS) method. Jones and Tennyson (2010) show the improvement in polarisabilities calculated for various molecules by including pseudostates in the calculation.

The MRMPS method is based on the use of a number of pseudostate wave functions in the close-coupling expansion. The pseudostates are not true eigenstates of the target, but represent a discretized version of the electronic continuum and also the high-lying target states not included in the close-coupling expansion. The pseudostates are normally obtained by diagonalizing the target electronic Hamiltonian described in an appropriate basis of configurations. A set of appropriate configurations are added in the CI expansion so that the pseudostates, used to represent target continuum states, are able to reproduce the electron density of the ionized system. To do this an extra set of orbitals, called pseudo-continuum orbitals (PCOs) are introduced to describe the ionized electron (Gorfinkiel and Tennyson, 2004). Hence, two sets of configurations are included in the CI expansion with the MRMPS method: the usual configurations in which all the electrons occupy molecular orbitals; and a new set of configurations where one-electron occupies a PCO.

An even-tempered basis set (Schmidt and Ruedenberg, 1979) of GTOs centred at the centre of mass of the system is used to represent the PCOs, in which the exponents of the GTOs are

$$\alpha_i = \alpha_0 \beta^{(i-1)} \quad i = 1, \dots, N \quad (3.49)$$

3.4 Molecular R -matrix with pseudostates method

which give different basis sets by choosing different values of α_0 and β . The use of different even-tempered exponents allows for convergence tests and helps avoid the effects of pseudoresonances. Furthermore the basis gives the completeness of the close-coupling expansion as N approaches infinity (Schmidt and Ruedenberg, 1979). Although smaller values of β produce a more complete set of pseudostates, it is more difficult to avoid linear dependence. In order to include all the important target states involved in the close-coupling expansion within the R -matrix box, parameters α_0 and β need to be chosen carefully. This means that in our method the amplitudes of the basis functions employed to expand the MOs must vanish at the R -matrix boundary.

To include PCOs in the calculation, an extra orthogonalization procedure has to be performed: Schmidt orthogonalization of the PCOs to the MOs and then symmetric orthogonalized among themselves. During this step a deletion threshold, in the range 10^{-4} to 10^{-5} , is used to delete near linear dependent pseudo orbitals. This gives a target orbital set in terms of the target MOs and the PCOs. Target CSFs are now represented by configurations of the form

$$(core)^m(CAS)^{N-m}$$

$$(core)^m(CAS)^{N-m-1}(PCO)^1$$

In the MRMPS scattering calculation, to avoid further difficulty with the orthogonalizing procedure, it is necessary to ensure that the exponents

$$\alpha_i^{PCOs} \geq \alpha_j^{continuum} \quad \forall i, j, \quad (3.50)$$

in which the largest exponents are deleted. This process does not misrepresent the scattered particle due to the fact that the PCO basis provides short-range GTOs.

It is very important to choose appropriate L^2 configurations when adding PCOs for positron-molecule scattering. We should note that in contrast to the electron case, the positron can occupy orbitals in the core. In principle, one would like to use the configuration

$$(core)^m(CAS)^{N-m}(COs)^{\mathbf{1p}}$$

$$(core)^m(CAS)^{N-m-1}(PCOs)^1(COs)^{\mathbf{1p}}$$

and the L^2 function can be represented by

$$(core)^m(CAS)^{N-m}(core, CAS, PCOs)^{\mathbf{1p}}$$

$$(core)^m(CAS)^{N-m-1}(PCOs)^1(core, CAS, PCOs)^{\mathbf{1p}}$$

Here the bold $\mathbf{1p}$ denotes positron occupies the current orbitals. Note that for these

3.5 The Partitioned R -matrix method

CSFs it is important to constrain the electronic wave function to have the correct spin state. Several models were performed for the positron-C₂H₂ system as shown in chapter 7.

In the standard R -matrix calculations, the most challenging computationally step is to diagonalise the (N+1) Hamiltonian matrix. Including the PCOs into the close-coupling expansion can make this matrix very large. This leads to the need for the partitioned R -matrix method.

3.5 The Partitioned R -matrix method

Calculations with the R -matrix method usually need all the eigenvalues and eigenvectors of the inner region Hamiltonian to construct the R -matrices. However, when a large number of the configurations are included in the calculations, the Hamiltonian matrix becomes too large to be completely diagonalised as it would require too much computational time and memory. Berrington and Ballance (2002) first introduced a partitioned R -matrix theory, aimed to make the calculations more efficient, by using only the lowest P solutions of the Hamiltonian matrix.

Usually, the R -matrix on the boundary can be written as equation (3.23) plus the Buttle correction \mathbf{R}^B (Buttle, 1967) at the collision energy considered

$$R_{il,i'l'}(a, E) = \sum_{k=1}^M \frac{\omega_{ilk}(a)\omega_{i'l'k}(a)}{E_k - E} + \delta_{ii'}\delta_{ll'}R_{il}^B \quad (3.51)$$

For calculations with a polyatomic target, we do not need to consider the Buttle correction. Equation (3.51) can be rewritten so that only some, P , of the solutions of the M-dimensional Hamiltonian matrix are explicitly required. Now one quantity needs to define: E_0 , which is an effective energy for the poles excluded when only the lowest P solutions of Hamiltonian are taken. This is determined by

$$E_0 = \frac{(\sum_{I=1}^M H_{I,I} - \sum_{k=1}^P E_k)}{M - P} \quad (3.52)$$

where the first sum gives the trace of the Hamiltonian matrix. Berrington and Ballance (2002) then gave an expression for the partitioned R -matrix

$$R_{il,i'l'}(a, E) = \sum_{k=1}^P \omega_{ilk}(a)\omega_{i'l'k}(a) \left(\frac{1}{E_k - E} - \frac{1}{E_0 - E} \right) + \delta_{ii'}\delta_{ll'} \left(\frac{s_{il}}{E_0 - E} + R_{il}^B + R_{il}^C \right) \quad (3.53)$$

3.6 Computational implementation

where R_{il}^C is the error correction term given by Berrington and Ballance (2002),

$$R_{il}^C = \sum_{j=J_i}^{n_{il}} (u_{ilj(a)})^2 \left(\frac{1}{E_{ilj} - E} - \frac{1}{E_0 - E} \right) \quad (3.54)$$

where E_{ilj} is the energy of the continuum basis function u_{ilj} . This point is chosen such that $E_{ilj} > E_P$, where E_P is the highest R -matrix pole explicitly enclosed in the summation in equation (3.53).

Several problems were carefully considered by Tennyson (2004) when the theory described above was applied. One is for the definition of the effective energy E_0 . The number of L^2 configurations increases when CI representation is used for the target molecule. Then the many high-lying L^2 functions contribute to the value of E_0 but not to the boundary amplitude due to the fact that all diagonal elements of the Hamiltonian matrix are included without considering whether the configuration involved makes any contribution to the boundary amplitude. Hence, only the configurations which contribute directly to the boundary amplitude are used to define E_0 . Normally, the Hamiltonian matrix is diagonally dominant to the calculation, so the lowest P diagonal element can be associated with the lowest P R -matrix poles. Then the value of E_0 can be obtained by averaging those non- L^2 diagonal elements of the Hamiltonian matrix, $H_{ilj,ilj}$, which do not belong to the lowest P diagonal elements.

Use of the partitioned R -matrix method also requires significant changes to the outer region R -matrix code. This method has proved a very efficient way to treat large ions and molecules, such as C_2^- (Halmová and Tennyson, 2008; Halmová et al., 2008) and Li_2 (Tarana and Tennyson, 2008).

3.6 Computational implementation

The programs used here for positron molecule scattering calculations are a modification of the UK polyatomic R -matrix code (Morgan et al., 1998). As the theoretical procedure described above, R -matrix computational calculations can be divided into two stages: inner region and outer region calculations. The inner region polyatomic suite is built on the 'Molecule-Sweden' quantum chemistry codes of Almlöf and Taylor (1984). Figures 3.2 and 3.3 show respectively the inner region N and $(N + 1)$ -electron calculations. The figure 3.4 gives a flow diagram for the outer region calculations. The inner codes comprises the following modules which are run in the sequence shown in

3.6 Computational implementation

the figures:

SWMOL3 produces one and two-electron integrals from the given GTO basis sets.

SWSCF carries out the Hartree-Fock self consistent field (HF-SCF) calculation to generate target molecular orbitals from linear combinations of atomic orbitals. SWSCF used the integrals obtained from SWFJK.

GAUSTAIL evaluates the contribution of each integral from the R -matrix boundary to infinity.

GAUSDELTA evaluates integrals of the Dirac-delta function (see Chapter 4). The procedure are similar to GAUSTAIL gives but uses delta integrals over atomic orbitals instead of a Coulomb integrals. This code was written by Dr. Jan Franz.

SWORD subtracts the 'tail' integrals derived from SWMOL3 and then reorders the integrals.

SWFJK builds up combinations of Coulomb and exchange integrals for the Fock matrix needed by the SCF calculation.

SWEDMOS constructs orthogonal molecular orbitals and boundary amplitudes for the continuum functions and GTO target functions. Schmidt orthogonalisation is used to orthogonalise each continuum orbital with the target orbitals. Then symmetric orthogonalisation is used to orthogonalise the continuum orbitals among themselves. A threshold for deleting the continuum orbitals with very small eigenvalues of the overlap matrix is required. SWEDMOS needs to run twice for MRMPs calculations to first orthogonalise the PCOs and then orthogonalise the COs.

SWTRMO implements the four-index transformation from atomic to molecular orbitals using the ordered integrals are generated by SWMOL3.

GAUSPROP produces the property integrals required by DENPROP.

CONGEN generates configuration state functions (CSFs) with appropriate spin and symmetry coupling for performing the configuration interaction (CI) calculations. The code also produces prototype CSFs for the target molecule and $(N+1)$ -system. An exotic particle flag (IPOSIT) needs to be set for positron runs. It should also be noted that when choosing the molecular orbitals, the positron and electrons share a common orbital set. The program also generates a phase factor for each target orbital, to ensure the phases between the target and $(N + 1)$ -electron system are consistent (Tennyson, 1996).

SCATCI carries out the CI calculation for target and $(N+1)$ -electron system. It

3.6 Computational implementation

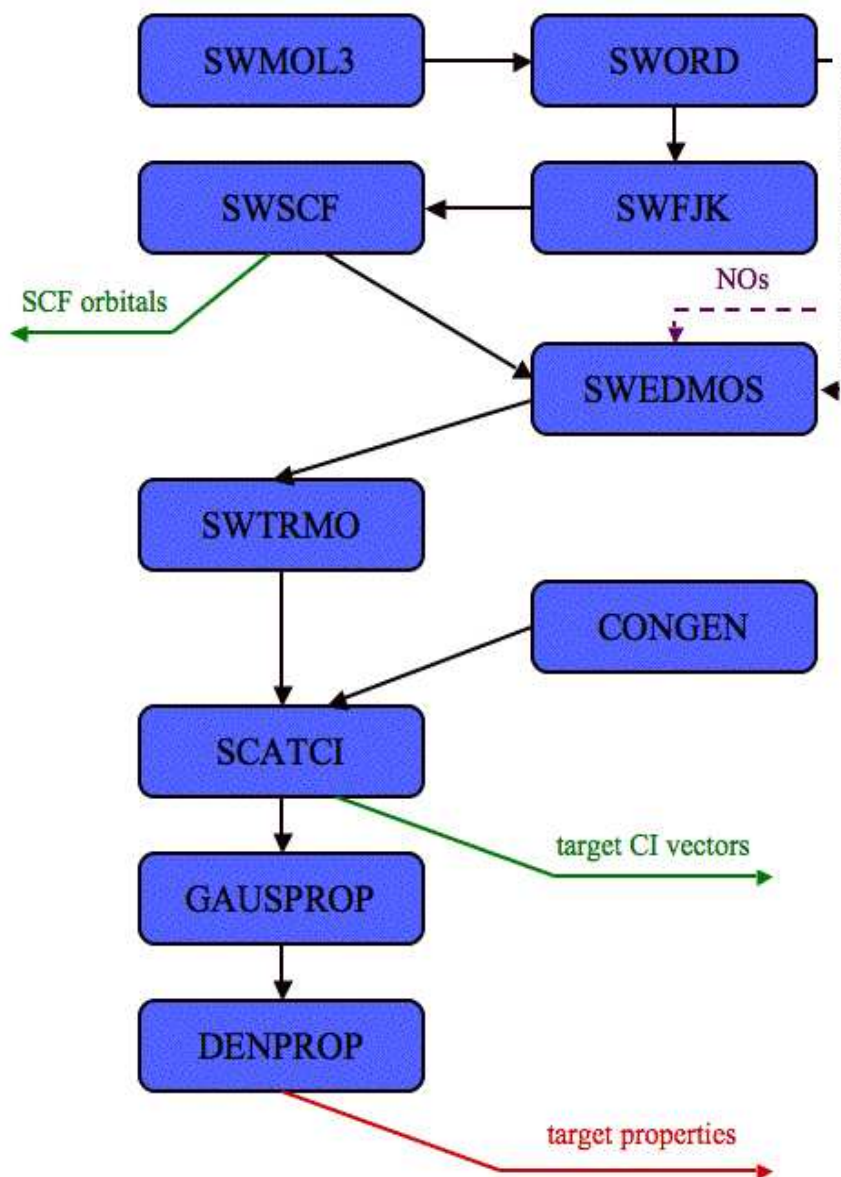


Figure 3.2: Flow diagram for the inner region target calculation using the UK *R*-matrix package. Red arrows indicate an input required by the scattering calculation. If NOs model is used, the modules SWFJK and SWSCF are skipped.

3.6 Computational implementation

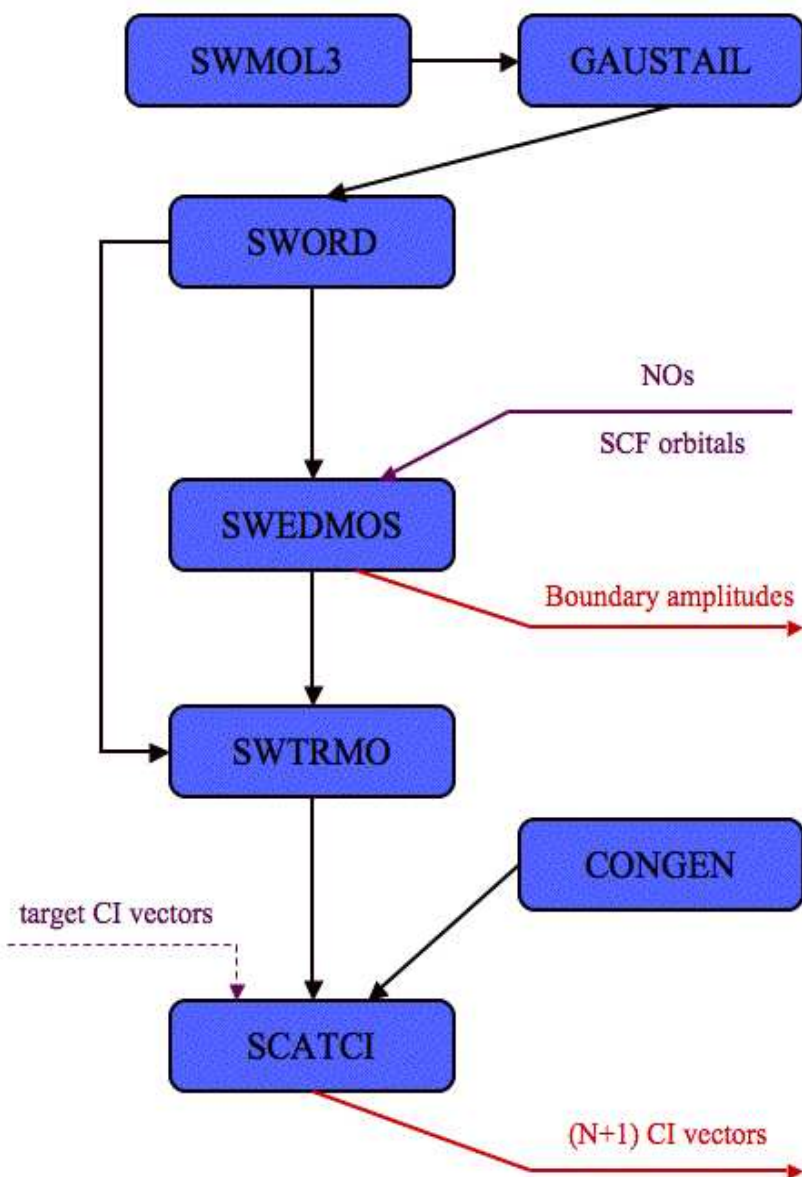


Figure 3.3: Flow diagram for the scattering calculation in the inner region. Red arrows indicate inputs required by the outer region runs. The modules used in this thesis are SWINTERF, RSOLVE, EIGENP, TMATRX and IXSEC.

3.6 Computational implementation

requires configurations generated by CONGEN and molecular integrals generated by SWTRMO to construct the Hamiltonian matrix. Then it diagonalises the Hamiltonian matrix to obtain the eigenvalues and eigenvectors. The prototype CSFs derived from CONGEN to do the contraction helps speeds the calculation very significantly. Different diagonalisation methods can be chosen; the ARPACK diagonaliser (Lehoucq et al., 1996) is used to treat large Hamiltonian matrices in the partitioned R -matrix method described above. Flag IPOSIT is also required to verify matrix elements for positron runs. Furthermore, SCATCI can write out the sequential indices representing the symbolic matrix elements (SME), which can be used for delta function calculations to perform Z_{eff} (see details in Chapter 4). This is important since SCATCI never generalise the actual inner region $N+1$ electron wave functions.

ZEFFMAT calculates delta functions as described in Chapter 4. It reads in the SMEs and eigenvectors derived from SCATCI and delta integrals generated by GAUS-DELTA and SWTRMO to build delta functions or Z_{eff} matrix. It should be noted that ZEFFMAT does not process any 1-electron integrals or intergrals not associated with the positron.

DENPROP generates properties such as permanent dipoles and polarisabilities obtained from input target wave functions. The target properties are then used in the outer region scattering calculation.

PSN produces pseudo-natural orbitals by diagonalising the density matrices produced by DENPROP. PSN can generate state-averaged NOs by choosing different weights for the target states.

SWINTERF supplies the interface between the inner and outer regions. It requires three input files obtained in the inner region calculations: boundary amplitudes from SWEDMOS, eigenvalues and eigenvectors of the $(N + 1)$ -electron Hamiltonian from SCATCI, target properties from DENPROP. It produces two files with channel data and R -matrix data.

RSOLVE requires the output files from SWINTERF and builds the R -matrix at the boundary, solves the outer region scattering equation (3.27) and then constructs fixed-nuclei K-matrices for specified energies. The R -matrix can be propagated to the asymptotic region. Alternatively, a procedure can be chosen to propagate an external wave function from the asymptotic region to the boundary. This procedure is discussed in Chapter 4. Note that the R -matrix propagation and the wave function

3.6 Computational implementation

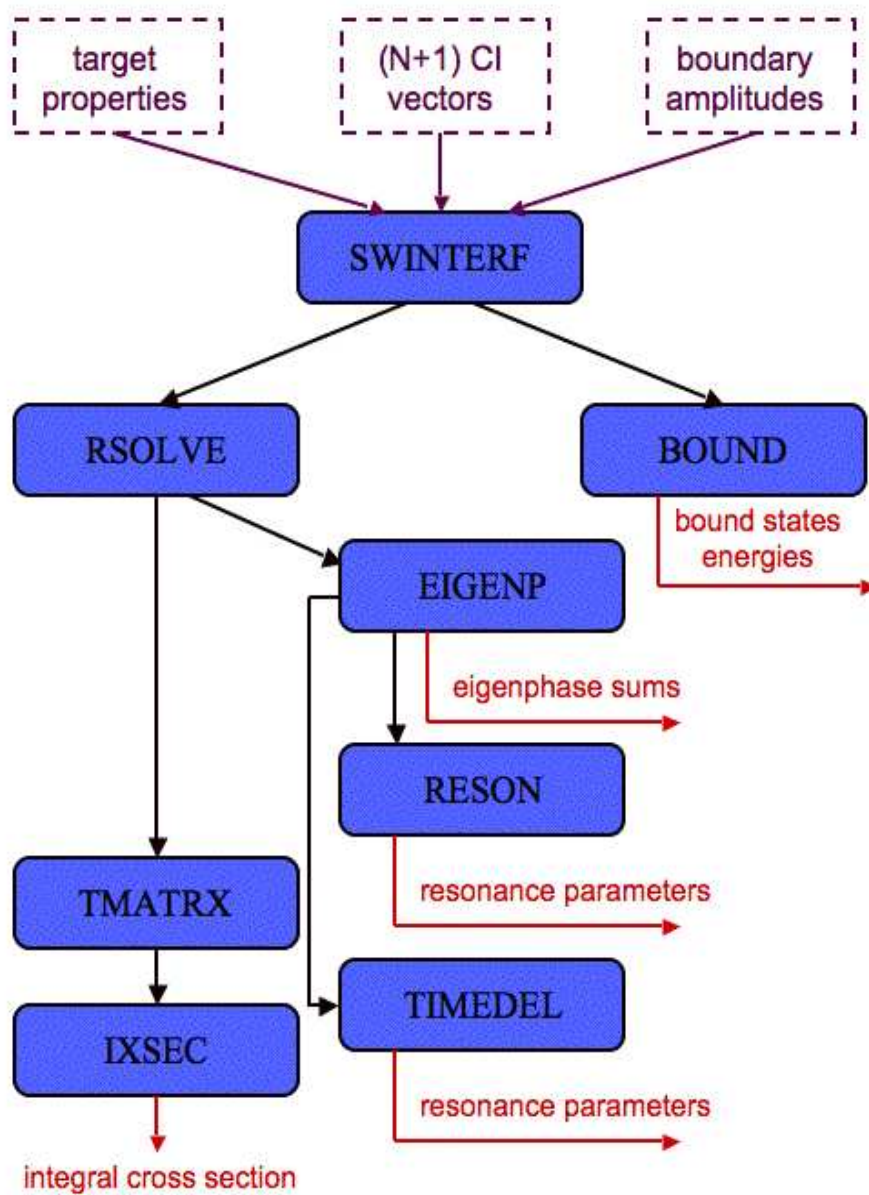


Figure 3.4: Flow diagram for the scattering calculation in the outer region. Red arrows indicate outputs of required quantities.

3.6 Computational implementation

propagation cannot be performed at the same time otherwise an improper K -matrixes given which result in incorrect eigenphases. The Z_{eff} calculation is included as an option in RSOLVE. It works by specifying the propagated wave function to obtain A_{Ek} coefficients, and then reading in the delta function matrix generated in ZEFFMAT.

EIGENP diagonalises the K -matrixes from RSOLVE and sums over all channels (n_a) to get the eigenphase sums given in equation (3.38).

TMATRIX generates the T -matrixes from the K -matrix.

IXSECS computes the integral cross sections from the T -matrixes produced by TMATRIX.

POLYDCS gives the rotationally elastic and inelastic DCSs for a variety of molecular system with different symmetries (e.g. C_{2v} , C_{3v}). The codes was written by Sanna and Gianturco (1998) POLYDCS requires K -matrix, rotational constant, dipole and quadrupole moments and incident energies.

Positron Annihilation

4.1 Introduction

Normally, positrons are thermalized in atomic or molecular gases before annihilation happens. At room temperature $T=296$ K, the energy of a positron is 0.037 eV. At this energy, s-wave scattering gives the dominant contribution to Z_{eff} .

Usually, the value of Z_{eff} is larger than the actual number of electrons in target, Z , due to the fact that the positron distorts the density of target electrons. One counter example is the neon atom, which has 10 electrons per atom; the experimental value of $Z_{eff}=5.99\pm 0.06$ (Coleman et al., 1975). As can be seen from table 4.1, for positron annihilation with helium, the measurement gives $Z_{eff}=3.94\pm 0.02$ (Coleman et al., 1975) at room temperature, compared to the theoretical result of $Z_{eff}=3.88\pm 0.01$ using Kohn variational calculations. It was found by Wright et al. (1983) for many atoms and simple molecules that

$$Z_{eff} \approx (18 \pm 3)\alpha^{1.05\pm 0.06}, \quad (4.1)$$

where α is the dipole polarisability of target. However, for many organic molecules, the value of Z_{eff} is very much larger than Z , e.g., $Z_{eff}=3160$ for C_2H_2 and $Z_{eff}=11300$ for C_4H_{10} as shown in table 4.1. Murphy and Surko (1991) gives an empirical relationship for many organic molecules

$$\ln Z_{eff} \approx \frac{A}{E_i - 6.8 \text{ eV}} + B, \quad (4.2)$$

where E_i is the ionization potential of target. A and B are constants.

4.1 Introduction

Table 4.1: Experimental values of Z_{eff} for various atoms and molecules at room temperature 296 K.

species	Z	experimental Z_{eff}
He	2	3.94 ^a
Ne	10	5.99 ^a
H ₂	2	14.6 ^b
N ₂	14	30.5 ^c
CO ₂	22	54.7 ^d
H ₂ O	10	319 ^e
NO ₂	23	1090 ^c
NH ₃	10	1600 ^c
CH ₄	10	142 ^d
C ₂ H ₂	14	3160 ^e
C ₂ H ₆	18	660 ^c
C ₃ H ₈	26	3500 ^c
C ₄ H ₁₀	34	11300 ^e

^a Coleman et al. (1975), ^b Laricchia et al. (1987), ^c Heyland et al. (1982),

^d Wright et al. (1985), ^e Iwata et al. (1995)

In the first Born approximation, the total scattering wave function can be written as a plane wave which is used to represent positron multiplied by the undistorted target wave function:

$$\Psi \underset{r \rightarrow \infty}{\sim} \exp(i\mathbf{k} \cdot \mathbf{r}_p) \Phi(\mathbf{r}_1, \dots, \mathbf{r}_Z). \quad (4.3)$$

So the $Z_{eff}=Z$.

For the R -matrix method, in the no potential case, only one positron integrals are allowed in the calculation. The Σ_g^+ symmetry contribution to Z_{eff} can be obtained as smoothly decreased results starting with $Z_{eff}=Z$. Adding to the results calculated with symmetries Π_u , Π_g and Σ_u^+ , constant value equal to Z can be obtained for positron energies below the positronium formation threshold.

As discussed in Chapter 1, Z_{eff} can be obtained from the elastic scattering wave function. Calculated value of Z_{eff} give an important indication of the accuracy of the wave functions. Below the method used for these calculations is presented.

4.2 Dirac delta functions

Substituting the inner region continuum wave function into equation (1.14), Z_{eff} can be expressed in terms of the coefficient A_{Ek} ,

$$Z_{eff}(E) = \sum_{k,k'} \sum_{i=1}^N \frac{4\pi}{kk'} \int A_{Ek}^* \langle \psi_k | \delta(\mathbf{r}_p - \mathbf{r}_i) | \psi_{k'} \rangle A_{Ek'}. \quad (4.4)$$

where it is only necessary to integrate over the inner region since it is assumed that the target wave function is zero outside this region. This expression (4.4) can be rewritten as the following equation if the delta function matrices elements are denoted by matrix $Z_{kk'}$,

$$Z_{eff} = \sum_{k,k'} \frac{4\pi}{kk'} A_{Ek}^* Z_{kk'} A_{Ek'} \quad (4.5)$$

Dr. Jan Franz modified program GAUSTAIL, which is used to evaluate the tail contribution to each Hamiltonian integral, to give a new program GAUSDELTA. GAUSDELTA evaluates the Dirac-delta integrals instead of the usual Hamiltonian integrals located in GAUSTAIL. Much of the remaining procedure is the same for the annihilation calculation as the scattering ones for inner region runs. Therefore, SWTRMO can still be used to give the four-index transformed integrals.

According to the formation of the Hamiltonian matrix given by Tennyson (1996), the target wave function can be expanded as,

$$\Phi_{in} = \sum_{m=1}^M c_{imn} \eta_{im}(\mathbf{r}_1 \cdots \mathbf{r}_Z) \quad (4.6)$$

The integrals used to construct matrix elements of (N+1) Hamiltonian, can be addressed by the orbital numbers. Therefore, the Hamiltonian can be written in the form:

$$H_{in,j,i'n'j'} = \langle \phi_{in} u_{ij} | \hat{H} | \phi_{i'n'} u_{i'j'} \rangle = \sum_{\beta} D_{in,j,i'n'j'}^{\beta} X(I_{ij,i'j'}^{\beta}) \quad (4.7)$$

where D^{β} are the coefficients multiplying each integral X ; I^{β} are the sequential indices of the constructed symbolic matrix elements which point to the required location of integrals. The subscripts i, n, j represent index of the symmetry of target states, index of target states for each symmetry and index of continuum orbitals, respectively. Using a Dirac delta functions instead of the Hamiltonian in equation (4.7), we can write

$$Z_{in,j,i'n'j'} = \langle \phi_{in} u_{ij} | \delta | \phi_{i'n'} u_{i'j'} \rangle = \sum_{\beta} D_{in,j,i'n'j'}^{\beta} Y(I_{ij,i'j'}^{\beta}). \quad (4.8)$$

4.3 Normalisation of elastic scattering wave function

A new program ZEFFMAT was designed for calculating equation (4.8). The symbolic matrix elements and coefficients set (I^β, D^β) are obtained from SCATCI (Tennyson, 1996) runs. The appropriate delta integrals obtained from SWTRMO are chosen by these symbolic matrix elements. Figure 4.1 shows the flow diagrams for inner region Z_{eff} calculation.

It should be noted that matrix element $Z_{inj,i'n'j'}$ requires no one-electron integrals or two-electron integrals without a positron involved. After considering the coefficients a_{ijk} and b_{lk} in equation (3.5) which are generated by normalising the Hamiltonian matrix, one can get the matrix $Z_{kk'}$.

As mentioned in Chapter 3, usually there is no need to calculate outer region wave functions in the R -matrix method. However, the exact form of wave function is required to calculate Z_{eff} and enters via the coefficient A_{Ek} .

4.3 Normalisation of elastic scattering wave function

The expression for the outer region wave functions has been introduced in Chapter 3. The normalisation of this wave functions needs to be treated carefully. Hence, for calculating Z_{eff} , the accurate description of the external wave function and its derivatives become an important part of determining the coefficients A_{Ek} .

To normalise the wave function, the density of the incident beam should be one positron per unit volume.

For channels with the same l , diagonal elements of wavefunction solutions should be the same. Hence, the normalisation of wavefunction should be $\frac{\sqrt{4\pi}}{k}(1 - i\underline{K})$. Therefore the required wavefunction is in the form of

$$\underline{\mathcal{F}} = (1 - i\underline{K})(\underline{F} + \underline{KG}). \quad (4.9)$$

Runge-Kutta-Nystrom integration (Brankin et al., 1989) is used to solve the second-order differential equation (3.27). The RKN12(10)17M coefficients (Baker et al, 1999) were used to integrate the outer region wave function to the boundary. It is necessary to integrate the asymptotic expansion inwards from $r = a'$, typically 30 to 50 a_0 , as the initial value to the R -matrix boundary at $r = a$. According to equation (3.20) or (3.25), coefficients A_{Ek} can then be obtained straight forwardly. In principle, the two expressions of A_{Ek} (equation (3.20) and (3.25)) should get the same results. However, the term $E_k - E$ in the denominator may leads to poles on Z_{eff} . According to the

4.3 Normalisation of elastic scattering wave function

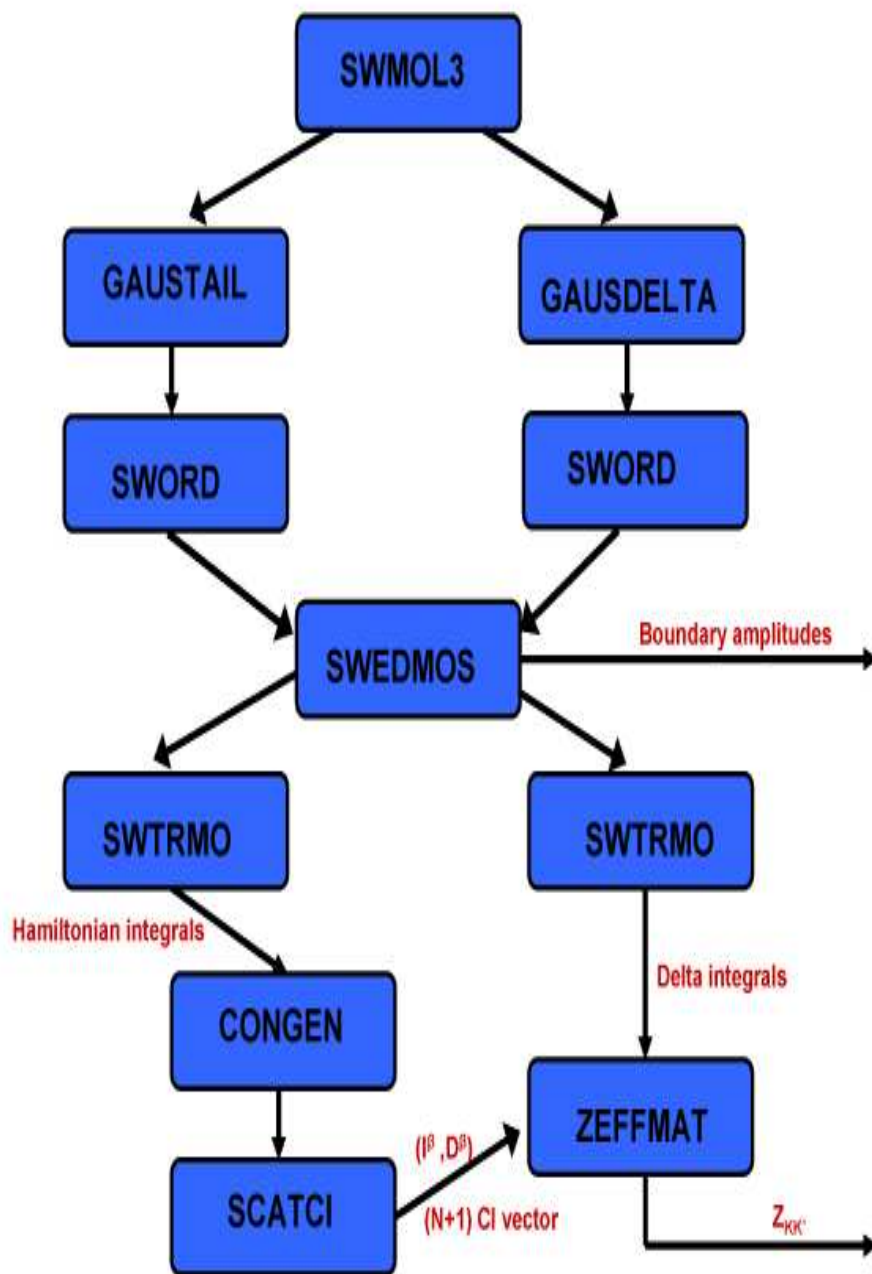


Figure 4.1: Flow diagram for the inner region Z_{eff} calculation.

4.4 Annihilation tests

definition of R -matrix, these poles can be removed when equation (3.20) is employed to compute A_{Ek} . So equation (3.20) is usually used to determine A_{Ek} . Sequentially, value of Z_{eff} can be obtained.

4.4 Annihilation tests

Initial tests of our Z_{eff} theory applied it to positron annihilation with 1-electron "atoms". For these systems, the value of Z_{eff} should behave as $\frac{1}{1+k^2}$ for the no interaction case and $\frac{1}{1+K^2}$ for annihilation in a square well potential for Σ_g^+ symmetry. The form of wave function for positron interaction by a square potential well:

$$V(r) = \begin{cases} V_0, & r \leq a \text{ (inner region)} \\ 0, & r > a \text{ (outer region)} \end{cases}$$

gives a good test case. The time-independent Schrödinger equations are given by

$$-\frac{1}{2}\nabla^2\psi + V_0\psi = E\psi, \quad r \leq a \quad (4.10)$$

$$-\frac{1}{2}\nabla^2\psi = E\psi, \quad r > a \quad (4.11)$$

Inserting $\psi = \frac{f_l(r)}{r}Y_l^m(\theta, \phi)$ into equations (4.10) and (4.11), we can obtain

$$f_l'' - \frac{l(l+1)}{r^2}\frac{f_l}{r} + 2(E - V_0)f_l = 0, \quad r \leq a \quad (4.12)$$

$$f_l'' - \frac{l(l+1)}{r^2}\frac{f_l}{r} + 2Ef_l = 0, \quad r > a \quad (4.13)$$

The solutions of equations (4.12) and (4.13) are the spherical Bessel functions $\hat{j}_l(Kr)$ and $\hat{j}_l(kr)$, respectively, where $K^2 = 2(E - V_0)$ and $k^2 = 2E$.

For the case of $l = 0$,

$$f_0 = \begin{cases} A \sin Kr, & r \leq a \\ B \sin(kr + \delta_0), & r > a \end{cases}$$

where δ_0 is the s-wave scattering phase shift. Considering the boundary conditions for a square potential well, we can obtain the matching equation and its derivative,

$$\begin{cases} \sin Ka & = C \sin(ka + \delta_0) \\ K \cos Ka & = Ck \cos(ka + \delta_0) \end{cases}$$

where $C = \frac{B}{A}$. The s-wave phase shift can be easily obtained by solving $k \tan Ka = K \tan(ka + \delta_0)$ which gives

$$\delta_0 = \arctan\left(\frac{k}{K} \tan Ka\right) - ka \quad (4.14)$$

4.4 Annihilation tests

The normalization factor C is obtained as

$$C = \sin Ka \sin ka + \frac{K}{k} \cos Ka \cos ka. \quad (4.15)$$

So the wave function used to calculate Z_{eff} for s-wave scattering by a square potential well is

$$f_0 = (\sin Ka \sin ka + \frac{K}{k} \cos Ka \cos ka)(\sin kr + \underline{K}_{00} \cos kr) \quad (4.16)$$

where \underline{K}_{00} is the K -matrix with $l=0$. Substituting the wave function into equation (3.20) or (3.25) to obtain A_k coefficients, allows Z_{eff} to be calculated. A Z_{eff} calculation for an H atom in a square well potential at energies below the positronium formation threshold is shown in figure 4.2.

Figure 4.2 shows the no potential and square well potential calculations of Σ_g^+ symmetry using the Z_{eff} theory described above for positron-H annihilation in terms of incident positron energies. For no interaction calculation, the K -matrix and phase shift are equal to zero. By adding the Z_{eff} values of Π_u , Π_g and Σ_u^+ symmetries, a constant value of one is obtained for the no interaction case and 0.87 if the square well potential $V_0=-2$ eV for incident energy below the positronium formation threshold. This supports the validity of the formulation of wave function. The pole in the results for Z_{eff} with square-well potential arises from the K -matrix poles at 2.6 eV.

More models are calculated to test positron annihilation with H atom: static model, SP model and close-coupling models with MRMPs method (see fig 4.3). Calculated Z_{eff} for scattering in the static potential are even smaller than the number of electrons in the H atom. One gets better results for calculations with the MRMPs method than static and SP model. As higher pseudo-continuum orbitals are included in the target representation using the MRMPs method, better results are obtained, particularly at lower energies. In the outer region only one target state is included in this calculation. The R -matrix radius was chosen as 13 a_0 . The wave function for positron-H calculations was propagated from 30 a_0 to the R -matrix boundary 13 a_0 using Runge-Kutta-Nystrom integrator.

Z_{eff} for positron- H_2^+ annihilation is also calculated in the static and SP level. It gives the similar results as positron-H calculations. This becomes another touch-stone calculation for testing our Z_{eff} codes.

Gribakin and Ludlow (2002) reported that the values Z_{eff} converge as $1/(l + \frac{1}{2})$, where l is the partial-wave quantum number. Details about it is shown in Chapter 8.

4.4 Annihilation tests

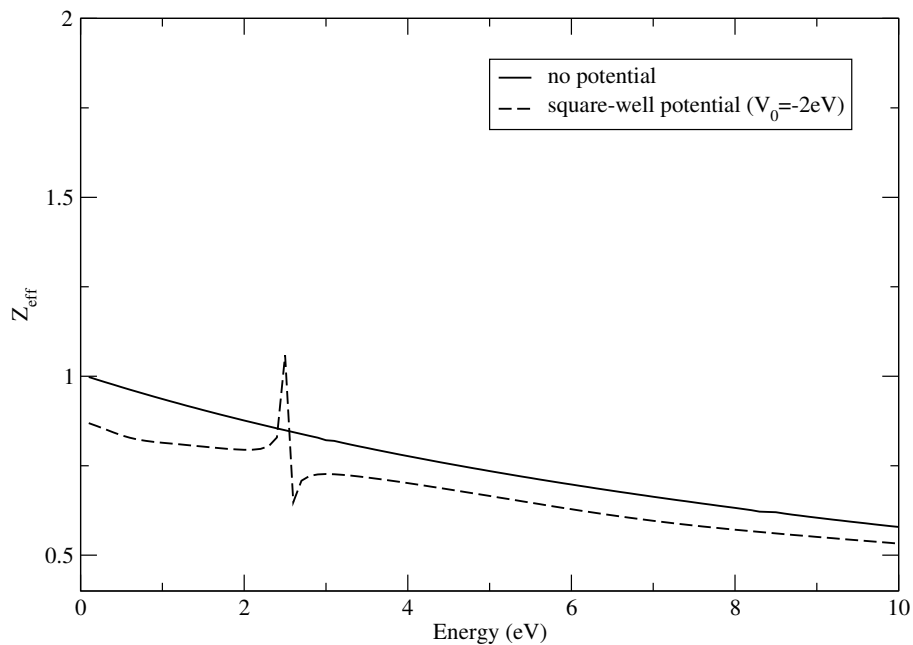


Figure 4.2: Z_{eff} for positron-H annihilation of A_g symmetry with no potential and a square-well potential as a function of positron scattering energy.

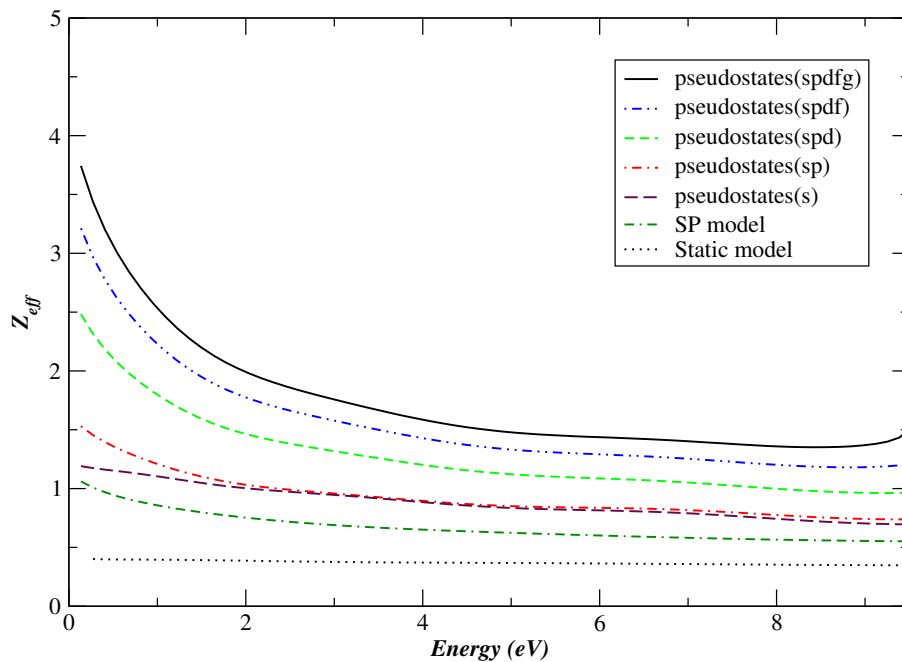


Figure 4.3: Z_{eff} for H atom calculated for several methods as a function of the collision energies.

4.5 Conclusion

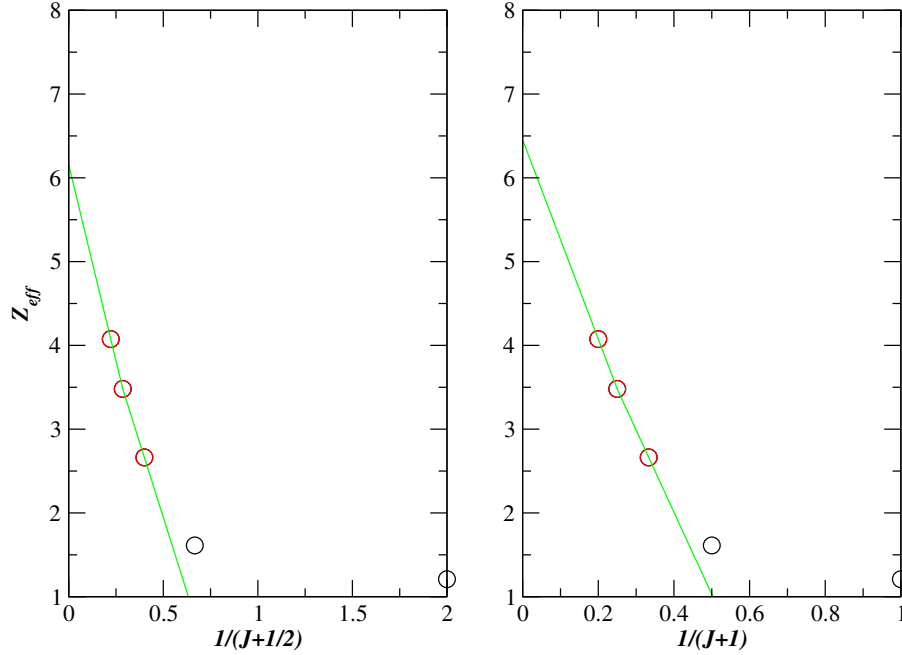


Figure 4.4: Z_{eff} for H atom in terms of J .

Enlightened by this behaviour of Z_{eff} , we tried to fit the Z_{eff} values based on models with MRMPs method using one target state only. As shown in figure 4.4, the values of Z_{eff} at 0.1 eV using different models with MRMPs method from s-PCOs model to spdfg-PCOs model are fitted in terms of $1/(J + \frac{1}{2})$ where J is the value of highest l included in the PCO expansion. It gives fitted $Z_{eff}=6.45$ at zero energy, compared to previous calculated results of 8.39 using Kohn variational calculations (van Reeth and Humberston, 1998) and 7.96 using many-body theory calculations (Gribakin and Ludlow, 2004).

4.5 Conclusion

A new code used to calculate annihilation parameter Z_{eff} is presented in this Chapter. This code gives the accurate form of outer region wave function for positron annihilation with atoms and molecules. Tests for positron-H annihilations at energies below the formation threshold are reported with no potential, square-well potential and various multipole potential models. Calculations for positron annihilation with H_2 molecule is reported in Chapter 8.

Positron collisions with water

5.1 Introduction

The study of interaction of charged particles with polar atoms and molecules plays an important role in many fields in astrophysics and radiation biological physics. Water is one of the most abundant substance in the universe and is the most significant component in living organisms. This molecule is very important for astrophysics, atmospheric physics and biophysics research. Humankind has been trying to understand water for more than two thousands years. As far back a 700 BC, water was regarded as one of the five significant elements in the whole natural world.

Calculations on electron collisions with water molecules using the R -matrix method (Faure et al., 2004*a,b*) have been reported, in which the differential cross sections and momentum transfer cross sections are in excellent agreement with corresponding measurements (Čurík et al., 2006)). The most recent comparison Zhang et al. (2009) of total cross sections between theory and new experiment (Khakoo et al., 2008) on electron-water collision also gives good agreement at energies up to 7 eV. The vibrationally elastic and rotationally inelastic total cross sections gives a very large forward scattering peak because of the big permanent dipole moment of the target. This causes difficulties with performing low-energy collisions in experiments. Several calculations (Baluja and Jain, 1992; Gianturco et al., 2001; Nishimura and Gianturco, 2004) on positron-water scattering have been performed. The single center expansion (SCE) calculations (Gianturco et al., 2001) are used to compare with our results. A num-

5.1 Introduction

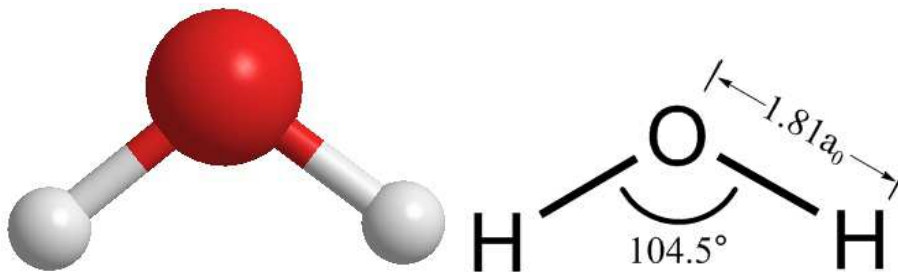


Figure 5.1: The equilibrium nuclear configuration of water

ber of measurements (Sueoka et al., 1986; Kimura et al., 2000; Zecca et al., 2006; Beale et al., 2006) have been carried out on positron-water collisions and gave rather different elastic cross sections.

Unlike positron collisions with non-polar molecule (Tennyson, 1986; Danby and Tennyson, 1988, 1990b, 1991), the low-energy cross section for collisions with strongly polar molecule are dominated by the forward scattering because of the long-range nature of the dipole potential. Although more partial waves must be included in the positron wavefunction expansion for strongly polar systems, the truncation in the expansion can be dealt with by using the dipole-Born approximation. Electron collisions with polar molecules (Lane, 1980; Padial et al., 1981; Gianturco and Jain, 1986; Morrison, 1988) also have this problem. For testing this, two calculations were performed: direct Born correction to the cross section and the Born correction from the frame transformation as implemented in the program POLYDCS (Sanna and Gianturco, 1998). This procedure is discussed in section 5.4. At energies approaching the rotational excitation thresholds, all thresholds are considered to be degenerated based on the adiabatic nuclei rotation (ANR) approximation we use.

In this chapter, elastic cross sections are reported for the incident positron energy range 0.025-10 eV. The results of R-matrix calculations using state-averaged natural orbitals model (NOs) are compared with the single center expansion (SCE) calculations (Gianturco et al., 2001) and the experimental results (Sueoka et al., 1986; Kimura et al., 2000; Zecca et al., 2006; Beale et al., 2006).

5.2 Target calculation

5.2 Target calculation

The water molecule is polar. It belongs to the C_{2v} point group, and its X^1A_1 ground state has the electronic configuration $1a_1^2 2a_1^2 3a_1^2 1b_1^2 1b_2^2$. We performed fixed-nuclei calculations at the experimental molecular geometry of H_2O (see Figure 5.1), $r_{OH}=1.81 a_0$ and $\widehat{HOH}=104.5^\circ$ (Csaszar et al., 2005).

The target wavefunctions of H_2O molecule are calculated at the self-consistent field (SCF) level using Gaussian-type orbitals (GTOs). We used two different GTO basis sets for H and O atoms of target. One of them we chose was double zeta plus polarization (DZP) of Dunning Jr (1970) as the GTO basis set for O and triple zeta (TZ) basis of Dunning Jr (1971) for H with an added diffuse s function and two p functions (Gorfinkiel et al., 2002), which gives an orbital space of (19,6,12,3), i.e. 19 molecular orbitals of a_1 symmetry, 6 of b_1 , 12 of b_2 and 3 of a_2 and (3,1,1,0) of them are occupied orbitals in the ground state of target and the rest are virtual orbitals. Within the SCF calculation, this basis sets yields a dipole moment of 1.983 D; it gives an improved value of 1.897 D with the natural orbital model described below, which is close to the experimental data of 1.854 D (Suresh and Naik, 2000). A smaller DZP basis set was also tested and gives (15,5,10,3) for the total target orbital space. The later basis set gives a target dipole moment of 1.986 D. Calculations presented below were performed with the larger basis. Table 5.1 shows the vertical excitation energy calculated using NOs model and compares them to previous studies on water (Gorfinkiel et al., 2002; van Harrevelt and van Hemert, 2000; Winter et al., 1975). The NOs model we used here is based on a configuration interaction calculation for singlet states. In this model, we obtained state-averaged natural orbitals (NOs) by performing a singles and doubles configuration interaction (SD CI) calculation from the completed active space (CAS) of $(2a_1, 3a_1, 4a_1, 5a_1, 1b_1, 2b_1, 1b_2)^8$. In our scattering calculation, we selected the lowest singlet states of each symmetry in the close-coupling expansion. The NOs model gives a good representation for all the target states in the calculation. We performed several tests on the state averaging NOs and chose the best case of lowest singlet state of each symmetry X^1A_1 state, 1B_1 , 1B_2 and 1A_2 with weights 40, 5, 5 and 5, respectively, which gives the best threshold energy and dipole moment. When the full CAS S CI and CAS SD CI models were used to represent the target states, they gave similar results.

5.3 Scattering calculation

Table 5.1: Vertical excitation energy for H₂O target states. N is the number of configurations. Basis 1 and basis 2 refer to the two different basis sets which give orbital space of (19,6,12,3) and (15,5,10,3) respectively, based on the NOs model. Compare to: (A) Gorfinkiel et al. (2002), (B) van Harrevelt and van Hemert (2000) and (C) Winter et al. (1975)

State	N		Vertical excitation(eV)				
	Basis 1	Basis 2	Basis 1	Basis 2	A	B	C
¹ A ₁	5144	6588	-76.107	-76.107	-76.092	-	-
¹ B ₁	4964	6348	9.88	7.54	7.51	7.63	7.49
¹ B ₂	5072	6432	15.86	13.52	14.02	11.11	10.0
¹ A ₂	4910	6210	12.32	10.80	13.12	9.60	-

5.3 Scattering calculation

The scattered positron is described by continuum orbitals using GTOs basis set with l up to g wave placed at the centre of mass of the target molecule. Three different R -matrix radii were tested for scattering calculation based on the static and static plus polarization model which are explained below: 10 a_0 , 13 a_0 and 14 a_0 . Among these tests, R -matrix radius of $a = 10 a_0$ gives the stablest eigenphase below the positronium formation threshold. Therefore, all calculations present in next section were performed within R -matrix radius of $a = 10 a_0$. The GTOs basis set for R -matrix radius of $a = 10 a_0$ is the same as the set used for electron-water calculation using the R -matrix method (Faure et al., 2002).

In order to find out how sensitive of polarization effects contributing to positron-water collision using close-coupling expansion, we carried out scattering calculations in three different models: static model, the static plus polarization (SP) model and a close-coupling model based on the use of Natural orbitals (NOs). In the static model no relaxation of the target is allowed but the positron can occupy both target occupied and virtual orbitals as well as continuum orbitals of each symmetry.

In the SP model, one electron excitations of the target are added to allow for short-range electron-positron correlation effects into full virtual states. In this calculation, 125 singlet excited target states were generated, 49 states of A₁ symmetry, 24 of B₁, 39 of B₂ and 13 of A₂.

5.4 Results and discussion

In both methods, the positron was allowed to occupy all continuum, all frozen and active target orbitals.

5.4 Results and discussion

Due to the strongly dipolar nature of water, the dipole Born approximation was used to augment the total collision cross sections which compensates for the truncated partial wave contribution. Two different methods were performed to test this: direct Born correction to the cross section and the Born correction from the frame transformation as implemented in the program POLYDCS (Sanna and Gianturco, 1998). The two approaches are compared in Figure 5.2. The frame-transformation approach (POLYDCS), which we used for performing our rotationally resolved cross sections, gave similar results to the direct Born correction approach above 1 eV. At lower energy region, the frame-transformation approach is deemed to more reliable following the study of Okamoto et al. (1993) who showed that DCS can be computed by the ground rotational state of target molecule at very small angle.

Results for elastic integral cross section for different models are shown in Figure 5.3 in the incident energy range 0.25-7 eV. It can be seen from this figure that the Born correction leads to a very substantial contribution to our calculation, particularly at low collision energies. Due to the strong dipole moment of molecule water, there is not much difference among our static, SP and NOs model results. The results are also compared with the single centre expansion (SCE) calculation of Gianturco et al. (2001), which are also performed at the SP level. However, their calculation did not include the Born correction, although it gets similar results to our Born-corrected results. This is because their SCE calculation includes many partial waves in the wavefunction expansion to get satisfactorily converged results.

The three different models we used to carry out differential cross section (DCS) give rather similar results due to the insensitivity to polarization effects. Here we only report Born-corrected results of DCS under using NOs model. The elastic (rotationally summed) differential cross sections are plotted for collision energy of 0.25 eV and 2 eV in Figure 5.4, 5 eV and 10 eV in Figure 5.5 The DCS are strongly peaked like electron water scattering in the forward direction, due to the dipole. Apparently, from these three figures we can see that the DCS are dominated by the dipolar (0-1) rotational

5.4 Results and discussion

transition. This has a significantly different behaviour from the electron-water results (Faure et al., 2004b) since for electron case, both the $\Delta J = 0$ component and $\Delta J = 2$ component give a crucial contribution to the DCS results.

Figure 5.6 presents the comparison between our rotationally summed cross section (Born-corrected NOs model) and experimental cross sections obtained by (Sueoka et al., 1986; Kimura et al., 2000; Zecca et al., 2006; Beale et al., 2006). Our theoretical results lie higher than the three of four experimental results below 7 eV which indicates the low angle scattering may be missed in determining contributions to cross sections in these experiments. The experiment whose measured cross section is higher than our calculated cross section corrected the forward scattering based on the measurement of Sueoka et al. (1987), using a procedure of unmodified dipole-Born approximation. This procedure appears to overestimate the forward scattering in the lower energy region.

One of above measurements (Beale et al., 2006) gives an experimental acceptance profiles. We used these to estimate forward scattering contribution to the cross sections at low energies. This procedure is discussed in the next section.

Figure 5.7 gives the rotationally resolved integral cross sections (ICS) for collision energies in the energy range of 0.1-10 eV, and then compares with the equivalent integral cross sections for electron-water collisions of Faure et al. (2004b). Cross sections for electron collision have the same value as positron's at energies near zero. The difference increases with increasing energy and that indicates the contribution of polarization effects to electron and positron scattering. It also can be seen from this figure that the cross sections are dominated by the $\Delta J = 1$ transition as DCS.

Momentum transfer cross sections are presented as a function of collision energy in Figure 5.8, which are also compared with the equivalent cross sections for electron case (Faure et al., 2004b) whose results have good agreement with measure values by Cho et al. (2003). As is expected, the momentum transfer cross sections are higher for electron than for positron particularly at low projectile energies.

5.4 Results and discussion

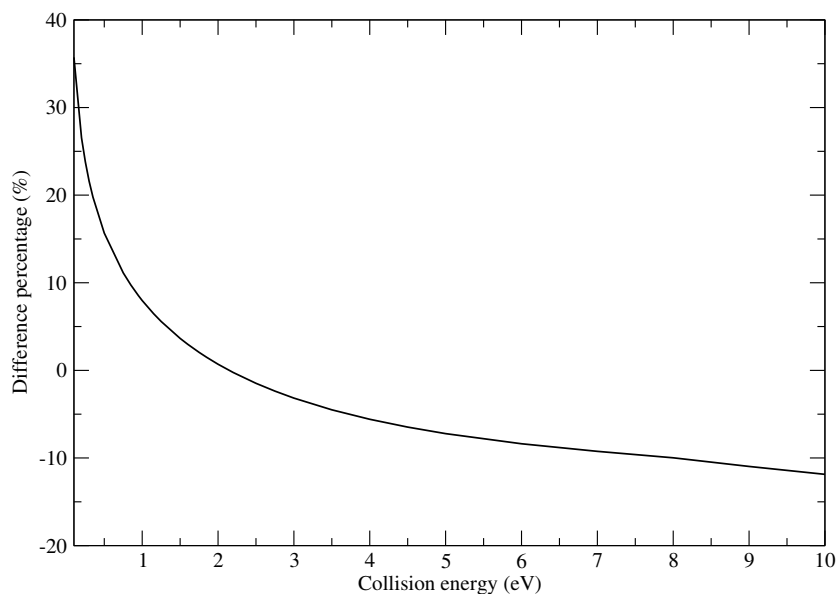


Figure 5.2: Comparison of the dipole Born corrections between the frame transformation correction by program POLYDCS (Sanna and Gianturco, 1998) and direct Born correction of the elastic cross section by Baluja et al. (2000). The difference is defined as percentage difference between POLYDCS and the simple Born calculation. This calculation based on NOs model which is explained in detail below.

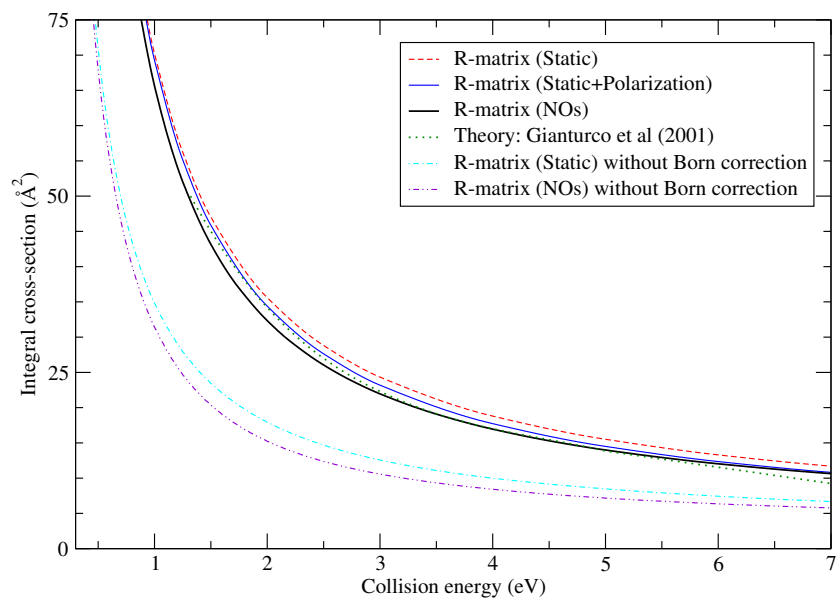


Figure 5.3: Elastic (rotationally summed) integral cross sections for positron-water collisions for several theoretical models with *R*-matrix method and previous study of Gianturco et al. (2001)

5.4 Results and discussion

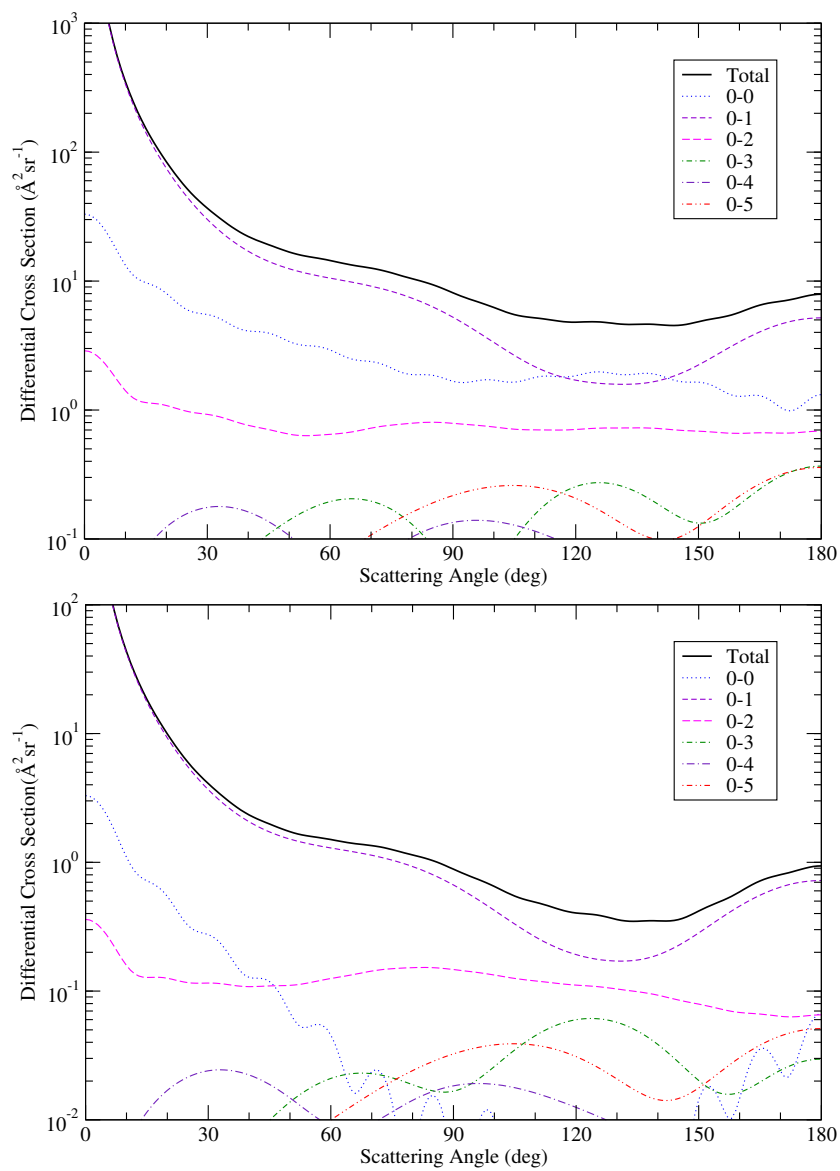


Figure 5.4: Differential cross section (DCS) for positron-water collisions at 0.25 eV (upper) and 2 eV (lower). The solid line gives the total DCS while the other give the rotationally resolved partial state-to-state DCS.

5.4 Results and discussion

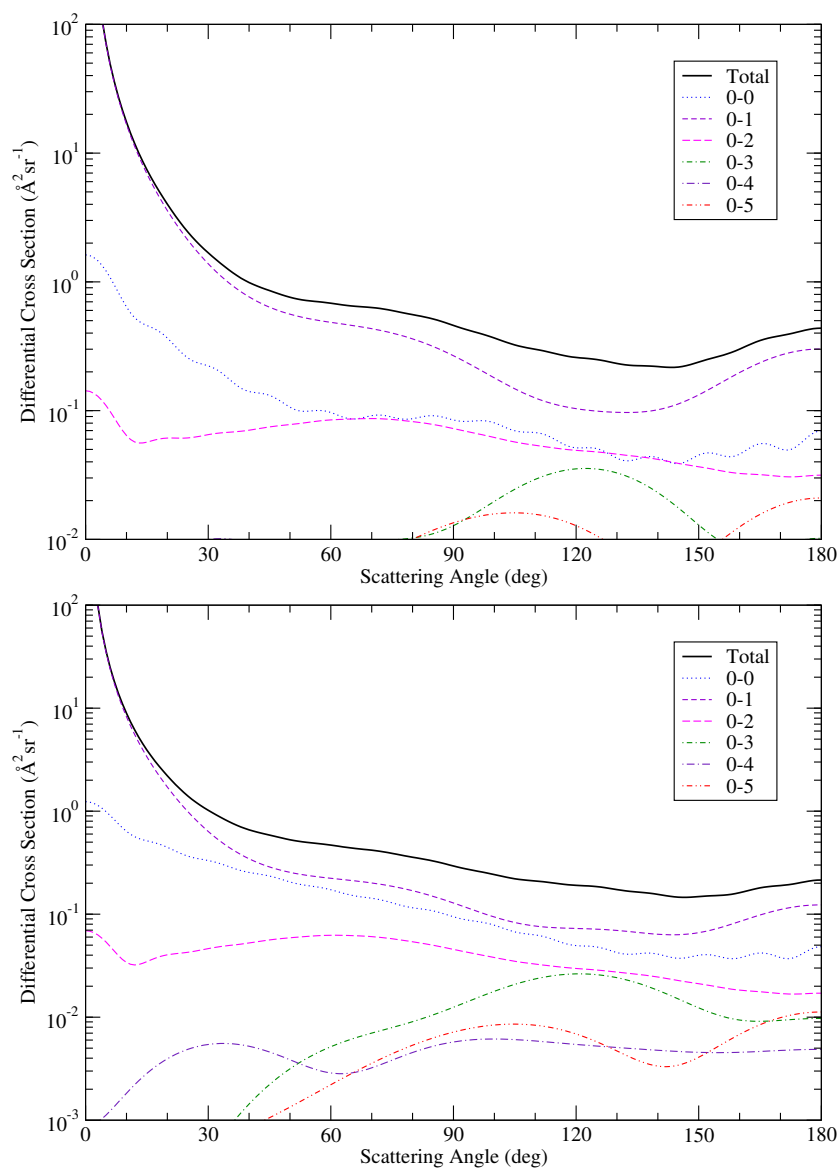


Figure 5.5: Same as Figure 5.4 except incident energies at 5 eV(upper) and 10 eV(lower) respectively

5.4 Results and discussion

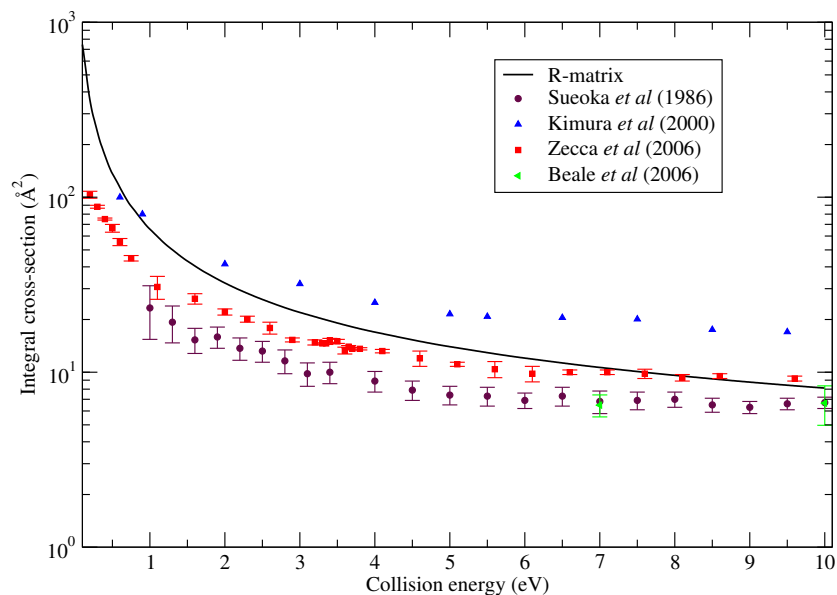


Figure 5.6: Comparison of experiment with theory for the elastic (rotationally summed) integral cross sections for positron-water collisions as a function of the collision energy.

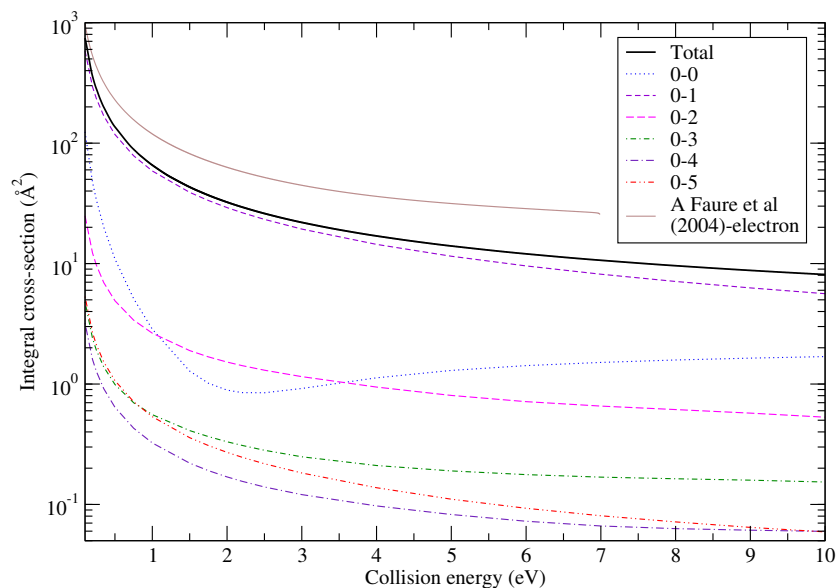


Figure 5.7: Calculated elastic (rotationally summed) integral cross sections for positron-water collisions as a function of the collision energy compared to the equivalent cross sections for electron collisions Faure *et al.* (2004*b*). Also shown are the rotationally resolved cross sections for positron collisions.

5.4 Results and discussion

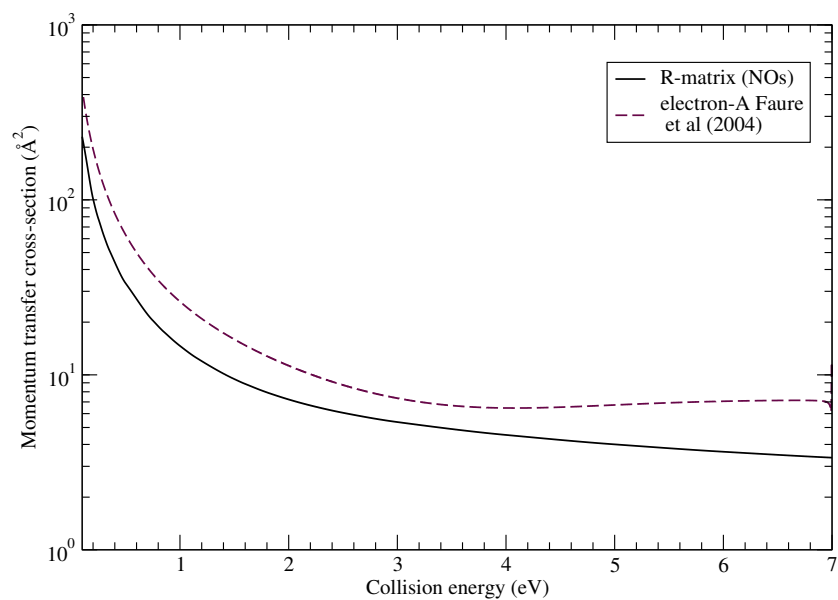


Figure 5.8: Elastic (rotationally summed) momentum transfer cross sections for position (this work) and electron (Faure et al., 2004b) water scattering as a function of the collision energy.

5.5 DCS correction

Table 5.2: Coefficients for fit function given by eq. (5.1) used to represent the angular behaviour of the positron (and electron) DCS in the forward region. Angles are given in degrees for a DCS in $\text{\AA}^2/\text{°}$. A separate fit is given for each collision energy, E .

	electron	positron	positron
E	7 eV	7 eV	10 eV
C_0	0.918729	-0.292103	-0.578577
C_1	0.0717311	0.033907	0.129589
C_2	0.383493	0.386788	0.265902
C_3	-0.00129725	-0.0000131518	0.0000463739

5.5 DCS correction

As mentioned above, experiments on positron-water collision gave very different cross sections to our calculation and, even to each other, due to the missing or overestimate consideration of low angle scattering. Among these measurements, Beale et al gives the acceptance profiles, which depends on the details of the apparatus and method used in the measurements. The corrected TCS for electron are similar to positron case, provided the acceptance profiles $x(\theta)$ is the same in both cases, which is revealed that fitting electron case is valid for water.

The partial-wave expansion used in our R -matrix calculations does not converge in the fixed-nuclei approximation due to the long-range dipolar interaction. Based on the reality that the charged particle does not penetrate the wave function of the target molecule for high partial wave, we used dipole Born approximation to deal with this problem. We found a polynomial fit to our calculated differential cross section which gives a good representation of the low angular data,

$$F(\theta) = C_0 + \sum_{i=1}^3 C_i \theta^i \quad (5.1)$$

Several different forms of $F(\theta)$ were tested, and among them we chose one fit function that gives closest angular behaviour of the low angle DCS, Table 5.2 gives the coefficients of the fits for the case of water. The residuals are less than 1% below 10° . The fit function equation (5.1) was then integrated analytically in whole range 0-180 degree.

$$\sigma^{\text{corr}} = \int x(\theta) F(\theta) \sin\theta d\theta \quad (5.2)$$

5.6 Conclusion

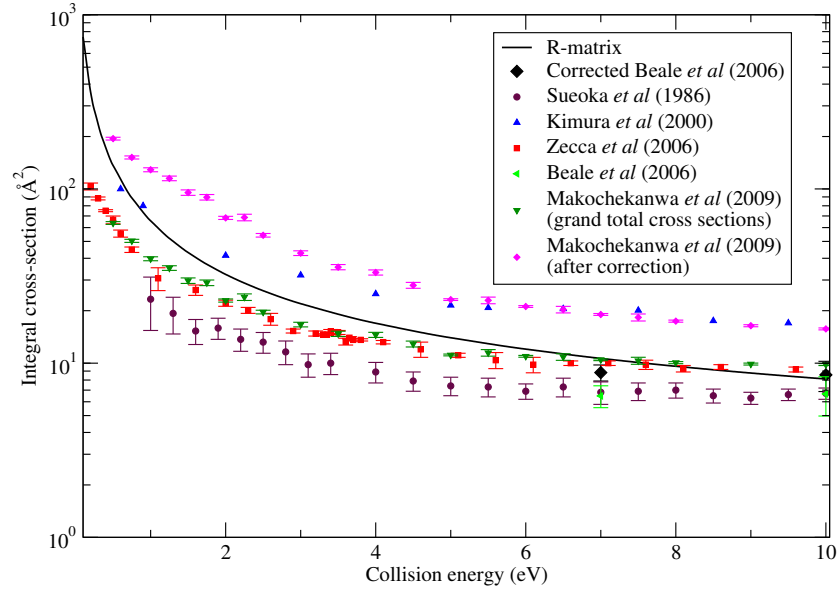


Figure 5.9: A comparison of theory Baluja et al. (2007) with uncorrected experiment Sueoka et al. (1986); Kimura et al. (2000); Zecca et al. (2006); Beale et al. (2006) and corrected one for integral cross sections for positron-water collisions as a function of the collision energy.

where $x(\theta) = e^{-\lambda\theta^2}$ is the angular acceptance profile from Beale et al. (2006), and $\lambda = 0.0206$ at 7 eV, 0.0266 at 10 eV. In practice, $x = 0$ for θ greater than 14° . For positrons, the correction at 7 eV is $\sigma^{\text{corr}} = 2.346 \text{ \AA}^2$ which is very close to the corrected electron differential cross sections data given by Faure et al. (2004b), 2.340 \AA^2 .

Figure 5.9 shows the comparison of our theoretically calculated total cross sections, published experimental results (Sueoka et al., 1986; Kimura et al., 2000; Zecca et al., 2006; Beale et al., 2006) and our corrected Beale et al. (2006) results. We can see that the corrected data give better agreement than uncorrected results. The error bars for corrected experimental results are the same as original experimental results (Beale et al., 2006) and therefore must be on underestimate of the error. Figure 5.9 also shows the latest measurement performed by Makochekanwa et al (2009) which gives the grand total cross sections (GTCS) and the ones with the forward scattering correction. This corrected measurement lies above our calculated results at energies below 10 eV.

5.6 Conclusion

We report rotationally resolved elastic differential cross sections, integral cross sections and momentum transfer cross sections for positron collision with polar molecule water

5.6 Conclusion

at incident energies below 10 eV. Unlike positron scattering with apolar molecules, our results are insensitive to the models we used and degree of polarization included in our calculations. The Born correction contributes an important part to the elastic cross sections, particularly at lower energies.

There is excellent agreement between our results using static plus polarization (SP) and NOs models, and the SCE results which are also performed at the SP level. Due to the large permanent dipole nature of the target, there is therefore not much difference between our static, SP model and Natural orbital model results. We compared our results with four published measurements (Sueoka et al., 1986; Kimura et al., 2000; Zecca et al., 2006; Beale et al., 2006) at collision energies below the positronium formation threshold. Given the fact that the positron-water collision is strongly forward peaked, it's difficult to perform this process in experiment at lower energies. Three of these four lie below our calculated results. We believe none of them did the forward scattering correction and therefore miss significant part of the total cross section. Although Kimura et al. (2000) gave the correction to low angle scattering by measurement Sueoka et al. (1986), it appears to overestimate the forward scattering correction to the cross sections. By contrast, our theoretical results are more reliable for positron collisions with dipolar molecule. We also calculated differential cross sections (DCS) in the positron energy range 0.25-10 eV using the POLYDCS program of Sanna and Gianturco (1998). This program takes our K -matrices as input and calculates elastic and inelastic rotational DCS which includes contributions for all rotor states up to $J=5$ which yields converged results. There is no other theoretical or experimental data available to compare our DCS results. Momentum transfer cross sections for the vibrationally elastic scattering of positron from water are also reported and compared to corresponding electron-water scattering (Faure et al., 2004*b*). In section 5.5, we give a theoretical correction to measured integral cross section (Beale et al., 2006) at low energies, based on given experimental angular acceptance profiles obtained by the same experimental group. Given the fact that no experimental DCS has been available so far, we correct the integral cross sections based on our calculated DCS for energies below 10 eV. The corrected results give better agreement with our theoretical results (Baluja et al., 2007) than the uncorrected ones. We suggest that our calculations give the most reliable results for positron collisions with water molecule at low energy.

Positron collisions with H₂ molecule

6.1 Introduction

H₂, the simplest molecule and serves as a benchmark system. Collisions with positrons and H₂ have been well studied in theory (Danby and Tennyson, 1990b; Armour et al., 1990; Gibson, 1992; Reid et al., 2004; Arretche et al., 2006; Mukherjee and Sarkar, 2008; Zhang et al., 2009) and experiment (Hoffman et al., 1982; Charlton et al., 1983; Deuring et al, 1983; Zecca et al., 2009). It is hard to model the polarization effects between the scattered positron and the electrons in the H₂ target due to the attractive nature in the collision. Unlike positron collisions with dipolar molecule, polarization effects play a dominant role in collisions with non-polar molecule. The calculations are particularly sensitive to the degree of polarization for energies below the positronium formation threshold at 8.63 eV.

The MRMPS method has been applied to solve electron impact with H₂ and H₃⁺ (Gorfinkiel and Tennyson, 2004, 2005), C₂⁻ (Halmová et al., 2008) and Li₂ (Tarana and Tennyson, 2008), which are found to lead to an excellent target polarizability and polarization potential. In this chapter, the MRMPS method is used to treat positron collisions with H₂ molecule at energies up to 10 eV. As part of this study, polarizabilities of H₂ were calculated using different models. The model which gives best polarizability was chosen to carry on scattering calculations. Comparison are made between our MRMPS calculations method and previous calculations performed by Armour et al. (1990); Arretche et al. (2006); Mukherjee and Sarkar (2008); Tennyson (1986); Danby

6.2 Calculations

and Tennyson (1990b); Gibson (1992); Reid et al. (2004) at low energies. Tennyson (1986) and Danby and Tennyson (1990b) are earlier R-matrix calculations that did not include enough short-range representation of polarization in Σ_g^+ symmetry, which is very important for lower energies cross sections. It seems that Gibson (1992) also had this problem in their calculation. Calculation with Kohn variational method of Armour et al. (1990) gave eigenphase sums and annihilation parameter below 13.61 eV. Arretche et al. (2006) presented the static and static plus polarisation calculation using Schwinger multichannel method. The most recent theoretical calculation (Mukherjee and Sarkar (2008)) reported integral cross sections at energies from 1 eV up to 1000 eV. This is the only available theoretical run that gave intermediate-energy results for positron-H₂ collision. Zhang et al. (2009) also reported scattering lengths.

Positron-H₂ collisions were also studied by some experimental groups (Hoffman et al., 1982; Charlton et al., 1983); these studies gave very similar cross sections to each other. The most recent measurement performed by Zecca et al. (2009) give very different integral cross sections from previous experiments below 10 eV. However, these three measurements and another attempt (Deuring et al, 1983) which gave the integral cross section from 8 eV to 400 eV, are in excellent agreement at energies above 10 eV. Among these measurements, only Zecca et al. (2009) presented cross sections below 1 eV. Although positron-H₂ collisions have been well studied, we still chose it as a touch-stone calculation for testing the MRMPS method employed to treat positron calculations. Comparisons are also made with simple calculations without MRMPS methods for eigenphase sums and integral cross sections at collision energies below the positronium formation threshold.

6.2 Calculations

We start from simple models for positron-H₂ calculation: the static model, static plus polarization model and close-coupling model without the MRMPS method. For the target calculation, we used the same basis set that Gorfinkiel and Tennyson (2005) employed, the 6-31 G** basis set of Hariharan and Pople (1973).

As mentioned in the theory chapter, we started by building Hartree-Fock molecular orbitals (MOs) for H₂⁺. The PCOs exponents generated with $\beta = 1.4$ and $\alpha_0 = 0.17$ after several tests with $\alpha_0 = 0.16, 0.18, 0.19$. We performed calculations with PCOs

6.2 Calculations

basis from (10s, 10p 6d) orbitals up to (10s, 10p 6d, 6f, 6g, 6h) orbitals, labelled as spd-PCOs, spdf-PCOs, spdfg-PCOs, spdfgh-PCOs, respectively. To avoid problems with linear dependence, a deletion threshold $\delta_{thrsh-tar}$ must be set at an appropriate value for orthogonalizing the PCOs to the MOs. Tests were performed for the spd-PCOs case and by choosing optimal β , α and $\delta_{thrsh-tar}$ value for our calculations. Comparisons of polarizability with $\beta = 1.4$ and various α with $\delta_{thrsh-tar}$ chosen as 2×10^{-4} are shown in table 6.1. Apparently, the polarizability given by the target calculation with $\beta = 1.4$ and $\alpha_0 = 0.16$ are better than other tests. These results are compared to given accurate values from Augspurger and Dykstra (1988). However, scattering calculation for PCOs with $\beta = 1.4$ and $\alpha_0 = 0.16$ shows less stable than for PCOs with $\beta = 1.4$ and $\alpha_0 = 0.17$. We carried out target calculations with $\beta = 1.4$ and $\alpha_0 = 0.10$ for different numbers of orbitals in the PCOs, see table 6.2. The $\alpha_0 = 0.10$ target was used in an attempt to perform scattering calculation with R -matrix radius of $13 a_0$. Because of the larger radius, bigger continuum basis have to be used in the scattering calculations. Although the target runs with $\beta = 1.4$ and $\alpha_0 = 0.10$ give good polarizabilities, it gives unstable eigenphase sums in the outer region calculation. To sum up, we choose the target runs with $\beta = 1.4$ and $\alpha_0 = 0.17$, which Gorfinkiel and Tennyson (2005) used to their electron- H_2 calculations with MRMPs method. All results shown in next section are with these values. In the case of $\beta = 1.4$ and $\alpha_0 = 0.17$, tests on different PCOs were performed, see table 6.3.

The target configurations used in our calculations with spd-PCOs basis in the irreducible representations of D_{2h} were:

$$(1-3a_g \ 1b_{2u} \ 1b_{3u} \ 1-2b_{1u} \ 1b_{2g} \ 1b_{3g})^2$$

$$1a_g^1(4-20a_g \ 2-8b_{2u} \ 2-8b_{3u} \ 1-5b_{3u} \ 3-10b_{1u} \ 2-6b_{2g} \ 2-6b_{3g})^1$$

where the orbitals in the first line are MOs and in the second line the PCOs placed in brackets. The target state distributions for different spd-PCOs basis are shown in figure 6.1, compared to a single CI calculation. For more complex PCOs, a greater number of PCOs are included in the calculations. For example, the spdfgh-PCOs calculation has the same MOs as spd-PCOs case but the PCOs were:

$$1a_g^1(4-28a_g \ 2-26b_{2u} \ 2-26b_{3u} \ 1-12b_{3u} \ 3-28b_{1u} \ 2-13b_{2g} \ 2-13b_{3g})^1$$

It's not easy to choose the three parameters (α , β , $\delta_{thrsh-tar}$) because there is another deletion threshold $\delta_{thrsh-scat}$ which has to be chosen carefully for the orthogonalization of the continuum GTOs to target orbitals for scattering calculation. For

6.2 Calculations

Table 6.1: Polarizabilities of H₂ for the basis of spd-PCOs with $\beta = 1.4$ for different α_0 . Accurate values are from Augspurger and Dykstra (1988)

α_0	α_{\parallel}	α_{\perp}
0.16	6.236	4.612
0.17	6.228	4.586
0.18	6.202	4.550
0.19	6.202	4.509
Accurate value	6.445	4.507

Table 6.2: Polarizabilities of H₂ for the basis of PCOs with $\beta = 1.4$ and $\alpha_0 = 0.10$.

PCOs	α_{\parallel}	α_{\perp}
(10s,10p,6d)	6.347	4.733
(12s,12p,6d)	6.345	4.735
(13s,13p,6d)	6.344	4.731

calculations with $\beta = 1.4$ and $\alpha_0 = 0.17$ for PCO basis, $\delta_{thrsh-tar} = 2 \times 10^{-4}$ and $\delta_{thrsh-scat} = 2 \times 10^{-7}$ gives smoother integral cross sections than other choices. These two deletion thresholds are different for various PCOs basis sets chosen.

We performed scattering calculations with spd-PCOs, spdf-PCOs, spdfg-PCOs and spdfgh-PCOs corresponding to the target calculations. The scattered positron is described by continuum Gaussian type orbitals with l up to g wave. Functions with largest exponent for the continuum orbitals (Faure et al., 2002) were deleted and (6s, 7p, 7d, 7f, 6g) was left. Calculations with PCO up to d wave carried with radius at $a = 10 a_0$, and $a = 13 a_0$. Comparisons of calculated integral cross sections for Σ_g^+ symmetry for

Table 6.3: Polarizabilities of H₂ for the basis of PCOs with $\beta = 1.4$ and $\alpha_0 = 0.17$.

PCOs	α_{\parallel}	α_{\perp}
spd	6.228	4.586
spdf	6.249	4.596
spdfg	6.249	4.597
spdfgh	6.266	4.595

6.2 Calculations

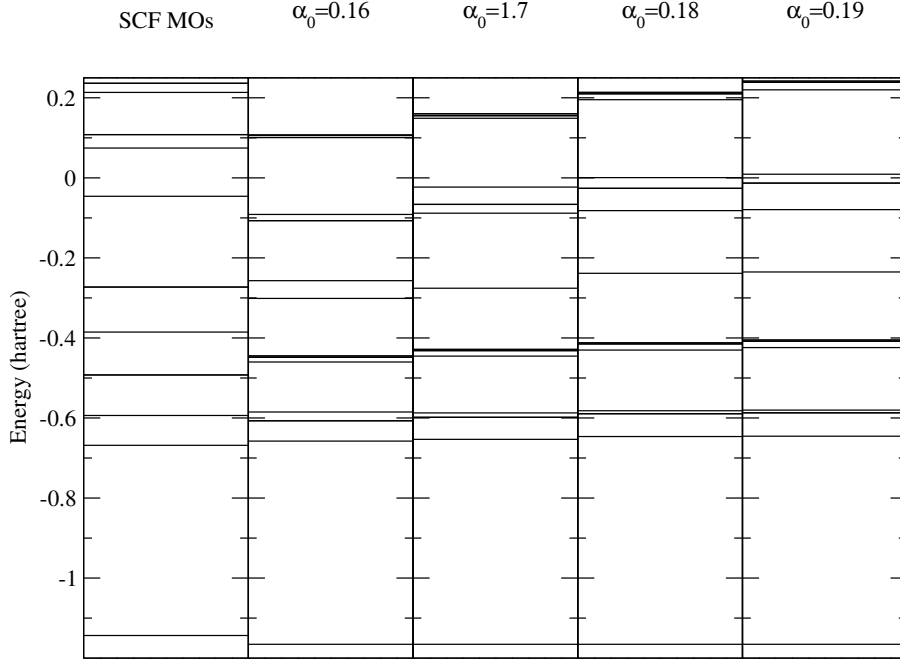


Figure 6.1: Target state distribution of Σ_g^+ symmetry for H_2 with $\beta = 1.4$ and deletion threshold $\delta_{thrsh-tar} = 2 \times 10^{-4}$

various R -matrix radius, PCOs basis and deletion thresholds are made in figure 6.2. These calculations were performed with spd-PCOs model. Results of eigenphase and cross sections for $a = 10 a_0$ are more stable than calculations with $a = 13 a_0$, so we used this radius for the rest of calculations. Although there is no significant difference among these calculations below the positronium formation threshold, the parameters $\beta = 1.4$, $\alpha_0 = 0.17$, $\delta_{thrsh-tar} = 2 \times 10^{-4}$ and $\delta_{thrsh-scat} = 2 \times 10^{-7}$ give smoother cross sections than other values.

As mentioned above, the deletion threshold for orthogonalizing between COs and target orbitals was set to 2×10^{-7} for all scattering calculations except those calculations with spdfg-PCOs and spdfgh-PCOs. Because $\delta_{thrsh-scat} = 2 \times 10^{-6}$ gives smoother eigenphase sum and corresponding cross sections than choosing $\delta_{thrsh-scat} = 2 \times 10^{-7}$ for the later two PCOs. 15 target states were included in the close-coupling expansion for spd-PCOs case, 22 for spdf-PCOs, 31 for spdfg-PCOs and 31 for spdfgh-PCOs.

6.3 Results and discussion

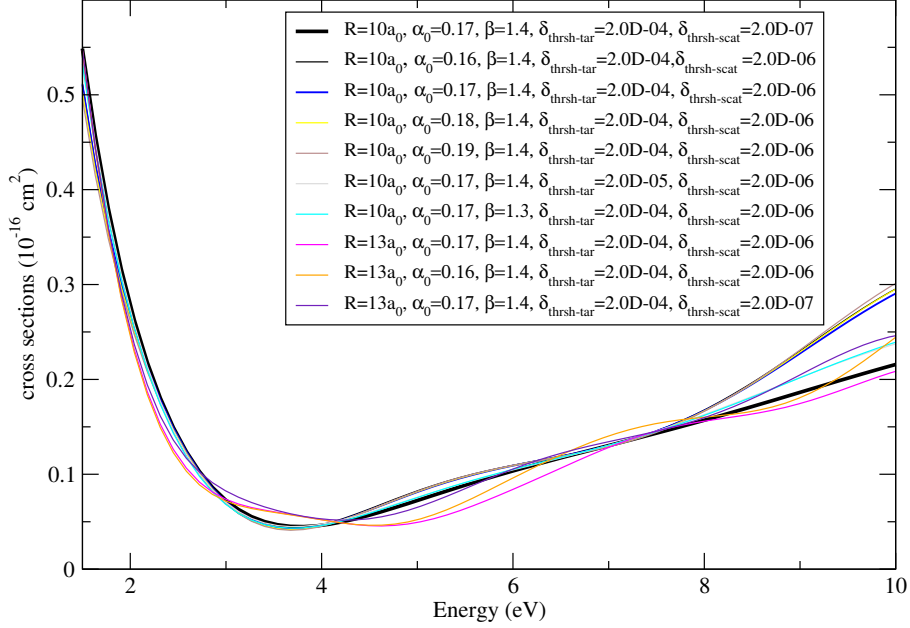


Figure 6.2: Cross sections of Σ_g^+ symmetry with various R -matrix radius, PCOs models and orthogonalizing deletion thresholds.

6.3 Results and discussion

Figure 6.3 shows the comparison of eigenphase sums for static model, SP model, close-coupling without MRMPS model and close-coupling with MRMPS model for Σ_g^+ symmetry. Apparently, results with the MRMPS method are much better than those for a SP calculation, which are without PCOs. It can be seen that only the static model gives negative eigenphase for the entire energies considered. Conversely, the eigenphase as for calculations with pseudostates stay positive at all energies below 10 eV. The SP model and close-coupling without MRMPS model eigenphases become negative at about 2.5 eV. However, the eigenphase given by non-pseudostate close-coupling model are higher than SP model at higher energies.

Figure 6.4 gives the eigenphase sums for Σ_g^+ symmetry, in radians, for different PCOs models used for representing pseudostates in comparison with Armour et al. (1990)'s theoretical results for energies up to 10 eV. All the calculations with PCOs shown in this figure employed PCOs basis with $\beta = 1.4$ and $\alpha_0 = 0.17$. As can be seen, the calculations with spdfg-PCOs and spdfgh-PCOs give very similar results to each other. It appears that our eigenphase calculated with the MRMPS method give converged results at low energies. Our results with MRMPS method show good

6.3 Results and discussion

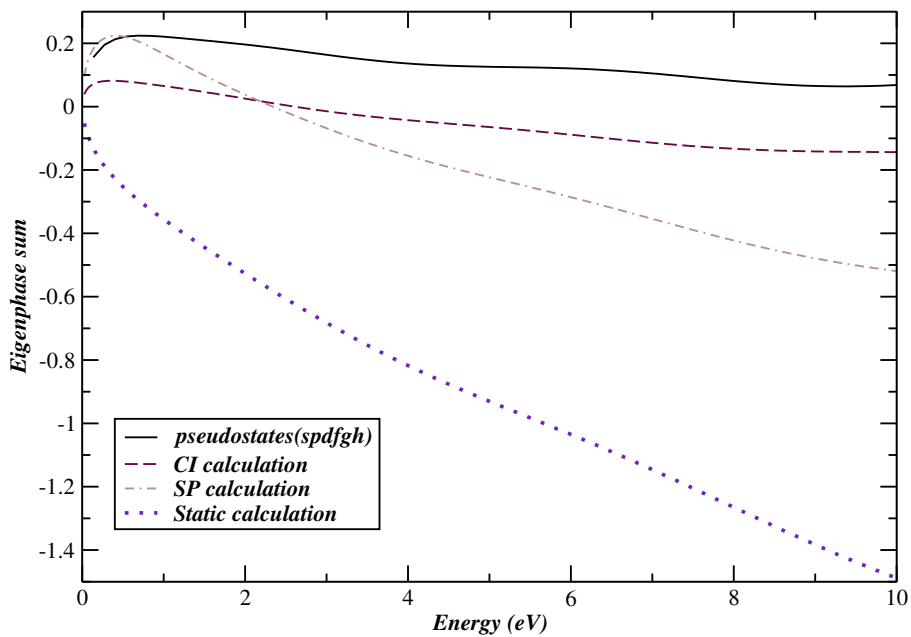


Figure 6.3: Comparison of eigenphase sums for Σ_g^+ symmetry for static model, SP model, close-coupling without MRMPS model and close-coupling with MRMPS model.

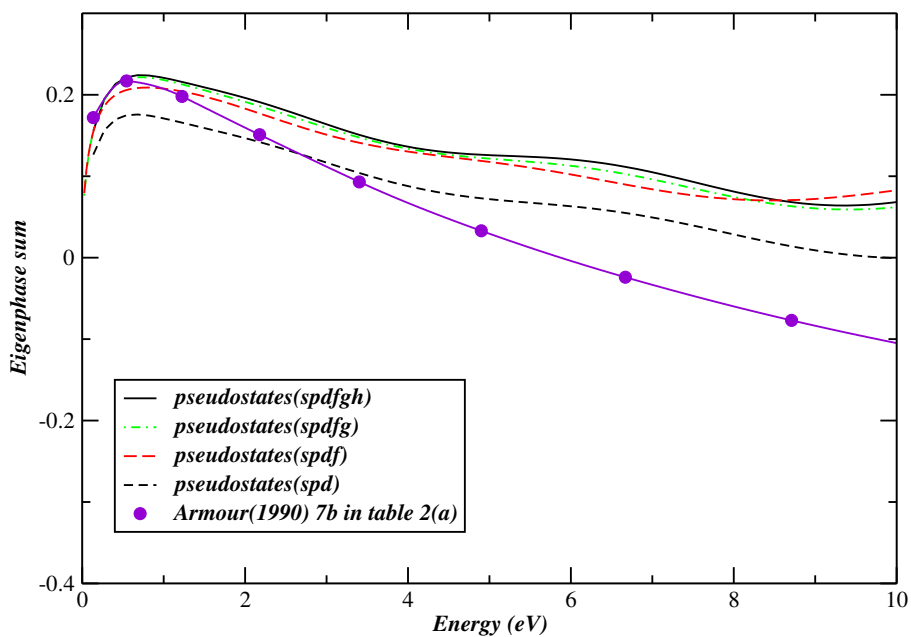


Figure 6.4: Comparison of eigenphase sums for Σ_g^+ symmetry with various PCOs models in the function of energies.

6.3 Results and discussion

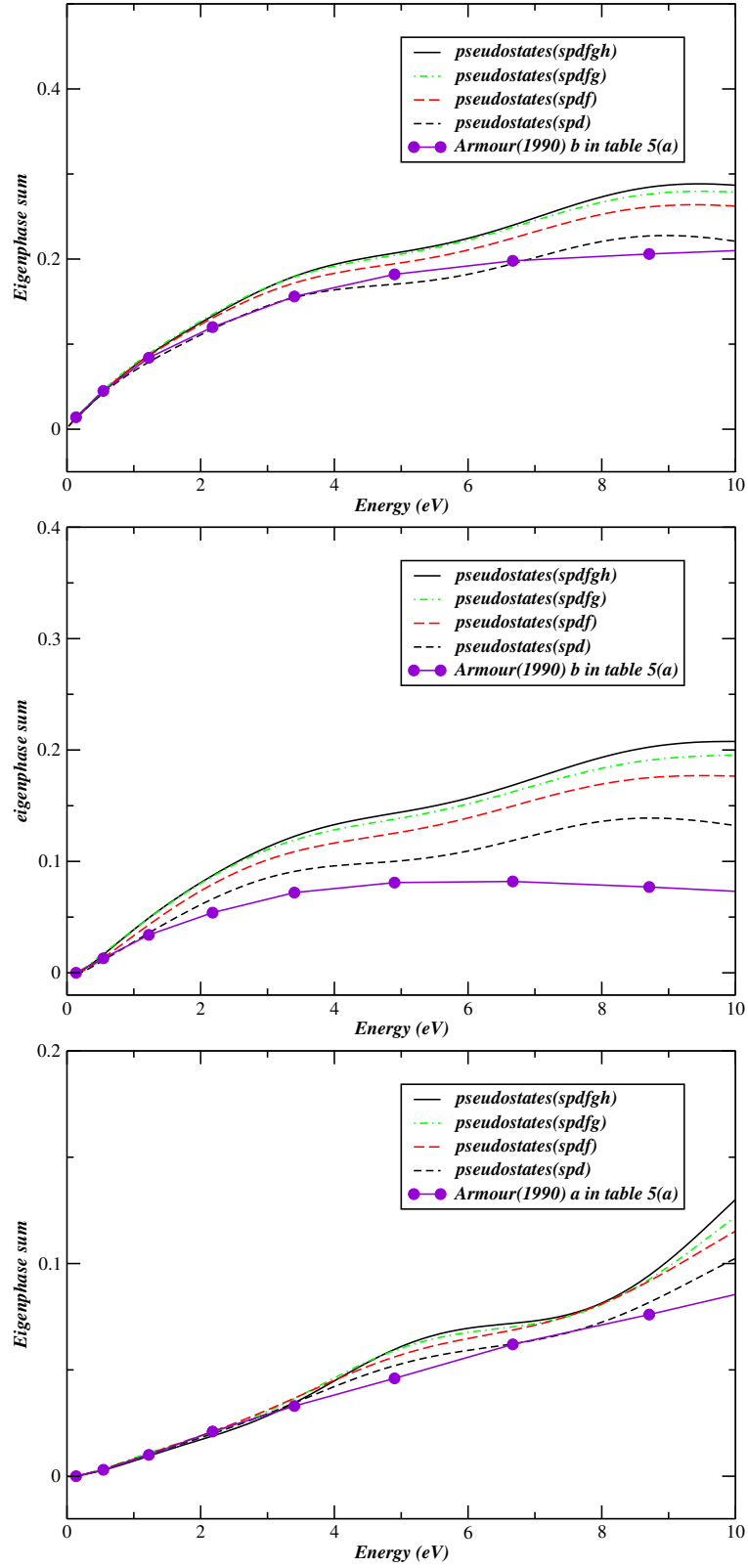


Figure 6.5: Comparison of eigenphase sums for Π_u, Σ_u^+ and Π_g symmetries, respectively.

6.3 Results and discussion

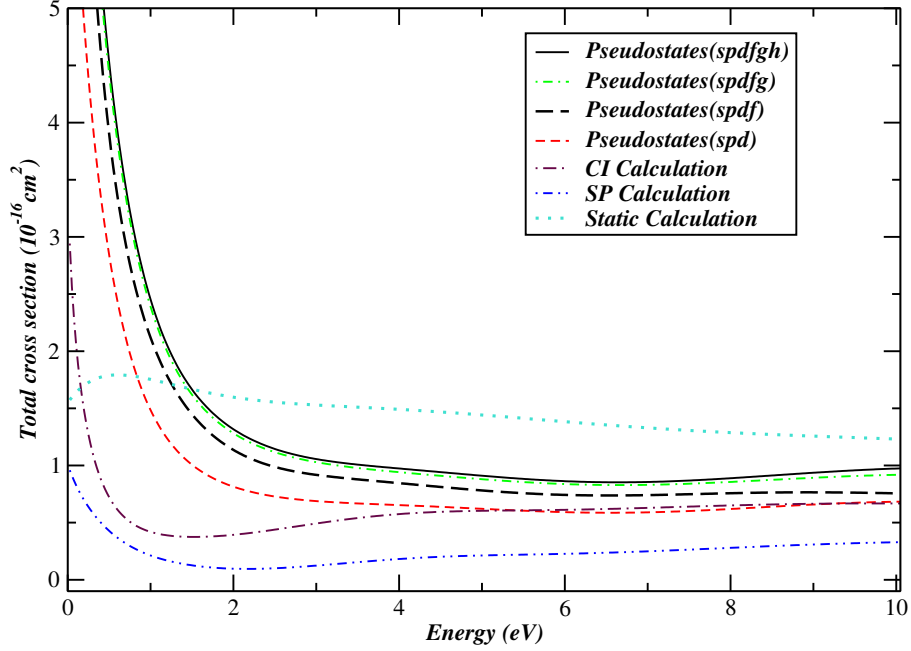


Figure 6.6: Total elastic cross sections for various models without and with MRMPS method.

agreement with Armour et al. (1990)'s eigenphase sums at lower energies, and are higher than Armour et al. (1990)'s results at incident energies above 5 eV. This is because only the lowest partial wave is included in their calculations. Similar behavior of eigenphase sums are given by Π_u , Σ_u^+ , Π_g symmetries in the function of energies, see figure 6.5.

Figure 6.6 presents total elastic cross sections given by various R -matrix models at energies below 10 eV. Obviously, our static and SP calculation are awful as the eigenphases above suggested. The static model does not even give forward-peaking behaviour at lower energies. At energies above 1.6 eV, total elastic cross sections for static model become larger than the MRMPS calculation with spdfgh-PCOs. Close-coupling without MRMPS calculation is better than SP model, but still much smaller at lower energies than calculations with MRMPS method. It turns out the polarization effects modelled by the MRMPS calculation play an important role for positron- H_2 collisions. Cross sections for calculations using MRMPS method with various PCOs give similar values. However the calculations with spdf-PCOs is better than the calculation with spd-PCOs. Judging by the eigenphase sum, the integral cross sections are converged for calculations with higher PCOs included.

Comparisons of our total elastic cross sections performed with MRMPS method with various available theoretical calculations are shown in figure 6.7. All studies give

6.3 Results and discussion

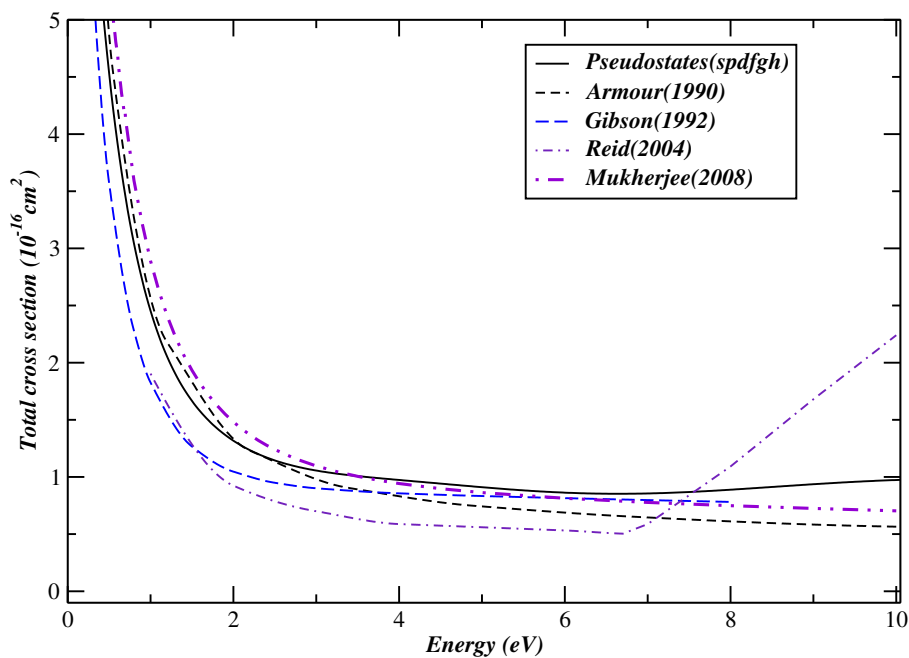


Figure 6.7: Calculated total elastic cross sections with MRMPS method compared with various available theoretical studies as a function of energy.

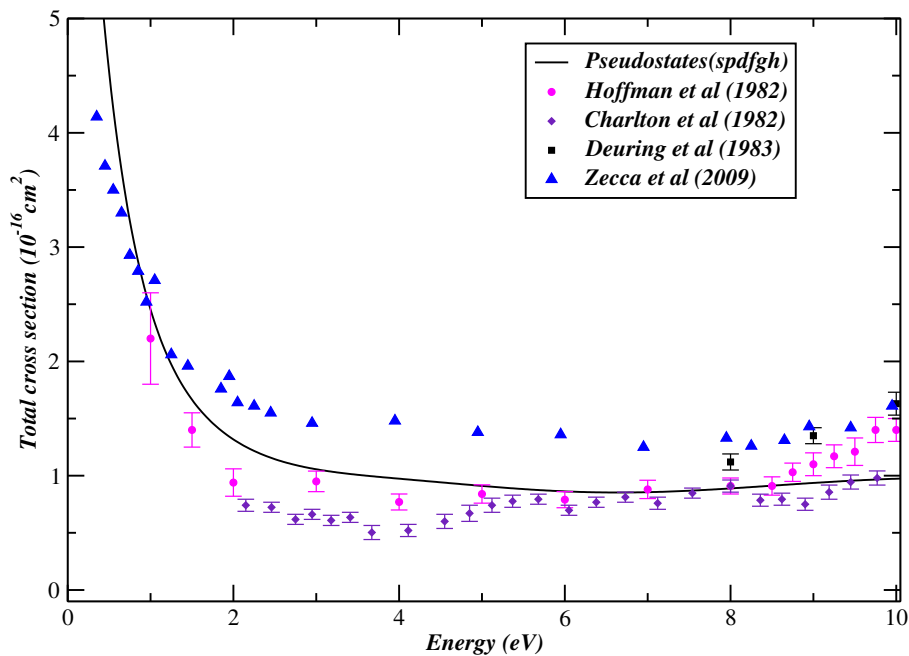


Figure 6.8: A comparison of experiment with our MRMPS calculation for total elastic cross sections for positron- H_2 collisions.

6.4 Conclusion

very similar cross sections at energies below the positronium formation threshold. In particular, our results with the MRMPS method give good agreement with Armour et al. (1990)'s integral cross sections, although there are minor differences between the corresponding eigenphase sums. At energies of 7 eV, Mukherjee and Sarkar (2008)'s cross sections increase rapidly due to the Ps formation included in their study. For energies above 10 eV, Mukherjee and Sarkar (2008) are in excellent agreement with experiments (Hoffman et al., 1982; Charlton et al., 1983; Deuring et al., 1983; Zecca et al., 2009).

Figure 6.8 compares our total elastic cross sections with spdfgh-PCOs with several experimental measurements (Hoffman et al., 1982; Charlton et al., 1983; Deuring et al., 1983; Zecca et al., 2009) for positron collisions with hydrogen molecule. Our results with MRMPS method are in excellent agreement with measurement of Hoffman et al. (1982) at energies below the positronium formation threshold. Zecca et al. (2009) is the only available measurement that gave total elastic cross sections below 1 eV. However, at energies above 1 eV, Zecca et al. (2009)'s result lies higher than our calculation. Charlton et al. (1983) lies below our results at energies from 2 eV to 6 eV, and then agree with them above 6 eV.

6.4 Conclusion

Total elastic cross sections for positron collision with H₂ molecule have been calculated using the MRMPS method at energies below the positronium formation threshold. We find excellent agreement between our results and other attempts performed by theoretical and experimental groups. The MRMPS method provides a good representation of polarization potential, so calculations with MRMPS method give much better results than calculations without MRMPS method. In our MRMPS calculation, appropriate parameters α_0 and β for the PCO basis need to be chosen carefully. The eigenphase sums and total elastic cross sections converged to MRMPS calculation with spdfgh-PCOs for models considered in our calculations. It reveals that MRMPS method give us a better representation of the polarization potential than other models we performed. It should be noted that the main contribution to total elastic cross sections is from Σ_g^+ symmetry under 2 eV. Positron collision with the more complicated, non-polar molecular system C₂H₂ are presented in next chapter. Calculations with the MRMPS method

6.4 Conclusion

for positron-H₂ collision developed in this chapter are employed to calculate the annihilation parameter Z_{eff} in chapter 8; this represents a crucial test for the method.

Positron collisions with C₂H₂

7.1 Introduction

In this chapter, calculated elastic integral scattering cross sections for positron-C₂H₂ collisions are obtained using the molecular *R*-matrix with pseudostates (MRMPS) method at energies below the positronium formation threshold. The MRMPS method is shown to be a successful procedure for dealing with positron-hydrogen molecule collision at low energies in last chapter. C₂H₂ is a non-dipolar molecule as H₂, but has a much more complicated electronic structure than the H₂ molecule. Acetylene is the simplest alkyne that has a large Z_{eff} , so we chose it as a benchmark system for a positron-molecule collision study.

Calculated integral cross sections and differential cross sections for positron collision with C₂H₂ using the *R*-matrix method has been performed with the static model and static plus polarisation model by Franz et al. (2008). These authors also gave the ICS and DCS results computed using semiempirical procedures based on density functional theory (DFT) and the distributed positron model (DPM). ICS and DCS calculations for positron-C₂H₂ collision were also performed by several theoretical groups (da Silva et al., 1998; de Carvalho et al., 2000, 2003; Nishimura and Gianturco, 2005). Total elastic scattering cross sections were measured by Sueoka and Mori (1989) for positron collision with acetylene at incident energies from 1 eV to 400 eV. Measured elastic DCS were reported by Kauppila et al. (2002) at 4, 6.75, 10, 20, 50, 100 eV.

The study of positron collision with acetylene molecule was performed at different

7.2 Target calculation

levels: the static, static plus polarisation and close-coupling with MRMPS method. Within the close-coupling with MRMPS method, our calculations are carried out based on the increasing levels of the PCOs included in target representations. We also analyze the existence of a virtual state by calculating the scattering length based on the s-wave eigenphase. The next sections describe the calculations in details.

7.2 Target calculation

All our calculations were carried out at the linear equilibrium geometry of HCCH, $r_{CC}=1.208 \text{ \AA}$ and $r_{CH}=1.058 \text{ \AA}$. The target GTO basis sets for C and H atoms are double zeta plus polarisation (DZP) set of Dunning Jr (1970). These give $9s \ 5p \ 1d$ basis for C and $5s \ 2p$ for H.

To understand how important the polarisation effects for positron-C₂H₂ collision at low energies, we performed the calculations using several different models, the same ones used for positron collision with hydrogen molecule reported in last chapter. We began from the simplest models, the static model and SP model. The target was frozen in its ground state $\tilde{X} \ ^1\Sigma_g^+$ state, which has the $1\sigma_g^2 \ 1\sigma_u^2 \ 2\sigma_g^2 \ 2\sigma_u^2 \ 3\sigma_g^2 \ 1\pi_u^4$ configuration. For both of the static and SP model, the target wavefunction was taken from a Hartree-Fock self-consistent field (HF-SCF) calculation.

For MRMPS calculations, several PCOs basis were tested with $(\alpha_0 = 0.16, 0.17, \beta = 1.4)$ and $(\alpha_0 = 0.10, \beta = 1.4)$ based on the *spd*-PCOs model. The deletion threshold for orthogonalizing the SCF MOs to PCOs is chosen as $\delta_{thrsh-targ} = 2 \times 10^{-4}$. The target state distribution for various (α_0, β) for model 4 (describes below), is shown in figure 7.1. The energy differences among these tests are fairly small among the three MRMPS model. The PCO basis set with $\alpha_0 = 0.17$ and $\beta = 1.4$ are used to run our target and scattering calculations up to $l=4$ for various MRMPS calculations.

C₂H₂ has 14 electrons, so the CI calculation can be very complicated. We tested different complete active space configuration interaction (CASCI) calculations for the target runs based on the MRMPS method and chose a model which gives good target energies and a relatively small Hamiltonian matrix size for the scattering calculation. Table 7.1 shows the CI models tested and the dimension of the Hamiltonian for each target calculation based on an *spd*-PCOs calculation, represented by the notation of $D_{\infty h}$ point group.

7.2 Target calculation

Table 7.1: Target configurations of different models. N is the size of hamiltonian matrix for Σ_g^+ symmetry. PCO represents pseudo-continuum orbitals.

Model	N	Configurations
1-1	2739	$(1\sigma_g 1\sigma_u)^4 (2\sigma_g 3\sigma_g 4\sigma_g 5\sigma_g 2\sigma_u 3\sigma_u 1\pi_u 1\pi_g)^{10}$ $(1\sigma_g 2\sigma_g 3\sigma_g 1\sigma_u 2\sigma_u 1\pi_u)^{13}$ (PCOs) ¹
1-2	827	$(1\sigma_g 1\sigma_u)^4 (2\sigma_g 3\sigma_g 4\sigma_g 2\sigma_u 3\sigma_u 1\pi_u 1\pi_g)^{10}$ $(1\sigma_g 2\sigma_g 3\sigma_g 1\sigma_u 2\sigma_u 1\pi_u)^{13}$ (PCOs) ¹
2	122	$(1\sigma_g 2\sigma_g 3\sigma_g 1\sigma_u 2\sigma_u)^{10} 1\pi_u^3 (4\sigma_g 3\sigma_u 1\pi_g)^1$ $(1\sigma_g 2\sigma_g 3\sigma_g 1\sigma_u 2\sigma_u)^{10} 1\pi_u^2 (4\sigma_g 3\sigma_u 1\pi_g)^2$ $(1\sigma_g 2\sigma_g 3\sigma_g 1\sigma_u 2\sigma_u)^{10} 1\pi_u^3$ (PCOs) ¹ $(1\sigma_g 2\sigma_g 3\sigma_g 1\sigma_u 2\sigma_u)^{10} 1\pi_u^2 (4\sigma_g 3\sigma_u 1\pi_g)^1$ (PCOs) ¹
3	3415	$(1\sigma_g 1\sigma_u 2\sigma_g)^6 1\pi_u^4 (3\sigma_g 4\sigma_g 2\sigma_u 3\sigma_u 1\pi_g)^4$ $(1\sigma_g 1\sigma_u 2\sigma_g)^6 1\pi_u^3 (3\sigma_g 4\sigma_g 2\sigma_u 3\sigma_u 1\pi_g)^5$ $(1\sigma_g 1\sigma_u 2\sigma_g)^6 1\pi_u^4 (3\sigma_g 4\sigma_g 2\sigma_u 3\sigma_u 1\pi_g)^3$ (PCOs) ¹ $(1\sigma_g 1\sigma_u 2\sigma_g)^6 1\pi_u^3 (3\sigma_g 4\sigma_g 2\sigma_u 3\sigma_u 1\pi_g)^4$ (PCOs) ¹
4	860	$(1\sigma_g 1\sigma_u)^4 (2\sigma_g 3\sigma_g 4\sigma_g 2\sigma_u 3\sigma_u 1\pi_u 1\pi_g)^{10}$ $(1\sigma_g 2\sigma_g 3\sigma_g 1\sigma_u 2\sigma_u)^{10} 1\pi_u^3$ (PCOs) ¹ $(1\sigma_g 2\sigma_g 3\sigma_g 1\sigma_u 2\sigma_u)^{10} 1\pi_u^2 (4\sigma_g 3\sigma_u 1\pi_g)^1$ (PCOs) ¹
5-1	1511	$(1\sigma_g 1\sigma_u)^4 (2\sigma_g 3\sigma_g 4\sigma_g 2\sigma_u 3\sigma_u 1\pi_u 1\pi_g)^{10}$ $(1\sigma_g 1\sigma_u)^4 (2\sigma_g 3\sigma_g 2\sigma_u 1\pi_u)^9$ (PCOs) ¹ $(1\sigma_g 1\sigma_u)^4 (2\sigma_g 3\sigma_g 2\sigma_u 1\pi_u)^8 (4\sigma_g 3\sigma_u 1\pi_g)^1$ (PCOs) ¹
5-2	3656	$(1\sigma_g 1\sigma_u)^4 (2\sigma_g 3\sigma_g 4\sigma_g 5\sigma_g 2\sigma_u 3\sigma_u 1\pi_u 1\pi_g)^{10}$ $(1\sigma_g 1\sigma_u)^4 (2\sigma_g 3\sigma_g 2\sigma_u 1\pi_u)^9$ (PCOs) ¹ $(1\sigma_g 1\sigma_u)^4 (2\sigma_g 3\sigma_g 2\sigma_u 1\pi_u)^8 (4\sigma_g 5\sigma_g 3\sigma_u 1\pi_g)^1$ (PCOs) ¹
6	6384	$(1\sigma_g 1\sigma_u)^4 (2\sigma_g 3\sigma_g 4\sigma_g 2\sigma_u 3\sigma_u 1\pi_u 1\pi_g)^{10}$ $(1\sigma_g 1\sigma_u)^4 (2\sigma_g 3\sigma_g 2\sigma_u 1\pi_u)^9$ (PCOs) ¹ $(1\sigma_g 1\sigma_u)^4 (2\sigma_g 3\sigma_g 2\sigma_u 1\pi_u)^8 (4\sigma_g 3\sigma_u 1\pi_g)^1$ (PCOs) ¹ $(1\sigma_g 1\sigma_u)^4 (2\sigma_g 3\sigma_g 2\sigma_u 1\pi_u)^7 (4\sigma_g 3\sigma_u 1\pi_g)^2$ (PCOs) ¹
7	16112	$(1\sigma_g 1\sigma_u 2\sigma_g)^6 (3\sigma_g 4\sigma_g 2\sigma_u 3\sigma_u 1\pi_u 1\pi_g)^8$ $(1\sigma_g 1\sigma_u 2\sigma_g)^6 (3\sigma_g 4\sigma_g 2\sigma_u 3\sigma_u 1\pi_u 1\pi_g)^7$ (PCOs) ¹
8	188924	$(1\sigma_g 1\sigma_u)^4 (2\sigma_g 3\sigma_g 4\sigma_g 5\sigma_g 2\sigma_u 3\sigma_u 1\pi_u 1\pi_g)^{10}$ $(1\sigma_g 1\sigma_u)^4 (2\sigma_g 3\sigma_g 4\sigma_g 5\sigma_g 2\sigma_u 3\sigma_u 1\pi_u 1\pi_g)^9$ (PCOs) ¹

7.2 Target calculation

Table 7.2: Polarisabilities of C₂H₂ in a_0^3 for the basis of PCOs with $\beta = 1.4$ and $\alpha_0 = 0.17$ for different models. The experimental data are from Nakagawa (1995).

Model	α_{\parallel}	α_{\perp}
1-1	26.51	15.65
1-2	26.33	15.67
2	6.78	4.18
3	33.84	15.65
4	26.89	14.88
5	24.37	12.83
6	27.23	13.82
7	26.87	14.20
8	27.13	13.04
exp.	30.73	18.83

Take Model 1-1 as an example, the first line gives the CAS SCFs only related to target MOs, while the PCOs in the second line are represented by the configurations as

6-22a_g 2-8b_{2u} 2-8b_{3u} 1-5b_{3u} 4-10b_{1u} 2-6b_{2g} 2-6b_{3g}

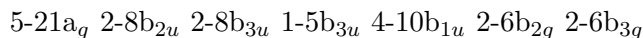
Figure 7.2 shows the target state distributions of different CI models for Σ_g^+ symmetry with $\alpha_0=0.17$, $\beta = 1.4$ and deletion threshold $\delta_{thrsh-tar} = 2 \times 10^{-4}$ with PCO comprising 10s, 10p and 6d orbitals. The chosen states span energies up to about 45 eV above the ground target state.

We need to chose an optimal model that gives fairly small Hamiltonian matrix and good polarisabilities. As shown in table 7.1, the only difference between Model 1-1 and 1-2 is that there is one more σ_g orbital in the CAS for model 1-1 than 1-2. These make the number of target configurations decrease from 2739 to 811. The second configuration in model 1-1 and 1-2 are the same which keeps thirteen electrons freely placing in $1\sigma_g$ $2\sigma_g$ $3\sigma_g$ $1\sigma_u$ $2\sigma_u$ $1\pi_u$ orbitals, one electron was in the PCOs. In model 2, ten electrons were frozen in $1\sigma_g$ $2\sigma_g$ $3\sigma_g$ $1\sigma_u$ $2\sigma_u$. So it gives much smaller size of the Hamiltonian matrix (122) than model 1. But the ground state of model 2 is A $^2\Pi_u$ instead of X $^2\Sigma_g$. Six electron were frozen in the core in model 3. The PCO

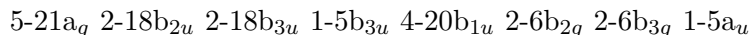
7.2 Target calculation

CSFs correspond to the MO CSFs, but with one electron was put into a PCOs from $3\sigma_g$ $4\sigma_g$ $2\sigma_u$ $3\sigma_u$ $1\pi_g$. Model 4 was constructed using the MO CSFs from model 1-2 and the two PCO CSFs from model 2. This model gives a Hamiltonian matrix of size 860, which is fairly a good choice for continuing calculations. The MO CSFs for model 5 and model 6 are the same as model 4, and several configuration for the PCO CSFs were generated by placing one or two electron in the $4\sigma_g$ $3\sigma_u$ $1\pi_g$ orbitals. The extra PCO CSFs in model 6 leads to a larger Hamiltonian matrix of dimension 6384 compared to 1511 for model 5. Obviously, model 7 and 8 give significantly more configurations than the models designed above. Model 8 is the ideal model for MRMPS calculation. However, the large size of Hamiltonian matrix would require an extremely high specification for the computer to do the implied scattering calculation. In order to choose an appropriate model, the polarisabilities for each model are shown in Table 7.2. The parallel component (α_{\parallel}) of the polarisability tensor derives from $^1\Sigma_u^+$ states, while the perpendicular component (α_{\perp}) are determined by $^1\Pi_u^+$ states. Both α_{\perp} and α_{\parallel} of model 2 gives rather small values compared to experimental values (Nakagawa, 1995), it is because the pure target representation without PCOs does not match to the representation with PCOs, which augments the denominator of the definition of the polarisability. Model 3 gives the biggest polarisability among these given models, but it also gives a fairly large size of Hamiltonian matrix (3415).

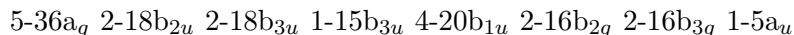
Given the criteria for choosing an appropriate model, model 4 was chosen as the target representation. Model 4 gives the PCOs in the configurations represented as in D_{2h} notation:



for *spd*-PCOs calculation.



for *spdf*-PCOs calculation.



for *spdfg*-PCOs calculation.

Polarisabilities for various MRMPS calculations shown in table 7.3 are performed based on model 4 with $\beta = 1.4$ and $\alpha_0 = 0.17$. Improved polarisabilities for both parallel component and perpendicular component are give with the more complicated PCO models.

7.3 Scattering calculation

Table 7.3: Polarisabilities of C_2H_2 for the basis of PCOs with $\beta = 1.4$ and $\alpha_0 = 0.17$ for different MRMPs calculations based on model 4.

Model	α_{\parallel}	α_{\perp}
<i>spd</i>	26.89	14.88
<i>spdf</i>	27.57	13.49
<i>spdfg</i>	27.64	15.26

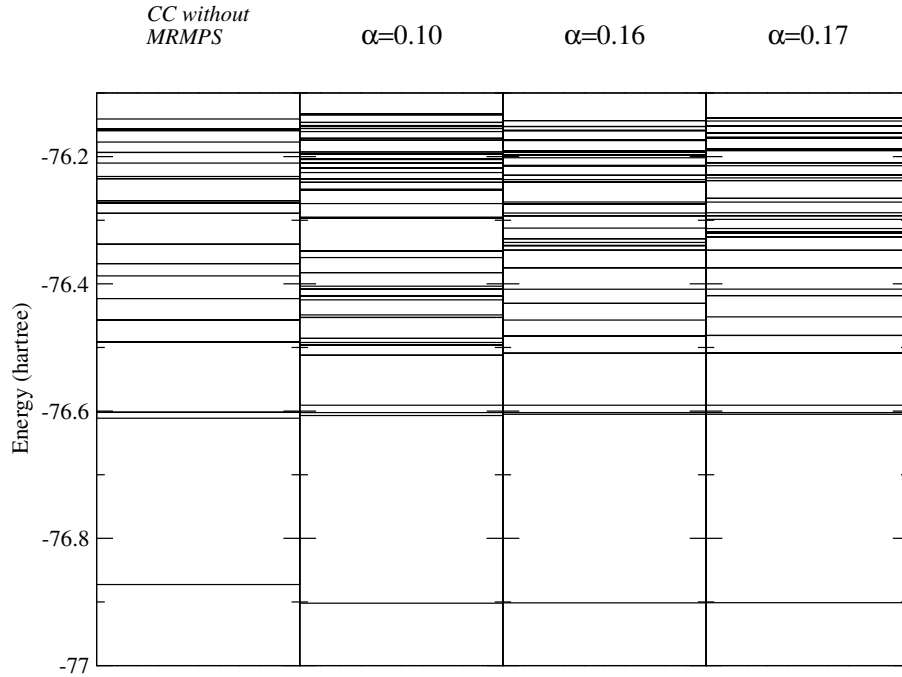


Figure 7.1: Target state distributions of Σ_g^+ symmetry for various α_0 with $\beta = 1.4$ and deletion threshold $\delta_{thrsh-tar} = 2 \times 10^{-4}$ based on *spd*-PCOs model.

7.3 Scattering calculation

Scattering calculations were performed starting from a study at the static level. The continuum basis set used to describe the incident positron is from Faure et al. (2002), which gives the continuum orbitals as (9s,7p,7d,7f,6g) for R -matrix radius $a = 10 a_0$. As described in the previous chapter, positron can be placed all target and continuum orbitals. For the SP model, a number of single excited target configurations were generated by allowing single excitations of one target electron which occupies a virtual orbital.

7.3 Scattering calculation

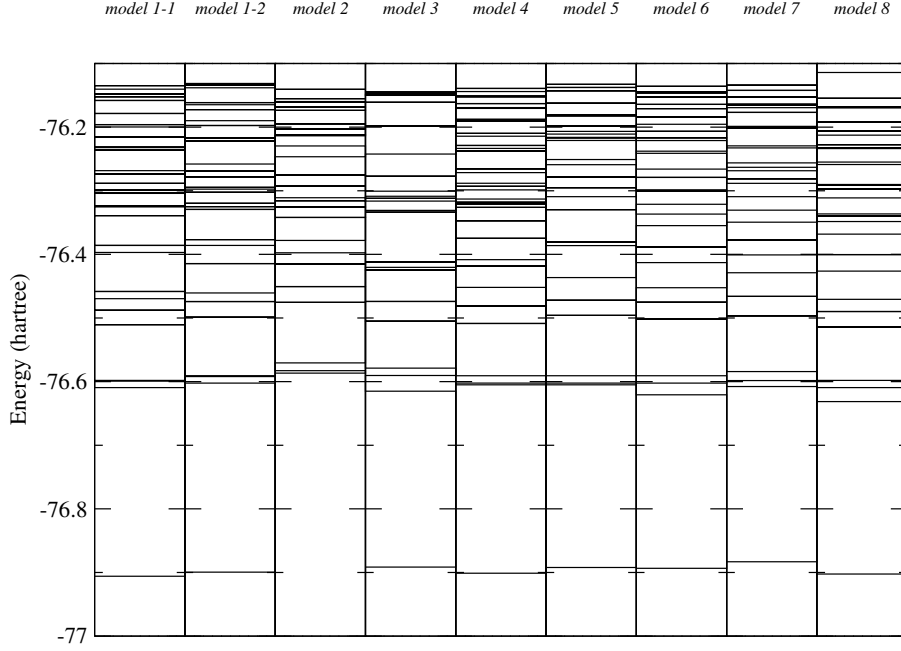


Figure 7.2: Target state distributions of Σ_g^+ symmetry for C_2H_2 .

For the MRMPs calculation, since some exponents of the continuum orbitals are higher than those in the PCO basis, they must be removed from the basis. The continuum orbitals used in the calculations were (6s,7p,7d,6f,6g) when $\alpha_0 = 0.17$. The deletion threshold for orthogonalizing the COs to PCOs were chosen as $\delta_{thrsh-scatt} = 2 \times 10^{-6}$. The target states energies are chosen up to about 20 eV above the ground state. 42 singlet target states are included in the close-coupling expansion for *spd*-PCOs model, 64 states for *spdf*-PCOs model and *spdfg*-PCOs model. The CI models used in our calculation can be represented as:

$$(1\sigma_g 1\sigma_u)^4 (2\sigma_g 3\sigma_g 4\sigma_g 2\sigma_u 3\sigma_u 1\pi_u 1\pi_g)^{10} (\text{COs})^{1p}$$

$$(1\sigma_g 2\sigma_g 3\sigma_g 1\sigma_u 2\sigma_u)^{10} 1\pi_u^3 (\text{PCOs})^1 (\text{COs})^{1p}$$

$$(1\sigma_g 2\sigma_g 3\sigma_g 1\sigma_u 2\sigma_u)^{10} 1\pi_u^2 (4\sigma_g 3\sigma_u 1\pi_g)^1 (\text{PCOs})^1 (\text{COs})^{1p}$$

and L^2 CSFs:

$$(1\sigma_g 1\sigma_u)^4 (2\sigma_g 3\sigma_g 4\sigma_g 2\sigma_u 3\sigma_u 1\pi_u 1\pi_g)^{10} (\text{CAS+PCO})^{1p}$$

$$(1\sigma_g 2\sigma_g 3\sigma_g 1\sigma_u 2\sigma_u)^{10} 1\pi_u^3 (\text{PCOs})^1 (\text{CAS+PCO})^{1p}$$

$$(1\sigma_g 2\sigma_g 3\sigma_g 1\sigma_u 2\sigma_u)^{10} 1\pi_u^2 (4\sigma_g 3\sigma_u 1\pi_g)^1 (\text{PCOs})^1 (\text{CAS+PCO})^{1p}$$

Although we chose a model which gives a fairly small size of Hamiltonian matrix among the models we designed, it still gives huge dimension of Hamiltonian for scat-

7.4 Results

Table 7.4: Dimension of the Hamiltonian matrix for scattering calculations for different MRMPS calculations.

	<i>spd</i>	<i>spdf</i>	<i>spdfg</i>
Σ_g^+	52196	87711	141332
Π_u	50249	85544	138281
Σ_g^-	49363	84588	137572
Σ_u^+	51803	87593	140888
Π_g	50897	86602	140179
Σ_u^-	49340	84540	137496

tering calculation (see table 7.4). So the partitioned R -matrix method (Tennyson, 2004) was used to cut the job time. The final number of solutions retained from the Hamiltonian matrix is 3000 for all MRMPS calculations we performed.

7.4 Results

The eigenphase sums of Σ_g^+ symmetry for positron- C_2H_2 scattering were calculated using various R-matrix models: static, SP and close-coupling with MRMPS. For calculations at the static level, the eigenphase are negative and decrease in the energy region below 5 eV, as shown in the upper panel of figure 7.3. The SP calculation gives slightly higher eigenphase than *spd*-PCOs calculations at energies below 0.3 eV. It falls through zero at about 2.2 eV, which predicts a minimum value of cross sections for Σ_g^+ symmetry. The eigenphase sums calculated with MRMPS method with model 4 (see table 7.1) shows progressively increasing results from the *spd*-PCOs calculation to the *spdfg*-PCOs calculation. For calculations with *spdfg*-PCOs, the eigenphase becomes negative at about 4.2 eV. The upper panel also gives the semi-empirical eigenphase sums calculated by Franz et al. (2008), whose value with π added, lies above all of our R-matrix calculations. The lower panel of figure 7.3 shows the same eigenphase sums of calculations with MRMPS method as upper panel, but with the collision energies up to 1.3 eV. Apparently, it shows the eigenphases peak at about 0.22 eV. Figure 7.5 represents the corresponding total elastic cross sections in \AA^2 for Σ_g^+ symmetry as a function of energy with different MRMPS calculations. The *spdfg*-PCOs model gives

7.4 Results

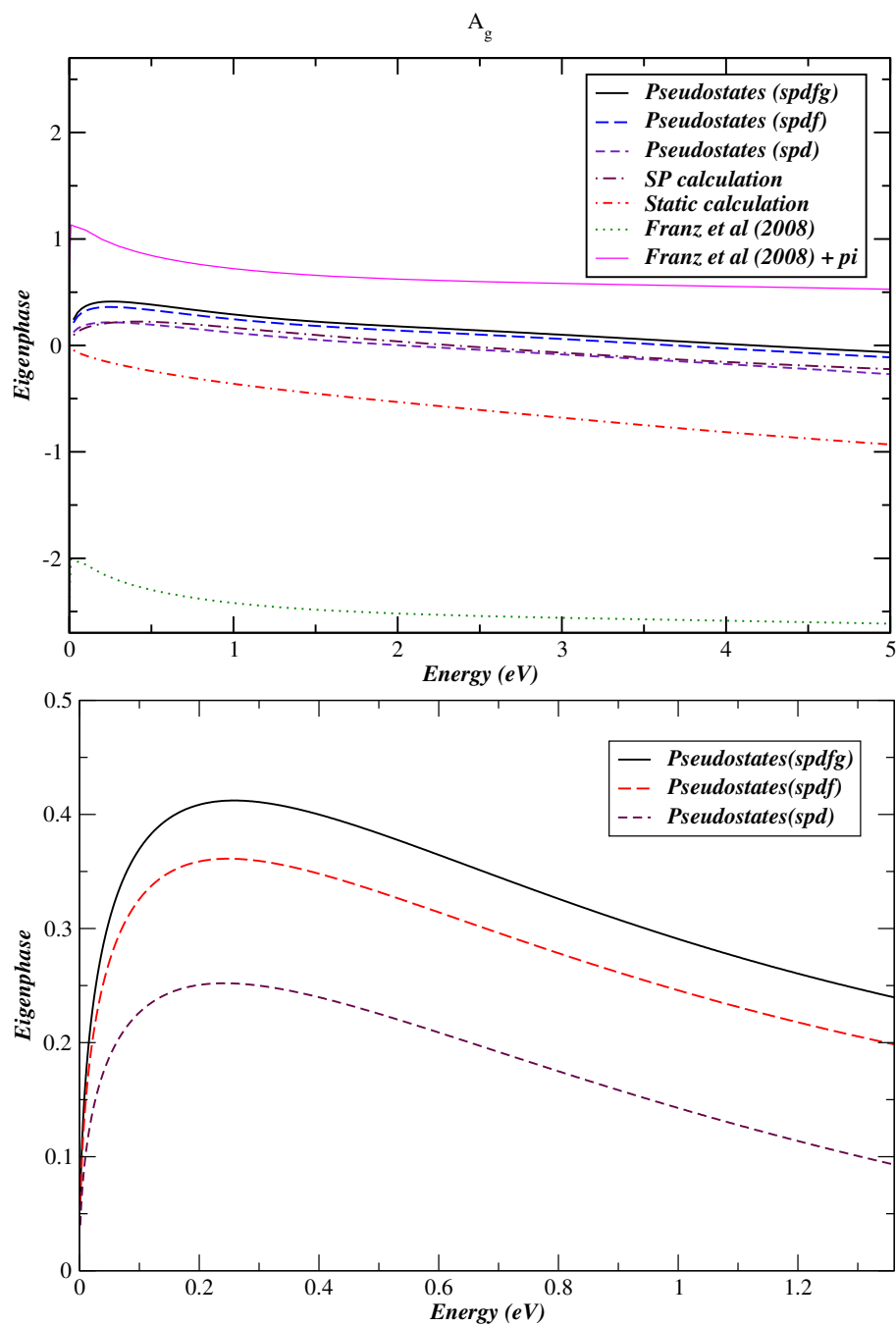


Figure 7.3: Comparison of eigenphase sums for different R-matrix calculations with semi-empirical results for Σ_g^+ symmetry.

7.4 Results

Table 7.5: scattering length a_{scat} for positron-C₂H₂ collision.

PCOs	$a_{scat}(a_0)$	$\sigma_{sl}(a_0^2)$	$\sigma_{tot}(a_0^2)$
<i>spd</i>	-4.130	214.2	202.6
<i>spdf</i>	-5.955	445.4	420.5
<i>spdfg</i>	-6.735	569.7	538.6

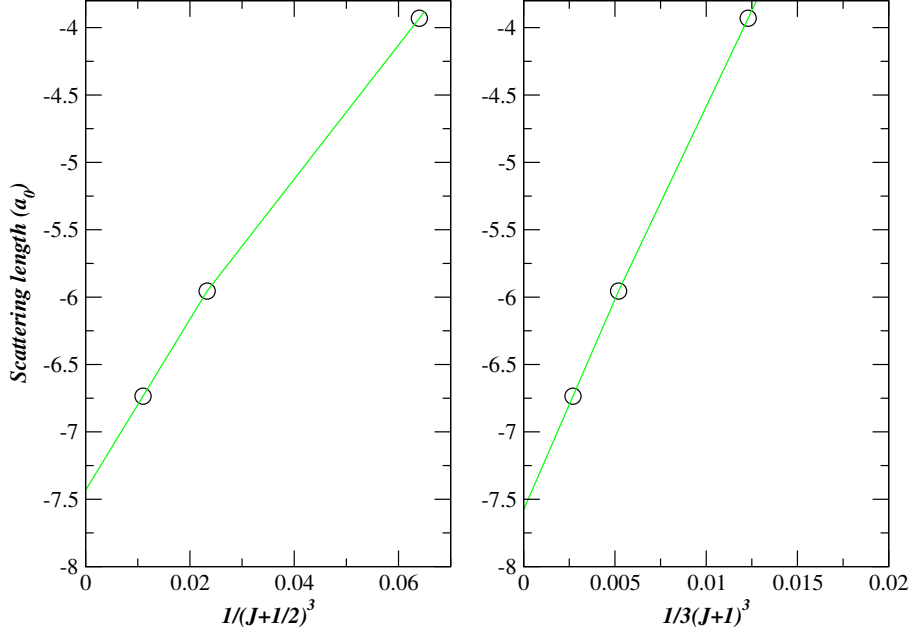


Figure 7.4: The scattering length for positron-C₂H₂ collision using MRMP method in terms of J .

the largest values at energies below 1.8 eV then *spdf* and *spd* models.

Figure 7.6 shows all our R -matrix calculations of integral scattering cross sections below the positronium formation threshold. The static calculation gives lower initial integral cross sections than other models. However, it increases from 0.4 eV. It even lies higher than *spd*-PCOs model above 1.8 eV. At near zero energies, results with MRMP gives higher results than static and SP models. While the most complicated *spdfg*-PCOs model employed for MRMP calculation gives the highest ICS. These results indicate that the application of the MRMP method leads to an improved representation for polarisation effects for positron collision acetylene at energies below 5 eV. Comparing with figure 7.5, the ICS is dominated by Σ_g^+ symmetry at lower energies.

For positron-C₂H₂ collision, the cross sections increase rapidly as the scattering en-

7.4 Results

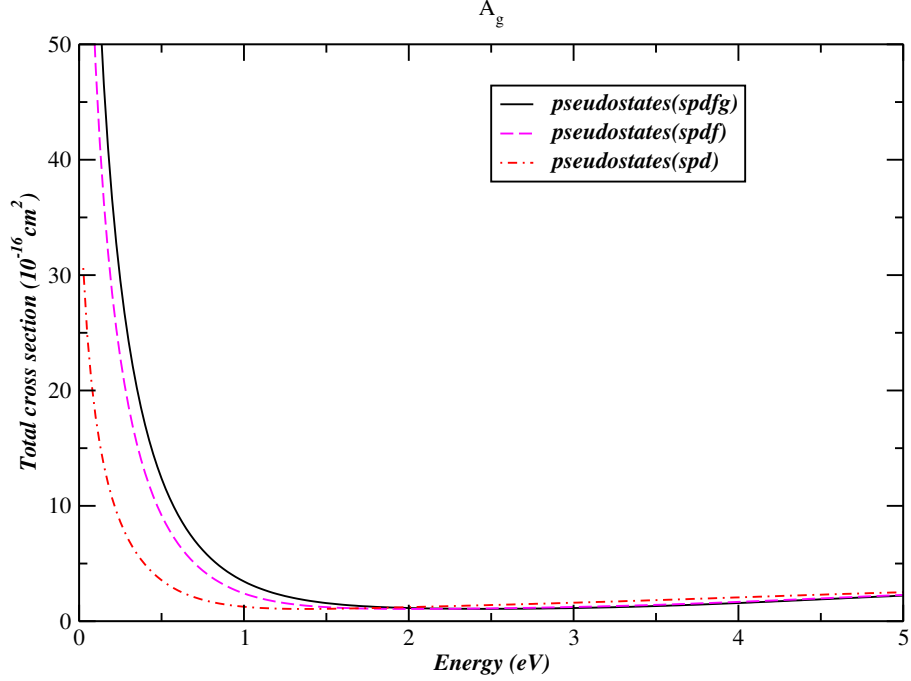


Figure 7.5: Calculated positron- C_2H_2 total elastic scattering cross sections for Σ_g^+ symmetry corresponding to different MRMPS calculations.

ergy goes to zero; the scattering length a_{scat} calculated from s-wave eigenphase increases as larger PCOs employed in our calculations, as shown in table 7.5. The negative scattering length we obtained suggests the presence of a virtual state rather than an s-wave bound states (Taylor, 1972). Table 7.5 also reports s-wave scattering cross sections derived by using the formula $\sigma_{sl}=4\pi|a_{scat}|^2$, compared to the s-wave total elastic cross sections at near zero energy. There is reasonable agreement between these two cross sections. However, the scattering length calculations by de Carvalho et al. (2003) gives $a_{scat}=-229 a_0$, and Nishimura and Gianturco (2005) gives $a_{scat}=-90.07 a_0$ for positron collision with C_2H_2 . An ideal virtual state should be derived when s-wave eigenphase as $\delta=\frac{\pi}{2}$. Accordingly, the position of virtual state given by $\kappa=\frac{1}{a_{scat}}$.

The scattering length for positron- C_2H_2 collision using different MRMPS models is also shown in figure 7.4 in terms of J , the value of highest l included in the PCO expansion. The scattering length converges to $-7.575 a_0$ as $1/3(J+1)^3$, which gives the $\sigma_{sl}=721.1 a_0^2$.

Comparisons of the calculated elastic integral cross sections from our MRMPS calculation with the *spdfg*-PCOs model were made with the experimental measurement

7.4 Results

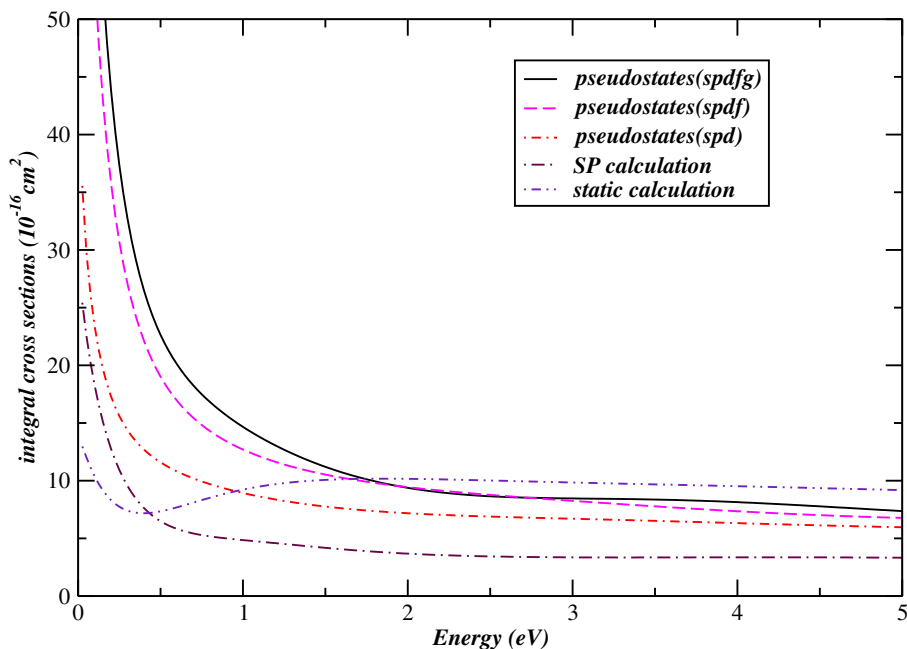


Figure 7.6: Elastic integral cross sections for positron-C₂H₂ collision using various R -matrix models.

Sueoka and Mori (1989) and the semi-empirical study of Franz et al. (2008). Figure 7.7 shows that Franz et al. (2008) gives a good agreement with experiment. Although our integral cross sections lie lower than the measurement, an MRMPS calculation with $spdfgh$ -PCOs can be assumed to give higher results than $spdfg$ -PCOs showed in figure 7.7.

Given the relatively poor agreement for our MRMPS calculation of model 4 with the experiment, more models were tested for calculating the total elastic cross sections (see figure 7.8). For the MRMPS calculation with spd -PCOs and A_g symmetry, four models have been carried out. Among them, model 3 gives the best results of the cross sections and leads to an important improvement for the energies below 2 eV compared to the other models. Furthermore, for model 1-1, calculation with $spdfg$ -PCOs gives a significant increment to the spd -PCOs one, particularly at very low energies. Hence, we can expect that for calculations of model 3 with $spdfg$ -PCOs, better agreement with the measured cross sections may be obtained. Such calculations are currently in progress. It is interesting to note that model 3 does not provide the most flexible target representation of those tested, but is the one with the best balance with the pure CAS-CI and PCO parts of the wave function. This observation may provide an

7.5 Conclusions

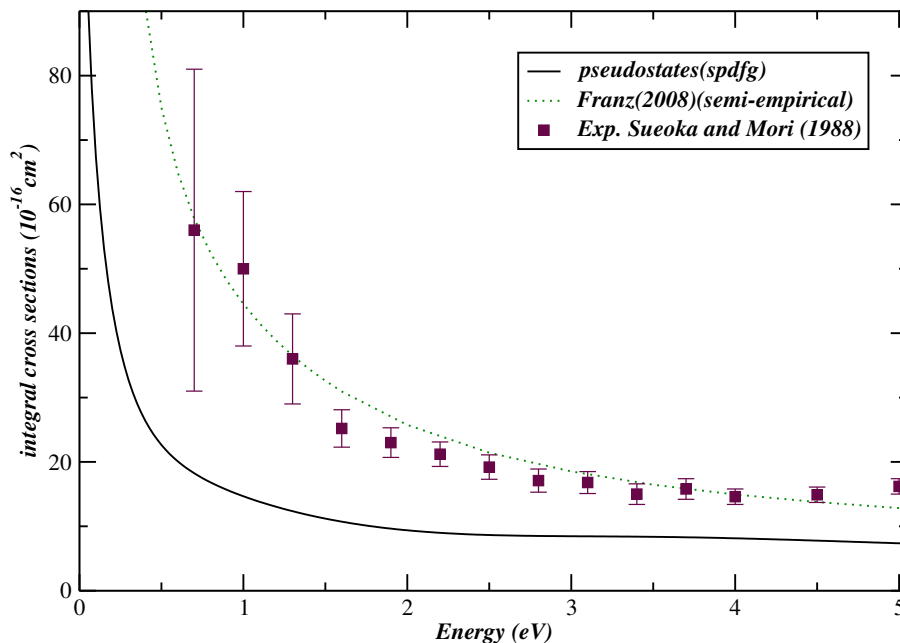


Figure 7.7: Comparisons of calculated integral cross sections with other theoretical and experimental studies for positron- C_2H_2 scattering at energies below 5 eV.

important pointer for designing future models.

7.5 Conclusions

Elastic integral scattering cross sections for positron- C_2H_2 collisions with pseudostates up to g orbitals are reported and compared to relevant measurement (Sueoka and Mori, 1989) and previous theoretical results (de Carvalho et al., 2000; Franz et al., 2008) at energies below the positronium formation threshold. Our MRMPs method calculations give better results than calculations using static and SP models. This suggests that again the MRMPs method gives a better representation for polarisation effects at the energies we consider. Preliminary results for the annihilation parameter Z_{eff} for C_2H_2 molecule based on the computational models described in this chapter are shown in next chapter.

7.5 Conclusions

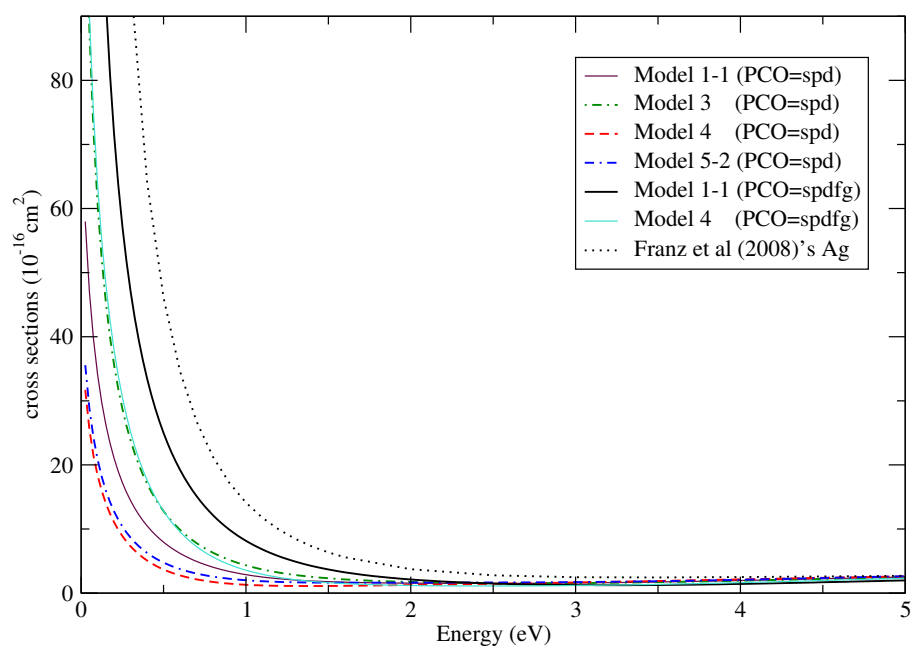


Figure 7.8: Comparisons of calculated integral cross sections with various models for positron-C₂H₂ scattering at energies below 5 eV.

Annihilation rates of low-energy positron scattering with molecules

8.1 Introduction

The value of Z_{eff} is the effective number of target electrons which are available for annihilating with incident positron. Theoretical studies can give accurate Z_{eff} values for simple atoms such as hydrogen (Humberston and Wallace, 1972) and helium (Campeanu and Humberston, 1977; McEachran et al., 1977). Most theoretical molecular positron annihilation studies focus on small molecules like H_2 due to the limitations in theory. Calculations of Z_{eff} for H_2 have been carried out using the Schwinger multi-channel method (Varello et al., 2002), the body-fixed vibrational-close-coupling method (Gianturco and Mukkerjee, 2000), the complex Kohn variational method (Cooper et al., 2008; Cooper and Armour, 2008) and confined variational method (Zhang et al., 2009). Franz et al. (2006) corrected Gianturco's calculation for lack of energy normalization of the wave function and also shows Z_{eff} values which additionally included an enhancement factor. The comparable experiments were performed by Laricchia et al. (1987) and Heyland et al. (1982).

Researchers are also interested in studying positron annihilation with organic molecules which gives very large value of Z_{eff} . Among these organic molecules, for example, acetylene C_2H_2 gives the value of $Z_{eff}=3160$. C_2H_2 is the simplest organic molecule that gives very large value of Z_{eff} . For molecules with large Z_{eff} , one needs to take

8.1 Introduction

account of the effect of nuclear motion which may strongly enhance the annihilation rates. Gribakin (2002) suggested that the low-energy positrons can be captured in vibrational Feshbach resonances with the target molecules to form a positron-molecule bound state. This means the positron is bound to a vibrationally excited state of the target. Then the positron couples to the vibrational positron-molecule complex, which causes the increasing probability of annihilation, at low incident energies. Gilbert et al. (2002) uses experimental work confirmed the importance of the molecular vibrations for processes that give large Z_{eff} . However, Gribakin and co-workers studies have all been based on very approximate treatment of the electronic/positronic motions.

Gribakin and Ludlow (2002) applied many-body theory to the calculation of positron binding energies and annihilation rates. They found convergence behaviours of the partial-wave expansions with rates of $1/(l + \frac{1}{2})^4$ and $1/(l + \frac{1}{2})^2$, respectively. In particular, they derived theoretically for Z_{eff} ,

$$Z_{eff}^l \sim Z_{eff}^{l-1} + \frac{C_{Z_{eff}}}{(l + \frac{1}{2})^2} \quad (8.1)$$

where $C_{Z_{eff}}$ is a constant. However, numerical experiments showed that this behaviour was only found at very high l . Gribakin and Ludlow (2004) found a fit for equation (8.1) based on the calculation with $l=9$ and $l=10$,

$$Z_{eff} = Z_{eff}^l + \sum_{L=l+1}^{\infty} \frac{C_{Z_{eff}}}{(L + \frac{1}{2})^2} \quad (8.2)$$

$$\approx Z_{eff}^l + \frac{C_{Z_{eff}}}{l + \frac{1}{2}} \quad (8.3)$$

Using this approximation, the value of Z_{eff} gives an error of about 10%. In the same way, scattering length can be given as:

$$A_{scat} \sim A_{scat}^l + \frac{C_{A_{scat}}}{(l + \frac{1}{2})^3}. \quad (8.4)$$

Mitroy and Bromley (2006) suggest a better approximation for equation 8.2 according to

$$\sum_{L=l+1}^{\infty} \frac{C_{Z_{eff}/A_{scat}}}{(L + \frac{1}{2})^n} \approx \frac{C_{Z_{eff}/A_{scat}}}{(n-1)(l+1)^{n-1}} \quad (8.5)$$

which gives an error about 0.1%.

Z_{eff} values for positron- H_2 calculated by Zhang et al. (2009) using the confined variational method, showed the scattering length and Z_{eff} in term of the internuclear distance and found that a virtual state is formed at $R=3.4 a_0$.

8.2 Calculations

A major difficulty in obtaining accurate value of Z_{eff} comes from the degree of accuracy required for the scattering wave function at low collision energies. A new computational code was developed to calculate Z_{eff} below the positronium formation using R -matrix method as discussed in Chapter 4. Various wavefunctions are used to calculate Z_{eff} according to models presented in Chapter 6 and Chapter 7.

8.2 Calculations

Obtaining accurate values of Z_{eff} is dependent on an accurate description of the scattering wave function. Here we use the H_2 and C_2H_2 wave functions calculated using several models described in Chapter 6 and Chapter 7 to obtain Z_{eff} . Calculations were initially performed for a test with no potential case, which means there is no interaction between the projectile and the target. Only one-electron and one-positron integrals are required in such a calculation. As expected, these calculations give constant results equal to the number of target electrons as $Z_{eff}=2$ for H_2 and 14 for C_2H_2 molecule for all energies below the positronium formation threshold.

For calculations of positron annihilation with H_2 , we used wave functions from the models presented in Chapter 6: the static model, static plus polarisation model and close-coupling models with the MRMPS method. Therefore, the same calculations are employed as the elastic scattering calculations shown previously. The most complex Z_{eff} calculation for H_2 with the MRMPS method is the spdfgh-PCOs calculation, in which 28 target states are included.

8.3 Z_{eff} results for H_2

The Z_{eff} results for H_2 molecule are shown in Figure 8.1 as a function of incident positron energy and model. Among these calculations, results for static model even gives the values of Z_{eff} smaller than the number of target electrons, while SP model produces higher Z_{eff} value of 2.57 at 0.037 eV than calculation with static potential. Calculations with the MRMPS method give a significantly higher values compared to the static and SP models. All the models behave similarly as a function of incident energy. At near zero energy $k \rightarrow 0$, the values of Z_{eff} increase to the largest number. Particularly for calculation with spdfgh-PCOs, it gives $Z_{eff}=8.26$ at incident positron energy of 0.037 eV.

8.3 Z_{eff} results for H_2

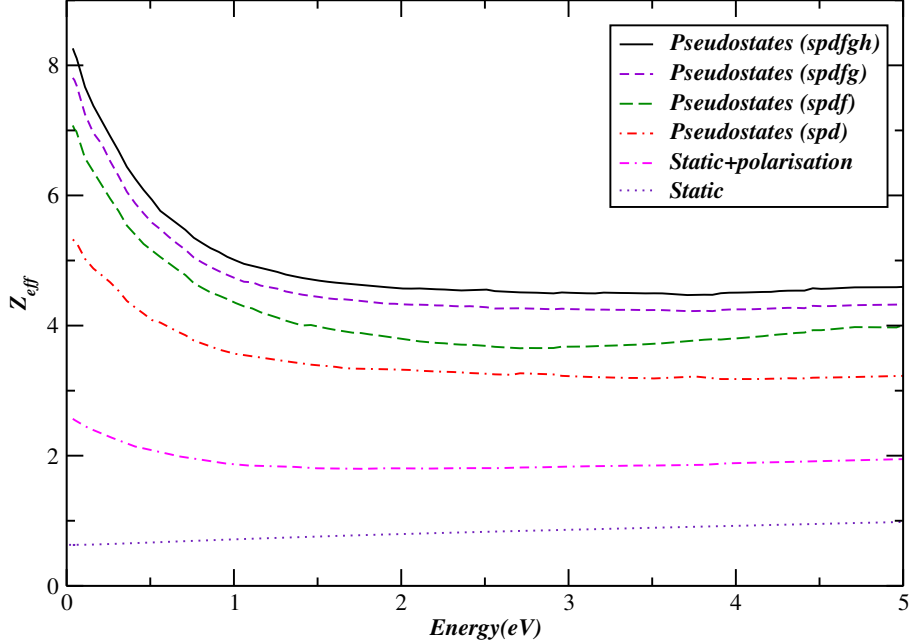


Figure 8.1: Z_{eff} for H_2 molecule in terms of energies for different models for all the symmetries.

It also can be seen from Figure 8.1 that the Z_{eff} values are very sensitive to the inclusion of polarisation in the calculation, particularly at low incident energies. The representations of polarisation effects modelled by the MRMPS method play a very important role not only for total cross section calculations but also for annihilation parameter Z_{eff} calculations at low incident positron energies. Therefore, more complex calculation such as the MRMPS method with spdfghi-PCOs should yield slight improvement compared to spdfgh-PCOs model at considered energies.

Figure 8.2 compares the Z_{eff} results of H_2 molecule with 1 target state and 28 target states included in the MRMPS calculation using the spdfgh-PCOs model, respectively, at energies below 5 eV. The difference between the results occurs at lower energies those below 0.8 eV. The main contribution to Z_{eff} at lower energy comes from the Σ_g^+ symmetry. The inclusion of more target states enhances the Z_{eff} value at near zero energies.

As discussed above, we can obtain improved results of Z_{eff} for H_2 molecule using MRMPS method at energies below 5 eV. Hence, we tried to plotted Z_{eff} results only with MRMPS method in term of factor $1/(J + \frac{1}{2})$ and $1/(J + 1)$ with increment of the pseudo-orbitals J from s-PCOs to spdfgh-PCOs calculations (see figure 8.3). After fitting our results, Z_{eff} converges to 10.30 and 10.53, respectively, as $J \rightarrow \infty$.

8.3 Z_{eff} results for H_2

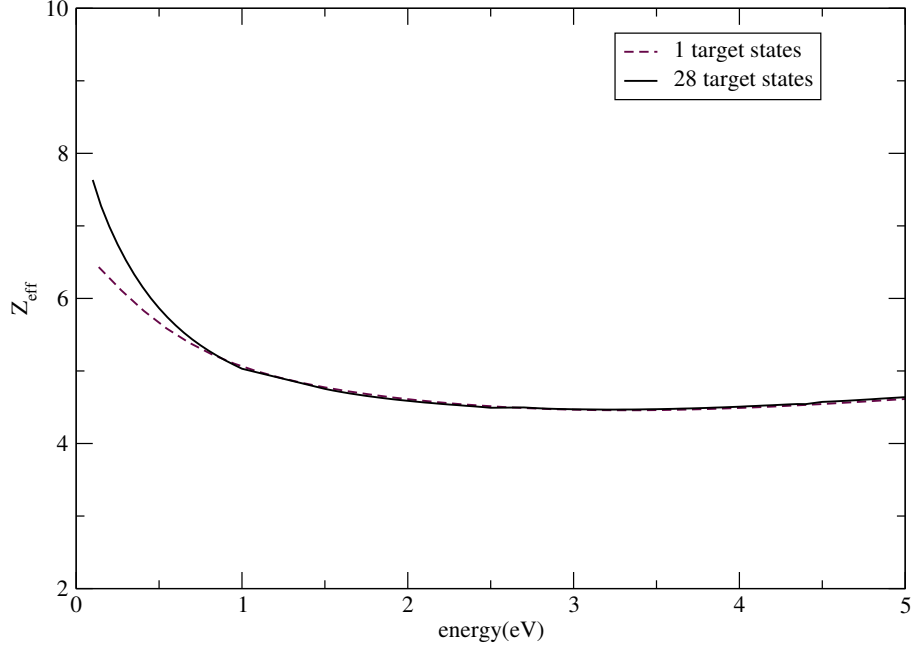


Figure 8.2: Z_{eff} of H_2 molecule for different number of target states included in the MRMPS calculation with spd fgh-PCOs.

Our results can be compared to the $Z_{eff}=6.67$ at incident positron energy of 0.1 eV calculated by Varello et al. (2002) using Schwinger multichannel method. Franz et al. (2006) used an enhancement factor to model the density of positron which yields $Z_{eff}=11.55$ at 0.001eV. $Z_{eff}=7.14$ was calculated using the Kohn variational method (Cooper and Armour, 2008) at 0.14 eV for thermal positrons at 297 K. A reliable nonempirical calculation, which used very accurate variational wave functions at low scattering energy, calculated by Armour et al. (1990) gives the value of $Z_{eff}=10.2$. The best Z_{eff} result is obtained by Zhang et al. (2009) so far, which yields $Z_{eff}=15.7$ at zero energy. The experimental result of Z_{eff} for elastic scattering of positron by hydrogen molecule at low energies is 14.61 ± 0.14 performed by Laricchia et al. (1987) at room temperature.

Figure 8.4 shows the Scattering length for positron- H_2 calculation with MRMPS method in terms of $(J+\frac{1}{2})^{-3}$ and $(J+1)^{-3}$. The scattering length presents a decreasing behaviour with increasing J . It gives the scattering length $a=-2.06$ at $J \rightarrow \infty$, compared to Zhang et al. (2009) which gives scattering length of -2.59.

8.3 Z_{eff} results for H_2

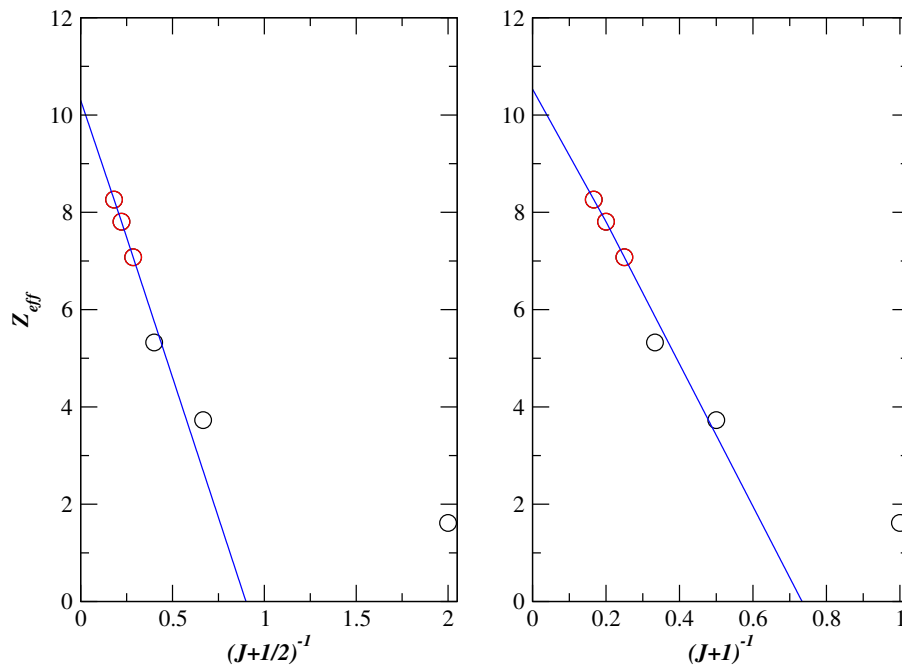


Figure 8.3: Z_{eff} using MRMPs method for H_2 molecule with 28 states at 0.037 eV.

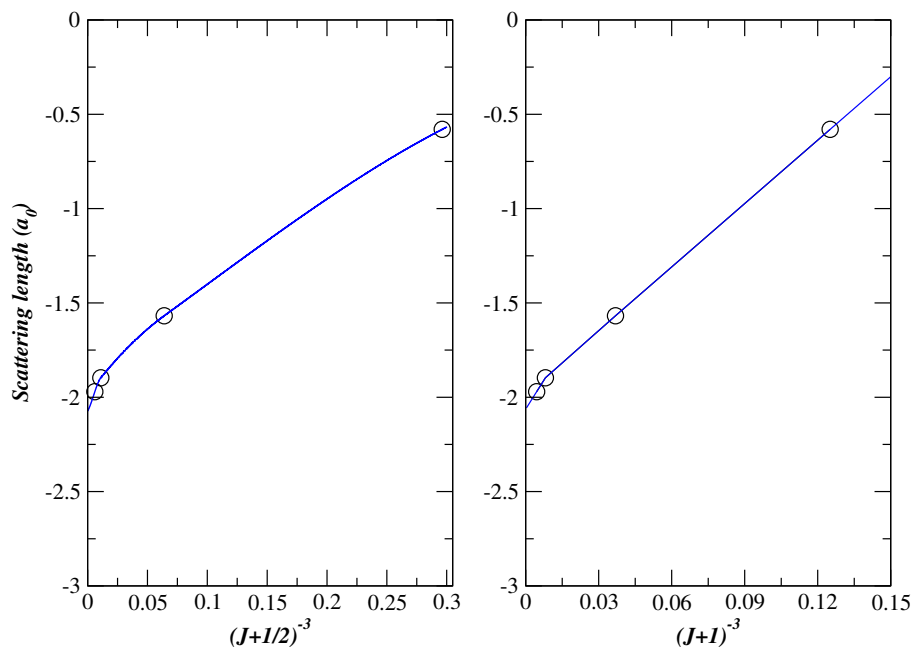


Figure 8.4: Scattering length using MRMPs method for H_2 molecule at 0.1 eV.

8.4 Z_{eff} results for C_2H_2

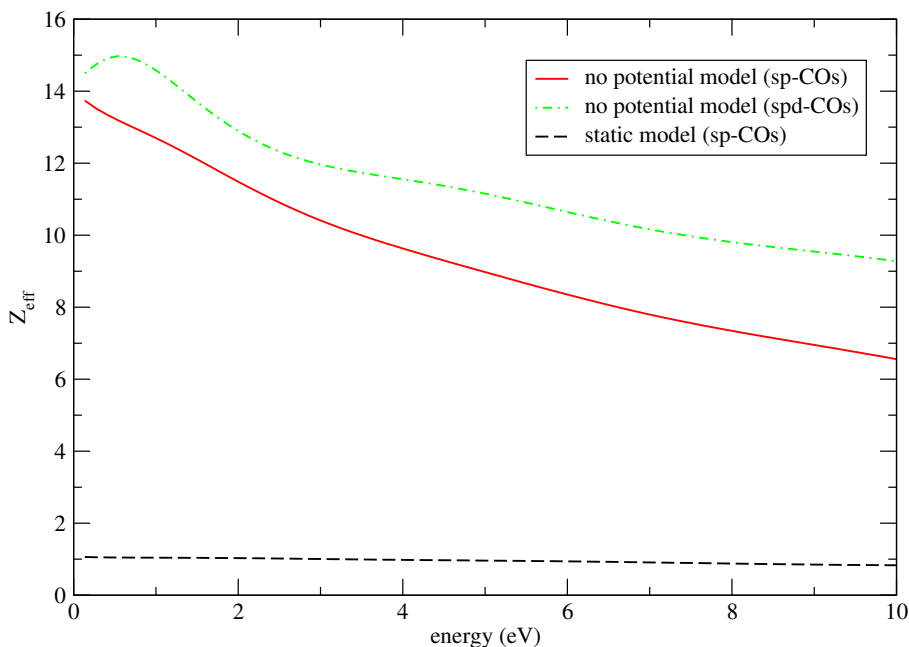


Figure 8.5: Z_{eff} for positron- C_2H_2 annihilation with no potential and static potential model.

8.4 Z_{eff} results for C_2H_2

Only very basic Z_{eff} calculations for positron- C_2H_2 annihilation are performed due to the unexpected behaviour for calculation with partial waves up to d wave. For no potential model with s and p continua, Z_{eff} is obtained as 14 at very low energy (see figure 8.5) and decreases monotonically with increasing energy. However, if d wave is added to above calculation, Z_{eff} rises to 15 at about 1 eV. Some possibilities may cause this problem: integrals involved the coupling of d with s or p orbitals; normalization of the wave function. The code correction is in progress.

8.5 Conclusion

Calculations of annihilation parameter Z_{eff} with H_2 and C_2H_2 molecules are presented at incident positron energy below the positronium formation threshold. The accuracy of the wave function is the most important challenge for calculating Z_{eff} . For H_2 , the use of MRMPs method is shown to give much better values for Z_{eff} than static and SP models. Although the best value of Z_{eff} obtained using MRMPs method can still underestimate the measured value, the results show the expectation if more complicated MRMPs calculation carries out.

Conclusion

Positron collisions with polar molecule H_2O , apolar molecules H_2 and C_2H_2 at incident energies below the threshold of positronium formation are studied using the R -matrix method. Previous studies of positron-molecule collisions using the R -matrix method only considered diatomic targets. The modified polyatomic R -matrix code was employed for the calculations of positron collision. A very efficient algorithm for Hamiltonian matrix construction (Tennyson, 1996) was used in our calculations. This thesis aims to use these developments to analyse the importance of polarisation effects, which is hard to model between the scattered positron and electrons in the target, for positron-molecule collisions. Various models were used to model polarisation in the calculations for each molecules.

Rotationally resolved elastic total cross sections, differential cross sections and momentum transfer cross sections for low energy positron scattering with water molecule using various models are calculated. These models, which include different levels of the polarisation effects, show very similar results due to the large permanent dipole moment of the target. The contribution of Born correction leads to a significant increase to the cross sections at considered energies from 0.25 to 7 eV.

Although both our results and all previous published measurements show strongly forward peaking behaviour for positron-water collision at low energy, our results lie above three of four experimental results. These three measurements neglect the effect of low angle scattering. The one lying above our results overestimates the forward scattering possibly due to the use of the electron DCS measurements to correct the

positron measurements.

Beale et al. (2006), which is the most recent experimental study, give the acceptance profile for the apparatus used. A theoretical correction to Beale *et al's* experimental total cross section is given based on our calculated DCS at low angles. After analysing the cross section, the corrected experimental data give better agreement with our calculated results than uncorrected ones at energies below 10 eV.

Calculations of positron collision with non-polar molecule H_2 were carried out below the positronium formation threshold using the MRMPS method. Unlike positron collisions with a polar molecule, the polarisation effects makes important contribution for positron collision with apolar molecule at low energy. Polarisabilities of H_2 generated using the MRMPS method give good agreement with accurate values calculated by Augspurger and Dykstra (1988). Eigenphase sums and integral cross sections using the close-coupling with MRMPS model show much better agreement with experiments than the static and SP models. The improvement using the MRMPS method in our results shows that a much better representation of polarisation effects at energies below the threshold of positronium formation is obtained. The higher the level of PCOs included in the calculation, the better are the results obtained, particularly at very low scattering energies. Furthermore, the MRMPS calculations give convergent results for the total cross section with increasing level of PCOs. Our best MRMPS calculation with spdfgh-PCOs model, which gives very similar results with spdfg-PCOs model, has excellent agreement with previous theoretical and experimental studies for positron collision with H_2 molecule. Calculation with the MRMPS method gives an excellent treatment of polarisation effects for low-energy positron- H_2 collision.

Non-dipolar molecule C_2H_2 was also treated using the MRMPS method. Various target configurations were performed. Due to the computational limitation, the ideal model which gives huge size of Hamiltonian matrix causes computationally intractable problem for scattering calculation. Hence, a MRMPS model which gives a fairly small size of Hamiltonian and good polarisabilites was chosen to apply to the scattering calculation. The partitioned R -matrix method was used to reduce the running time for diagonalizing the $(N+1)$ Hamiltonian. Although our calculation performed using close-coupling with MRMPS model gives better results than the static and SP models, our MRMPS calculation cross sections still lie below the semi-empirical calculation (Franz et al., 2008) and measurement (Sueoka and Mori, 1989). Although the best current

calculations still do not fully reproduce the experiment, it is indisputable that calculations with the MRMPS method provide a great improvement in the treatment of polarisation.

MRMPS models with a more complex CASCI are shown to give better results for the total cross section than the model we initially chose yielding results very close to the semi-empirical calculation (Franz et al., 2008) for A_g symmetry. It is realistic to expect that the three months long scattering calculations with the target model 3 of Chapter 7 will show good agreement with the experiment. The ideal model (models) with the huge size of Hamiltonian is also expected to give better results than the best presently performed calculations if it becomes computationally feasible. This could be achieved by moving the diagonalisation step to a large parallel computer. Something that is currently being investigated for electron-scattering as a part of the UK-RAMP project.

For the first time, the UK R -matrix code has been extended to calculate the annihilation parameter Z_{eff} at energies below the positronium formation threshold. The accuracy of Z_{eff} is greatly dependent on the accurate description of the scattering wave function. For Z_{eff} calculations of positron- H_2 annihilation, wave functions derived from models with MRMPS method were used. Given the success of the treatment for polarisation shown in the results of total cross section, Z_{eff} calculated using, MRMPS method gives very much better results than the static and SP model. However, the best value of Z_{eff} carried out using MRMPS method gives $Z_{eff}=7.56$ at incident positron energy of 0.1 eV which still underestimates the experiments. The values of Z_{eff} were fitted in terms of the MRMPS model performed from s-PCOs to spdfgh-PCOs calculations, and extrapolate to a value of 10.73 which compares well with the experimental value of Z_{eff} and previous theoretical studies. Several simple calculations of Z_{eff} were carried out for positron annihilation with C_2H_2 molecule below the positronium formation threshold but more work on this problems is required.

The numerical problems with the outer region wave function generation procedure still exists when both open channels and close channels are included in the calculation, especially for calculations with the MRMPS method which leads to a significant increase in the number of channels in the outer region. Propagation of the positron wave function regional $20 a_0$, as shown in this thesis, is unstable. Numerical problem with propagation of many-channel problems to larger radii such like $50 a_0$ need to be solved.

Bibliography

- Alder K and Winther A 1975 *Electromagnetic excitation: Theory of Coulomb excitation with heavy ions*, North-Holland.
- Alkhorayef M, Abuelhia E, Alzimami K, Marouli M, Chin M P W and Spyrou NM 2009 *J. Rad. and Nucl. Chem.* **280**, 315-318.
- Almlöf J and Taylor P R, eds 1984 *Advances theories and computational approaches to the electronic structure of molecules*, (ed. C.E. Dykstra) Dordrecht: Reidel.
- Anderson C D 1933 *Phys. Rev.* **43**, 491-494.
- Anderson C D and Anderson H L 1933 in L M Brown and L hoddeson eds 'The birth of particle physics', 135-136.
- Armitage S, Leslie D E, Beale J and Laricchia G 2006 *Nucl. Instrum. and Methods in Phys. Res. B* **247**, 98-104.
- Armour E A G 1983 *J. Phys. B: At. Mol. Phys.* **16**, 1295-1302.
- Armour E A G and Baker D J 1987 *J. Phys. B: At. Mol. Phys.* **20**, 6105-6119.
- Armour E A G, Baker D J and Plummer M 1990 *J. Phys. B: At. Mol. Phys.* **23**, 3057-3074.
- Arretche F, da Costa R F, Sanchez S D, Hisi A N S, De Oliveira E M, Varella M and Lima M A P 2006 *Nucl. Instrum. and Methods in Phys. Res. B* **247**, 13-19.
- Augspurger J D and Dykstra C E 1998 *J. Chem. Phys.* **88**, 3817-3825.
- Baker T S, Dormand J R and Prince P J 1999 *Appl. Numer. Math* **29**, 171-188.

BIBLIOGRAPHY

- Baluja K L and Jain A 1992 *Phys. Rev. A* **45**, 7838–7845.
- Baluja K L, Mason N J, Morgan L A and Tennyson J 2007 *J. Phys. B: At. Mol. Phys.* **33**, L677–L684.
- Baluja K L, Zhang R, Franz J and Tennyson J 2007 *J. Phys. B: At. Mol. Phys.* **40**, 3515–3524.
- Bartschat K, Hudson E T, Scott M P, Burke P G and Burke V M 1996 *J. Phys. B: At. Mol. Opt. Phys.* **29**, 115–123.
- Beale J, Armitage S and Laricchia G 2006 *J. Phys. B: At. Mol. Opt. Phys.* **39**, 1337–1344.
- Berrington K A and Ballance C P 2002 *J. Phys. B: At. Mol. Opt. Phys.* **35**, 2275–2282.
- Bloch C 1957 *Nucl. Phys.* **4**, 503–528.
- Bray I, Fursa D V, Kheifets A S and Stelvobics A T 2002 *J. Phys. B: At. Mol. Opt. Phys.* **35**, R117–R146.
- Brankin R W, Gladwell I, Dormand J R, Prince P J and Seward W L 1989 *ACM Trans. Math. Soft.* **15**, 31–40.
- Burke P G, Hibbert A and Robb W D 1971 *J. Phys. B: At. Mol. Opt. Phys.* **4**, 153–161.
- Burke P G and Robb W D 1975 *Adv. At. Mol. Phys.* **11**, 143–214. .
- Burke P G 1976 *Proc. 5th Int. Conf. on Atomic Physics ed. R.Marrus, M.Prior and H.Shugart (New York): Plenum* p. p.293.
- Burke P G, Mackey I and Shimamura I 1977 *J. Phys. B: At. Mol. Opt. Phys.* **10**, 2497–2512.
- Burke P G, ed. 1982 *Physics of electronic and atomic collisions* S. Datz, Amsterdam: North-Holland.
- Burke P G, Noble C J and Salvini S 1983 *J. Phys. B: At. Mol. Opt. Phys.* **16**, L113–L120.
- Buttle P J A 1967 *Phys. Rev.* **160**, 719–729.

BIBLIOGRAPHY

- Campeanu R I and Humberston J W 1977 *J. Phys. B: At. Mol. Phys.* **10**, 239–250.
- Canter K F, Coleman P G, Griffith T C and Heyland G R 1972 *J. Phys. B: At. Mol. Phys.* **5**, L167–169.
- Chandra N and Temkin A 1976 *Phys. Rev. A* **13**, 188–203.
- Chang E S and Fano U 1972 *Phys. Rev. A* **6**, 173–185.
- Charlton M, Griffith T C, Heyland G R and Wright G L 1983 *J. Phys. B: At. Mol. Phys.* **16**, 323–341.
- Charlton M and Humberston J W 2001 *Positron Physics*, Cambridge University Press.
- Cho H, Lee H S and Park Y S 2003 *Radiat. Phys. Chem.* **68**, 115–120.
- Cho H, Park Y S, Tanaka H and Buckman S J 2004 *J. Phys. B: At. Mol. Opt. Phys.* **37**, 625–634.
- Chu S I and Dalgarno A 1974 *Phys. Rev. A* **10**, 788–792.
- Clough S A, Beers Y, Klein G P and Rothman L S 1973 *J. Chem. Phys.* **59**, 2254–2259.
- Coleman P G, Griffith T C, Heyland G R and Killeen T L 1975 *J. Phys. B: At. Mol. Opt. Phys.* **8**, 1734–1742.
- Cooper J N and Armour E A G 2008 *Nucl. Instr. and Meth. in Phys. Res. B* **266**, 452–457.
- Cooper J N, Armour E A G and Plummer M 2008 *J. Phys. B: At. Mol. Opt. Phys.* **41**, 245201.
- Crawford O H 1967 *J. Chem. Phys.* **47**, 1100–1104.
- Csaszar A G, Czako G, Furtenbacher T, Tennyson J, Szalay V, Shirin S V, Zobov N F and Polyansky O L 2005 *J. Chem. Phys.* **122**, 214205.
- Čurík R, Ziesel J P, Jones N C, Field T A and Field D, 2006 *Phys. Rev. Lett.* **97**, 123202.
- Danby G and Tennyson J 1988 *Phys. Rev. Letts* **61**, 2737–2739.
- Danby G and Tennyson J 1990 in R J Drachman eds 'Proceedings of the workshop on annihilation in gasses and galaxie', 91–93.

BIBLIOGRAPHY

- Danby G and Tennyson J 1990 *J. Phys. B: At. Mol. Phys.* **23**, 1005–1016.
- Danby G and Tennyson J 1991 *J. Phys. B: At. Mol. Phys.* **24**, 3517–3529.
- da Silva E P, Germano J S E, Lino J L S, de Carvalho C R C, Natalense A P P and Lima M A P 1998 *Nucl. Instr. and Meth. in Phys. Res. B* **143**, 140-148.
- de Carvalho C R C, Varella M T D, Lima M A P, da Silva E P and Germano J S E 2000 *Nucl. Instr. and Meth. in Phys. Res. B* **171**, 33-46.
- de Carvalho C R C, Varella M T D, Lima M A P and da Silva E P 2003 *Phys. Rev. A* **68**, 062706.
- Deutsch M 1951a *Phys. Rev.* **83**, 207-208.
- Deutsch M 1951b *Phys. Rev.* **82**, 455-456.
- Dirac P A M 1928 *Proc. Roy. Soc. Lond. A* **117**, 610-624.
- Dirac P A M 1930 *Proc. Roy. Soc. Lond. A* **126**, 360-365.
- Dunning Jr T H 1970 *J. Chem. Phys.* **53**, 2823-2833.
- Dunning Jr T H 1971 *J. Chem. Phys.* **55**, 716-723.
- Deuring A, Floeder K, Fromme D, Raith W, Schwab A, Sinapius G, Zitzewitz P W and Krug J 1983 *J. Phys. B: At. Mol. Phys.* **16**, 1633-1656.
- Dora A, Tennyson J, Bryjko L and van Mourik T 1991 *J. Chem. Phys.* **130**, 164307.
- Faure A and Tennyson J 2001 *Mon. Not. R. astr. Soc.* **325**, 443-448.
- Faure A, Gorfinkiel J D, Morgan L A and Tennyson J 2002 *Computer Phys. Comms.* **144**, 224-241.
- Faure A, Gorfinkiel J D and Tennyson J 2004a *Mon. Not. Roy. astr. Soc.* **347**, 323–333.
- Faure A, Gorfinkiel J D and Tennyson J 2004b *J. Phys. B: At. Mol. Opt. Phys.* **37**, 801–807.
- Field T A et al., 2008, private communication.
- Fliflet A W and McKoy V 1980 *Phys. Rev. A* **21**, 1863–1875.

BIBLIOGRAPHY

- Franz J, Baluja K L, Zhang R and Tennyson J 2007 *Nucl. Instr. Meths. Phys. Res. B* **266**, 419–424.
- Franz J and Gianturco F A 2006 *Nucl. Instr. Meths. Phys. Res. B* **247**, 20–24.
- Franz J, Gianturco F A, Baluja K L, Tennyson J, Carey R, Montuoro R, Lucchese R R, Stoecklin T, Nicholas P and Gibson T L 2008 *Nucl. Instr. Meths. Phys. Res. B* **266**, 425–434.
- Gailitis M 1976 *J. Phys. B: At. Mol. Opt. Phys.* **9**, 843–854.
- Gianturco F A and Jain A 1986 *Phys. Rep.* **143**, 347–425.
- Gianturco F A, Meloni S, Paoletti P, Lucchese R R and Sanna N 1998 *J. Chem. Phys.* **108**, 4002–4012.
- Gianturco F A and Mukherjee T 2000 *Nucl. Instr. and Meth. B* **171**, 17–32.
- Gianturco F A, Mukherjee T and Occhigrossi A 2001 *Phys. Rev. A* **64**, 032715.
- Gibson T L 1992 *J. Phys. B: At. Mol. Opt. Phys.* **25**, 1321–1336.
- Gibson T L, Lima M A P, McKoy V and Huo W M 1987 *Phys. Rev. A* **35**, 2473–2478.
- Gilbert S J, Barnes L D, Sullivan J P and Surko C M 2002 *Phys. Rev. Lett.* **88**, 043201.
- Gillan C J, Tennyson J and Burke P G 1995 *in* W Huo and F. A Gianturco, eds, ‘Computational methods for Electron-molecule collisions’ pp. 239–254.
- Gorfinkiel J D, Morgan L A and Tennyson J 2002 *J. Phys. B: At. Mol. Opt. Phys.* **35**, 543–555.
- Gorfinkiel J D and Tennyson J 2004 *J. Phys. B: At. Mol. Opt. Phys.* **37**, L343–L350.
- Gorfinkiel J D and Tennyson J 2005 *J. Phys. B: At. Mol. Opt. Phys.* **38**, 1607–1622.
- Gorfinkiel J D, Faure A, Taioli S, Piccarreta C, Halmová G and Tennyson J 2005 *Euro. J. Phys. D* **35**, 231–237.
- Gribakin G F 2002 *Nucl. Instr. and Meth. in Phys. Res. B* **192**, 26–39.
- Gribakin G F and King W A 1994 *J. Phys. B: At. Mol. Opt. Phys.* **27**, 2639–2645.

BIBLIOGRAPHY

- Gribakin G F and Ludlow J 2002 *J. Phys. B: At. Mol. Opt. Phys.* **35**, 339–355.
- Gribakin G F and Ludlow J 2004 *Phys. Rev. Lett* **70**, 032720
- Halmová G and Tennyson J 2008 *Phys. Rev. Lett* **100**, 213202
- Halmová G, Gorfinkiel J D and Tennyson J 2008 *J. Phys. B: At. Mol. Opt. Phys.* **41**, 155201.
- Hariharan P and Pople J 1973 *Theor. Chimica Acta* **28**, 213–222.
- Haxton D J, Zhang Z, McCurdy C W and Rescigno T N 2004 *Phys. Rev. A* **69**, 062713.
- Henry R J W 1970 *Phys. Rev. A* **2**, 1349–1358.
- Heyland G R, Charlton M, Griffith T C and Wright G L, 1982 *Can. J. Phys.* **60**, 503–516.
- Hoffman K R, Dababneh M S, Hsieh Y F, Kauppila W E, Pol V, Smart J H and Stein T S 1982 *Phys. Rev. A* **25**, 1393–1403.
- Humberston J W 1978 *J. Phys. B.: At. Mol. Phys.* **11**, L343–346.
- Humberston J W and Wallace J B G 1972 *J. Phys. B.: At. Mol. Phys.* **5**, 1138–1148.
- Itikawa Y 2000 *Theor. Chem. Acc.* **105**, 123–131.
- Itikawa Y and Mason N 2005 *J. Phys. Chem. Ref. Data* **34**, 1–22.
- Iwata K, Greaves R G, Murphy T J, Tinkle M D and Surko C M 1995 *Phys. Rev. A* **51**, 473–487.
- Johnstone W M and Newell W R 1991 *J. Phys. B.: At. Mol. Opt. Phys.* **24**, 3633–3643.
- Jones M and Tennyson J 2010 *J. Phys. B: At. Mol. Opt. Phys.* **43**, 045101.
- Jung K, Antoni T, Muller R, Kochem K H and Ehrhardt H 1982 *J. Phys. B: At. Mol. Phys.* **15**, 3535–3555.
- Kauppila W E, Kwan C K, Przybyla D A and Stein T S 2002 *Nucl. Instr. and Meth. in Phys. Res. B* **192**, 162–166.
- Kernoghan A A 1996 Ph.D. thesis, Queens’s University of Belfast.

BIBLIOGRAPHY

- Khakoo M A, Silva H, Muse J, Lopes M C A, Winstead C and McKoy V 2008 *Phys. Rev. A* **78** 052710.
- Kimura M, Sueoka O, Hamada A and Itikawa Y 2000 *Adv. Chem. Phys.* **111**, 537–622.
- Lane N F 1980 *Rev. Mod. Phys.* **52**, 29-119.
- Lane N F and Thomas R G 1958 *Rev. Mod. Phys.* **30**, 257–353.
- Laricchia G, Charlton M, Beling C D and Griffith T C 1987 *J. Phys. B: At. Mol. Phys.* **20**, 1865–1974.
- Lehoucq R, Maschhoff K, Sorensen D and Yang C 1996 *ARPACK*
<http://www.caam.rice.edu/software/ARPACK/> .
- Lodi L, Tolchenov R N, Tennyson J, Lynas-Gray A E, Shirin S V, Zobov N F, Polyansky O L, Csaszar A G, van Stralen J and Visscher L 2008 *J. Chem. Phys.* **128**, 044304.
- Löwdin P O 1950 *J. Chem. Phys.* **18**, 365-375.
- Löwdin P O 1955 *Phys. Rev.* **97**, 1474-1489.
- Makochekanwa C, Bankovic A, Tattersall W, Jones A, Caradonna P, Slaughter D S, Nixon K, Brunger M J, Petrovic Z, Sullivan J P and Buckman S J 2009 *New J. Phys.* **11**, 103006.
- McEachran R P, Morgan D L, Ryman A G and Stauffer A D 1977 *J. Phys. B: At. Mol. Phys.* **10**, 663–677 and corrigendum and addendum, 1978 *J. Phys. B: At. Mol. Phys.* **11**, 951-953.
- Mills Jr. A P 1981 *Phys. Rev. Lett.* **46**, 717–720.
- Mitroy J and Bromley M W J 2006 *Phys. Rev. A* **73**, 052712.
- Morgan L A, Tennyson J and Gillan C J 1998 *Computer Phys. Comms.* **114**, 120–128.
- Morrison M A 1988 *Adv. At. Mol. Phys.* **24**, 51-156.
- Mukherjee T and Sarkar N K 2008 *J. Phys. B: At. Mol. Opt. Phys.* **41**, 125201.
- Murphy T J and Surko C M 1991 *Phys. Rev. Lett.* **67**, 2954-2957.
- Murtagh D J, Cooke D A and Laricchia G 2009 *Phys. Rev. Lett* **102**, 133202.

BIBLIOGRAPHY

- Nakagawa S 1995 *Chem. Phys.Lett* **246**, 256-262.
- Nestmann B M and Peyerimhoff S D 1990 *J. Phys. B: At. Mol. Opt. Phys.* **23**, L773-L777.
- Nestmann B M, Pfingst K and Peyerimhoff S D 1994 *J. Phys. B: At.Mol. Opt. Phys.* **27**, 2297-2308.
- Nishimura T and Gianturco F A 2004 *Nucl. Instr. and Meth. in Phys. Res. B* **221**, 24-29.
- Nishimura T and Gianturco F A 2005 *Phys. Rev. A* **72**, 022706.
- Okamoto Y, Onda K and Itikawa Y 1993 *J. Phys. B: At. Mol. Opt. Phys.* **26**, 745-758.
- Padial N T and Norcross D W 1981 *J. Phys. B: At. Mol. Phys.* **14**, 2901-2909.
- Paul D A L and Saint-Pierr L 1963 *Phys. Rev. Lett.* **11**, 493-496.
- Read F H and Channing J M 1994 *Rev. Sci. Instruments* **67**, 2372-2377.
- Reid D D, Klann W B and Wadehra J M 2004 *Phys. Rev. A* **70**, 062714.
- Rescigno T N, Lengsfield B H, McCurdy C W and Parker S D 1992 *Phys. Rev. A* **45**, 7800-7809.
- Sanna N and Gianturco F A 1998 *Comput. Phys. Commun.* **114**, 142-167.
- Schmidt M W and Ruedenberg K 1979 *J. Chem. Phys.* **71**, 3951-3962.
- Schneider B I 1975 *Phys. Rev. A* **11**, 1957-1962.
- Schneider B I and Hay P J 1976 *Phys. Rev. A* **13**, 2049-2056.
- Silva H, Muse J, Lopes M C A, and Khakoo M A 2008 *Phys. Rev. Lett.* **101**, 033201.
- Sinapius G, Raith W and Wilson W G 1980 *J. Phys. B: At. Mol. Phys.* **13**, 4079-4090.
- Slater J C, ed. 1960 *Quantum theory of atomic structure* McGraw-Hill.
- Stein T S, Kauppila W E, Pol V, Smart J H and jesion G 1978 *Phys. Rev. A* **17**, 1600-1608.
- Sueoka O, Mori S and Katayama Y 1986 *J. Phys. B: At. Mol. Phys.* **19**, L373-378.

BIBLIOGRAPHY

- Sueoka O, Mori S and Katayama Y 1987 *J. Phys. B: At. Mol. Phys.* **20**, 3237–3246.
- Sueoka O and Mori S 1989 *J. Phys. B: At. Mol. Phys.* **22**, 963-970.
- Suresh S J and Naik V M 2000 *J. Chem. Phys.* **113**, 9727-9732.
- Surko C M, Gribakin G F and Buckman S J 2005 *J. Phys. B: At. Mol. Opt. Phys.* **38**, R57-R126.
- Szabó A and Ostlund N S, eds 1996 *Modern quantum chemistry* Dover Publication, Inc.
- Tarana M and Tennyson J 2008 *J. Phys. B: At. Mol. Opt. Phys.* **41**, 205204.
- Taylor J R 1972 *Scattering Theory* (Wiley, New York) Chap. 13.
- Tennyson J, Noble C J and Salvini S 1984 *J. Phys. B: At. Mol. Phys.* **17**, 905-912.
- Tennyson J 1986 *J. Phys. B: At. Mol. Phys.* **19**, 4255–4263.
- Tennyson J and Morgan L A 1987 *J. Phys. B: At. Mol. Phys.* **20**, L641–L646.
- Tennyson J and Morgan L A 1999 *Phil. Trans. A* **357**, 1161-1173.
- Tennyson J and Danby G 1988 *J. Phys. B: At. Mol. Phys.* **169**, 111–121.
- Tennyson J 1996 *J. Phys. B: At. Mol. Opt. Phys.* **29**, 1817–1828.
- Tennyson J 2004 *J. Phys. B: At. Mol. Opt. Phys.* **37**, 1061–1071.
- Tennyson J 2010 *Phys. Rep.* (submitted).
- van Harrevelt R and van Hemert M C 2000 *J. Chem. Phys.* **112**, 5777–5786.
- van Reeth P, Humberston J W, Iwata K, Greaves R G and Surko C M 1996 *J. Phys. B: At. Mol. Opt. Phys.* **29**, L465–L471.
- van Reeth P and Humberston J W 1998 *J. Phys. B: At. Mol. Opt. Phys.* **31**, L231–L238.
- Varella M T D, Bettega M H F, Lima M A P and Ferreira L G 1999 *J. Chem. Phys.* **111**, 6396-6406.
- Varella M T D, de Carvalho C R C and Lima M A P 2002 *Nucl. Instr. and Meth. in Phys. Res. B* **192**, 225-237.

BIBLIOGRAPHY

- Watson D K and McKoy V 1979 *Phys. Rev. A* **20**, 1474–1483.
- Wigner E P 1946 *Phys. Rev.* **70**, 606–618.
- Wigner E P 1946 *Phys. Rev.* **70**, 15–33.
- Wigner E P and Eisenbud L 1947 *Phys. Rev.* **72**, 29–41.
- Winter N W, Goddard W A and Bobrowicz F W 1975 *J. Chem. Phys.* **62**, 4325–4331.
- Wright G L, Charlton M, Clark G, Griffith T C and Heyland G R 1983 *J. Phys. B: At. Mol. Phys.* **16**, 4065–4088.
- Wright G L, Charlton M, Griffith T C and Heyland G R 1985 *J. Phys. B: At. Mol. Phys.* **18**, 4327–4347.
- Zhang R, Faure A and Tennyson J 2009 *Phys. Scr.* **80**, 015301.
- Zhang J Y, Mitroy J and Varga K 2009 *Phys. Rev. Lett* **103**, 223202.
- Zecca A, Sanyal D, Chakrabarti M and Brunger M J 2006 *J. Phys. B: At. Mol. Phys.* **39**, 1597–1604.
- Zecca A, Chiari L, Sarkar A, Nixon K L and Brunger M J 2009 *Phys. Rev. A* **80**, 032702.